Three-Dimensional Finite Element Analysis of a Complex Excavation on the MIT Campus

by

Zhandos Y. Orazalin

Bachelor's Degree in Civil Engineering
Karaganda State Technical University, Kazakhstan (2008)

Submitted to the Department of Civil and Environmental Engineering
in Partial Fulfillment of the Requirements for the Degree of

Masters of Science in Civil and Environmental Engineering

at the

MASSACHUSSETTS INSTITUTE OF TECHNOLOGY

June 2012

Signature of Author.....
Department of Civil and Environmental Engineering
May 21, 2012

Certified by.....
Andrew J. Whittle
Professor of Civil and Environmental Engineering
Thesis Supervisor

Accepted by.....
Heidi M. Nepf
Chair, Departmental Committee for Graduate Students

Three-Dimensional Finite Element Analysis of a Complex Excavation on the MIT Campus

by

Zhandos Y. Orazalin

Submitted to the Department of Civil and Environmental Engineering on May 21, 2012
in Partial Fulfillment of the Requirements for the Degree of
Masters of Science in Civil and Environmental Engineering

ABSTRACT

Large excavation projects in urban areas are complex geotechnical problems when it is necessary not only to ensure the stability of the excavation and support system, but also to minimize impacts on adjacent buildings and structures. These problems require more comprehensive analyses that represent the four-dimensional (space-time) processes associated with performance of the excavation support system.

The goal of this research is to evaluate the use of three-dimensional finite element analysis in Plaxis 3D 2011 to simulate ground deformations, pore pressures, and diaphragm wall deflections for the very well instrumented excavation for the basement of the Stata Center on the MIT campus. The model predictions are compared with the field measurements that include vertical inclinometers, settlement points, magnet extensometers, and piezometers.

The Ray and Maria Stata Center building at MIT was designed with a basement for underground parking requiring a 42 ft deep excavation. The excavation was supported by a perimeter diaphragm wall that formed part of the permanent structure and extended 45 ft into a deep layer of underlying Boston Blue clay. The diaphragm wall was braced by a combination of prestressed tieback anchors, preloaded raker and corner bracing support elements. The control of ground movements was a critical aspect of the subsurface design due to the close proximity of the excavation to the historical MIT Alumni swimming pool building.

This study has shown that the three-dimensional finite element analysis can be effectively used for such a complex excavation project and is capable to achieve reasonably consistent predictions of wall deflections, ground movements, and pore pressures for tieback, corner-braced, and raker supported diaphragm walls despite of simplifications in the base case model. The simulation has also captured the three-dimensional effects causing the induced ground deformations to be smaller near the corner areas. Further numerical analyses are now needed to assess the importance of soil constitutive behavior on the observed field performance of the support system for the Stata Center basement.

Thesis Supervisor: Andrew J. Whittle
Title: Professor of Civil and Environmental Engineering

ACKNOWLEDGEMENTS

I would like to thank my thesis and research advisor, Professor Andrew Whittle, as well as my academic advisor, Professor Herbert Einstein for their support and continuous guidance. I am also very grateful for the opportunity to learn from Dr. John Germaine, Dr. Lucy Jen, and Professor Ruben Juanes. I express my deep appreciation to my father, Professor Yerbol Orazaly, and my mother, Azhimova Shara.

Also, I would like to thank all my friends and colleagues at MIT for their support and encouragement.

TABLE OF CONTENTS

List of Figures

List of Tables

1 INTRODUCTION

1.1 Problem Statement and Research Objectives

Large excavation projects in urban areas are complex geotechnical problems where it is necessary not only to ensure the stability of the excavation and support system, but also to minimize impacts on adjacent buildings and structures. These problems require more comprehensive analyses that represent the four-dimensional (space-time) processes associated with performance of the excavation support system. The goal of this research is to evaluate the use of three-dimensional finite element analysis (using a commercial Finite Element Analysis code, Plaxis 3D 2011) to simulate ground deformations, pore pressures, and diaphragm wall deflections for the very well instrumented excavation for the basement of the Stata Center on the MIT campus.

The Ray and Maria Stata Center building at MIT was designed with a basement for underground parking requiring a 42 ft deep excavation. The excavation was supported by a perimeter diaphragm wall that formed part of the permanent structure and extended 45 ft into a deep layer of underlying Boston Blue clay. The diaphragm wall was braced by a combination of prestressed tieback anchors, preloaded raker and corner bracing support elements. The control of ground movements was a critical aspect of the subsurface design due to the close proximity of the excavation to the historical MIT Alumni swimming pool building. The construction history and measured performance of the excavation support system were documented in the SM thesis by Olsen (2001).

The development of the three-dimensional finite element model for the Stata Center constitutes a challenging task, because it not only requires a reliable modeling of the constitutive behavior of the soil coupled with groundwater seepage flow, but also needs to represent a large

range of structural support system elements and a complex non-uniform excavation process. The complexity of the project has defied previous attempts at three-dimensional modeling. However, with the latest generation of Plaxis 3D 2011, we now have the advantage of a suitable three-dimensional flow-deformation analysis tool to create a comprehensive model of the entire excavation project with more than 300 tieback and raker support elements. This analysis is the first attempt to use these modern tools for a well-documented case history.

Therefore, the main research objective is to evaluate the use of three-dimensional finite element analysis to simulate ground deformations, pore pressures, and diaphragm wall deflections for this very well instrumented excavation. The model predictions are compared with the field measurements that include vertical inclinometers, settlement points, magnet extensometers, and piezometers. The thesis provides full results of the analysis and detailed directions to reproduce the base case model predictions.

This study is a part of research with the goal to investigate the key parameters affecting the excavation performance and the predictive capabilities of the three-dimensional finite element analysis applied to geotechnical engineering problems. Taking into account the complexity of the project and challenges of a three-dimensional analysis, a base case simulation with a simple soil model was needed in order to obtain preliminary results. Several models have been developed, calculated and carefully analyzed. Two of them are presented and discussed in detail - the Base Case Model (A), which assumes undrained conditions within the clay, and the Model (B), which takes into account the effects of partial drainage. Both models simulate the adjacent swimming pool building as a three-dimensional surface surcharge (1.28ksf). All three dimensional models are currently limited to a Mohr-Coulomb soil model, which represents a

reasonable "first-order" approximation of soil behavior and is defined by input parameters that specify the linear elastic behavior (E, ν') and yield conditions (c', ϕ').

1.2 Organization

Chapter 2 provides background information for this thesis and presents the description of the excavation project used as a case study for the three dimensional finite element analysis. The chapter includes a detailed overview of the excavation support system and construction history of the project. It also describes the subsurface soil and groundwater conditions of the site and geotechnical instrumentation used to monitor the excavation performance.

Chapter 3 describes the development of the three dimensional finite element model and the base case model assumptions. That includes the information on the soil profile, groundwater and boundary conditions and properties of the structural elements. The process of modeling complex geometries for large three dimensional analyses is also fully described.

Chapter 4 presents and evaluates the results obtained from the base case model. The model predictions include wall deflections, pore pressures, surface settlements, excavation heave and structural loads. These results are compared with the field measurements. Also, the observed three dimensional effects are discussed in detail.

Chapter 5 contains a summary of the thesis. The conclusions are summarized and recommendations from this work are presented. Chapter 5 is followed by three appendices. They include all the necessary details to recreate the three dimensional model of the excavation for the basement of the Stata Center at MIT in Plaxis 3D 2011.

2 BACKGROUND

2.1 Project Description

The Ray and Maria Stata Center is an academic complex designed by renowned architect Frank Gehry for the Massachusetts Institute of Technology (MIT). The building is home to the Computer Science and Artificial Intelligence Laboratory (CSAIL), the Laboratory for Information and Decision Systems (LIDS) and the Department of Linguistics and Philosophy. The Stata Center has become "iconic" and well known due to its impressive design featuring unusual shapes such as tilting towers and many-angled walls (Figure 2-2). It also has a great number of sustainable design elements that include innovative storm water retention and management system, as well as demand controlled ventilation system.

The underground part of the Stata Center building was complete in a period of 11 months from July 2000 to June 2001. Almost 5 months of this period were spent on the slurry wall construction which was accomplished in early November, 2000. The mass excavation for the Stata Center building started on November 14, 2000, and the project was believed to be the largest open excavation in the history of Cambridge (Joyce, 2004). Nevertheless, the excavation work and associated support system installation were successfully completed as scheduled on June 19, 2001. The construction dates with the time frame for the excavation and associated support system are summarized in Table 2-1.

The site for the MIT Stata Center has a very large rectangular plan area (approx. 320ft x 390ft), which abuts an existing building along its southern edge (Figure 2-3). A floating mat foundation system was designed so that the weight of the building is balanced against the weight of the soil extracted from the site. The excavation support system comprises a reinforced 30 inches thick concrete diaphragm wall that is supported through the use of: 1) three levels of

tiebacks on the west, south, and east sides, 2) two levels of corner bracing, and 3) two levels of raker supports on the north side.

Tiebacks were installed at an angle of 20 degrees from the horizontal at El. 10, El. -1, and El. –10 and preloaded from 112 to 128 kips. Two levels of corner bracing consisting of 36-in-diameter pipe struts were installed at El. 10 and El. –10.

The City of Cambridge prohibited the installation of tiebacks beneath the Vassar street such that two levels of inclined raker bracing (at El. 10 and El. –10) were used along the North side of the excavation. The raker bracing consisted of 36-in-diameter pipe struts extending from embedded plates in the diaphragm wall to kicker blocks embedded in the concrete mat foundation.

2.2 Subsurface Soil Conditions

The site is situated on filled land within the Charles River Basin at the east side of the MIT campus in Cambridge, Massachusetts (Figure 2-1). In preparation for the design and construction of the Stata Center a geotechnical exploration program and specialized laboratory testing (at MIT Geotechnical Laboratory) were undertaken to provide data on the engineering properties of the soil underlying the proposed building location. The subsurface exploration program consisted of 20 shallow test borings, 2 deep borings, and 10 piezocone tests advanced to refusal in the glaciomarine deposits or bedrock (Hewitt, et al., 2003). Piezocone testing was used to identify sand layers and lenses within the marine clay and to recognize relative changes in stress history and undrained shear strength profile.

A typical subsurface profile underlying the Stata Center in the middle of the site would consist of 11 ft of fill, 6 ft of organics, 14 ft of sand, 85 ft of clay, and 15 ft of glacial till. The

principal stratum is the marine clay (Boston Blue Clay) - which can be sub-divided into an upper overconsolidated clay crust and a lower normally consolidated unit. Five subsurface profiles (location is schematically drawn in Figure 2-5) showing soil and water conditions, adjacent structures, and the Stata Center excavation are shown in Figures 2-6 and 2-7.

The description of the subsurface layers can be found below, proceeding downward from the ground surface (Hewitt, et al., 2003):

1) Miscellaneous Granular Fill – the layer consists of coarse to fine sand or gravelly sand, with varying amounts of cinders, glass, brick, rubble, and wood. It varies in density from loose to dense with an average Standard Penetration Test N value of 15 and ranges in thickness from 5 to 19 ft.

2) Organic Silt and Peat – a deposit of organic silt and peat is a soft, gray, compressible layer containing some fibers, and interbedded with peat that is soft, brown, and fibrous. The stratum thickness varies from 4 to 22 ft. Some fine sand and shells are present.

3) Marine Sand – the marine sand stratum is a dense, gray, fine to medium sand with some gravel. It ranges in thickness from 0.5 to 16.5 ft and the top of the layer is located at depths ranging from 13 to 30 ft. (El. +7 ft to –11 ft). The Standard Penetration Test blow counts ranged from 19 to 32 blows/ft.

4) Marine Clay – the Boston Blue Clay consists of medium stiff to stiff, silty clay with occasional fine sand seams. This stratum is typical of the Boston area with an upper layer consisting of a stiff crust, becoming softer and more compressible with depth. The thickness of the clay varies from 55 to 90 ft within the location of the Stata Center. Undrained shear strength profiles (Figure 2-9) were developed from the laboratory CRS data using SHANSEP procedure. As recommended by Berman et al. (1993), the SHANSEP parameters m=0.77 and S=0.205 were

used to determine the undrained shear strength (Hewitt, et al, 2003). The profiles typically decrease from 1,600 psf to 1,300 psf at El. -55 ft, and then increase to a maximum of 1,900 psf at the bottom of the marine clay.

5) Glacial Till –a heterogeneous layer of dense sand, gravel, silt, clay and boulders was encountered underlying the marine deposits (Boston Blue Clay). This glaciomarine deposits appear to vary in thickness from 5 ft to possibly 20 ft in some places with it averaging roughly 12 ft in thickness.

6) Bedrock – the bedrock is a part of the Cambridge Argillite formation, which is a relatively soft gray sedimentary rock. Bedrock is encountered at depths approximately 131 ft (El. -110 ft).

2.3 Groundwater Conditions

Two groundwater observation wells were installed in the test borings HA-1 and HA-5 on the northeast and southwest sides of the site (Figure 2-4). Groundwater was observed in completed test borings at depths ranging from El. 5 ft to El. 11 ft. The water level in the wells was also checked right before excavation work began and was found to be at El. 14.0 ft and El. 14.2 ft, respectively. The groundwater table elevation is affected by a great number of factors with include below-grade structures, precipitation, local construction activity, pumping of dewatering systems, leakage from utilities, and seasonal variations. The water level in the Charles River is maintained in the range of El. 12 to El. 13. Although previous investigations have found that the water pressures in the clay and underlying till are higher than hydrostatic by about 5 ft to 7 ft of head (Berman, 1993), there was no evidence to support these conditions

during investigations or construction of the Stata basement. As a result, hydrostatic pressures were used for the design calculations (Olsen, 2001).

2.4 Adjacent Structures

As can be seen in Figure 2-3, the Stata Center site is surrounded by existing structures. The adjacent structures can impact both the performance and the design of the excavation support systems; therefore, all adjacent buildings were carefully studied and documented. Figure 2-3 shows the locations and foundation systems of for these adjacent buildings.

Building 36 is located to the west of the site near the northwest corner, 24-ft from the diaphragm wall, and is a 9-story concrete building with two belowgrade levels. The building is built on a mat foundation bearing on the marine sand at El. –2 ft.

Building 26 is a 5-story concrete structure with a penthouse and one below-grade level situated to the west of the site 54 ft from the diaphragm wall. The foundation system is footings bearing on the marine sand at El. 1 ft.

Building 57, the MIT Alumni Pool Building, is a 3-story building with a swimming pool that extends below grade. It is located to the south of the site at a distance of approximately 3.5 ft from the diaphragm wall. The structure is supported by belled concrete caissons bearing primarily in the marine sand at El. –12 ft with a typical shaft diameter of 3-ft with the bells varying from 3 to 10 ft. The loads supported by these caissons vary from 80 to 320 kips.

Building 70 was a parking garage (since demolished) with 8 stories with a below grade level located to the east of the site with the nearest point 28-ft from the Stata Center. The foundation system comprises pressure injected footings bearing in the marine sand at El. –6.25 ft.

Vassar Street is a two lane road that is approximately 45 ft wide located to the north of the site and at its nearest point is 20 ft from the diaphragm wall. A great number of utilities are located beneath the street which have affected the design of the excavation support system.

2.5 Excavation Support System

The wall system consists of a 30 in reinforced concrete diaphragm wall as the permanent basement wall. The slurry wall was comprised of 65 diaphragm wall panels that were installed with numbering starting in the southwest corner and continuing counter-clockwise around the perimeter. The wall was designed to extend to El. –50 ft (approximately 28 ft into the marine clay deposits) top elevation varying from El. 15.4 ft to El. 19.0 ft with the surface at El. 21.0 ft. The wall was designed to support loads through skin friction but not through end-bearing. The diaphragm wall was cast in-situ with sleeves pre-installed to simplify the installation of tieback anchors. The bearing plates were also used to strengthen the contact areas with corner braces and rakers.

The foundation consists of a 4.0 ft thick reinforced concrete slab (mat foundation). At the excavation level of El. –21 ft, a concrete mud mat was placed to stabilize the surface of the clay and to make it easier to construct the reinforcing cage for the slab, as well as to pour it. The top of the mat foundation is at El. –16.6 ft.

The support system was designed with a total of 289 tiebacks spread out on the south, east, and west sides of the site to provide lateral support. They were installed at El. 10.0 ft, -1.0 ft, and –12.0 ft and inclined at an angle of 20°. The design loads are 112 kips for the top level and 128 kips for the second and third levels. The tiebacks were designed to have total lengths of 90 ft, 48 ft, and 38 ft, with bond lengths of 40 ft, 50 ft, and 50 ft for first, second, and third levels respectively. A typical cross section showing the tiebacks and the diaphragm wall with the

excavation progress is in Figure 2-11. The tiebacks details can be found in Table 2-2. The tiebacks each consist of 4, 0.6 in. diameter high strength steel tendons (270 ksi) where the free lengths are sheathed with a polyethylene tube material to preclude bonding in that portion. The Type I/II Portland Cement with water to cement ratio of 0.49 by weight and a minimum 28 day compressive strength of 4,000 psi was used in the grouted anchors.

The tiebacks are drilled with a casing through the layers of fill, organics, and sand using internal flush methods deep into the overconsolidated clay crust. Each drilled hole is filled with grout and the tendon and post-grouting pipes are inserted while the casing is removed. The post-grouting pipe consists of a 0.75 in PVC pipe with holes, so post-grouting can be undertaken (instead of redrilling) if the anchor fails to achieve its proof load. The grout can be applied at pressures up to 800 psi if post-grouting is necessary. The tiebacks will then be locked-off at 100% of their design load once the grout has had time to set. All tiebacks are also proof tested to 130% of their design load.

The corner bracing consists of 36 in diameter steel pipe struts that are installed at El. 10 ft and El. –10 ft. The pipe struts were pre-loaded by jacking them in place at 50% of their design load. The details for corner bracing support can be found in Table 2-3 (design loads, jacking loads, and strut sizes). The numbering system used to identify each corner brace identifies the corner location, the bracing level (1 for El 10 ft and 2 for El –10ft), and its position from the corner (starting from the closest to the corner).

The support system for the north wall comprises two levels of raker struts that transfer earth pressures to the mat foundation (and transferring the load through basal shear resistance across to the south wall). The construction sequence assumes that a large portion of the site will be excavated to final grade leaving a 20 ft berm in front of the north wall. The foundation mat is

poured from the south wall and the rakers are then set in place and pre-loaded. Each raker comprises a 36 in diameter steel pipe strut that supports the wall (at El 10 ft and El –10 ft) and is inclined downward to a kicker block cast into the mat. They are also pre-loaded to 50% of their design load. Figure 2-12 shows a typical cross section of rakers and excavation progress. The details for each of the rakers can be found in Table 2-4.

2.6 Construction Sequence

The MIT Stata Center project started with the installation of the reinforced concrete diaphragm wall using the slurry trench method. This was accomplished from July to November 2000, a period of approximately 5 months. A grouting program was undertaken to strengthen the sand layer below building 57 to minimize settlements due to loss of ground for the wall directly adjacent to its foundation prior to installation of the south wall.

The excavation began approximately in November of 2000, after the perimeter diaphragm wall installation. Dewatering wells were installed within the excavation to maintain the water table below the excavation grade. Two groundwater observation wells were set up outside of the diaphragm wall (Figure 2-4) and recorded no appreciable lowering of the water table surrounding the site during this process. The excavation work developed a general trend of progressing from the southwest toward the northeast. At each grade elevation, the excavation progresses from the southwest corner northwards along the west wall to enable installation of tieback anchors (Figure 2-1). The next phases included the excavation along the south wall and then north along the east wall (#2 and #3 in Figure 2-10). The soil in the middle of the site was kept as a central surcharge to improve the stability of the lateral earth support system. Next, the excavation was gradually pulled back northward, as shown in Figure 2-10. This same pattern was repeated for each tieback levels. The north side was left to the end in order to install the raker

supports. Support installation progressed as quickly as the tiebacks could be installed by the drill rigs, as well as the corner bracing could be fabricated on site and put in place.

The excavation process was constantly monitored, described in the daily field logs and recorded on the webcams located around the site; numerous photos were also taken during the each construction phase. The summary of construction activities with corresponding dates is presented in Table 2-1.

2.7 Geotechnical Instrumentation

The performance of the excavation support was monitored throughout the excavation in order to ensure that movements were within acceptable limits and to mitigate possible damage to the surrounding structures. Any movement toward the excavation generates settlements and lateral deformations in the retained soil. Therefore, one of the main potential causes of damage to surrounding structures is the movement of the diaphragm wall into the excavation. This damage is primarily related to the differential settlement and lateral strain between structural supports (Boscardin, 1989). A system of instruments that included vibrating wire piezometers, magnetic extensometers, vertical inclinometers, groundwater observation wells, and settlement points was implemented in order to monitor the movements and provide advance warning of any potential failures.The instrumentation plan is shown in Figure 2-4.

The vibrating wire piezometers are used to determine changes in pore pressure within the clay layer and can reflect changes in groundwater pressure due to overburden release, pumping, or inflows into the excavation. This information is essential for calculating changes in the effective stress within the clay (and hence, estimating soil settlement).

The magnetic extensometers consist of magnets positioned at various depths in a borehole pipe. A probe passing through the pipe detects the adjacent magnets and its location is recorded. The distribution of vertical deformations can be measured within the soil column by recording these locations over time.

The vertical inclinometers are tubes that are located vertically within the diaphragm wall. The bottom of these pipes is fixed in the bedrock. Lateral deformations are measured by integrating tilt measurements from a torpedo probe pulled through the tube. The inclinometers are marked on all drawings as SC-x, where "x" is the number of the inclinometer.

The settlement points consist primarily of metal screws that are fixed to buildings or sidewalks. They are then optically surveyed to measure whether or not a building or the ground surface are moving. The measured data is logged over the full period of construction and beyond.

To sum up, a total of 11 inclinometers, 12 piezometers, 2 observational wells, 5 borehole extensometers, and between 100 and 150 settlement points were installed and monitored. These data are presented, analyzed and compared with the three dimensional finite element analysis results in Chapter 4.

Table 2-1: Summary of construction activities with corresponding dates

Construction activities			
Description	**Start Date**	**End Date**	**Duration**
Diaphragm Wall installation	July, 2000	November, 2000	~150 days
First Level of West Tiebacks	12/05/00	12/27/00	22 days
First Level of South-West Bracing	12/06/00	12/13/00	7 days
First Level of South Tiebacks	12/21/00	01/05/01	15 days
First Level of South-East Bracing	12/18/00	01/05/01	18 days
First Level of East Tiebacks	01/02/01	01/09/01	7 days
First Level of North-West Bracing	01/08/01	01/17/01	9 days
Second Level of West Tiebacks	01/02/01	01/18/01	16 days
Second Level of South Tiebacks	01/12/01	01/23/01	11 days
Second Level of East Tiebacks	01/23/01	02/01/01	9 days
Second Level of South-West Bracing	01/22/01	01/29/01	7 days
Third Level of West Tiebacks	01/29/01	02/09/01	11 days
Third Level of South Tiebacks	02/02/01	02/20/01	18 days
Second Level of South-East Bracing	02/02/01	02/16/01	14 days
Third Level of East Tiebacks	02/21/01	03/26/01	33 days
First Level of North-East Bracing	03/06/01	03/14/01	8 days
Second Level of North-West Bracing	04/25/01	05/01/01	6 days
Foundation slab at the center	03/03/01	04/25/01	53 days
First Level of Raker support	04/06/01	05/15/01	39 days
Second Level of Raker support	05/09/01	06/01/01	23 days
Second Level of North-East Bracing	05/30/01	06/06/01	7 days
Excavation process	11/14/00	06/19/01	~217 day

Table 2-2: Details for the tiebacks at the MIT Stata Center (adapted from Olsen, 2001)

Wall	Tiebacks	Number of Tiebacks	Design Load (kips)	Prestressing Load (kips)	Installed Angle (deg)	Free Length (ft)	Bond Length (ft)
South	S1-1 to S1-45	45	112	112	20	50	40
	S2-1 to S2-45	45	128	128	20	20	50
	S3-1 to S3-45	45	128	128	20	10	50
East	E1-1 to E1-25	25	112	112	20	50	40
	E2-1 to E2-25	25	128	128	20	20	50
	E3-1 to E3-25	25	128	128	20	10	50
West	W1-1 to W1-26	26	112	112	20	50	40
	W2-1 to W2-26	26	128	128	20	20	50
	W3-1 to w3-27	27	128	128	20	10	50

Table 2-3: Details for Corner Bracing at the MIT Stata Center (after Olsen, 2001)

Strut	Elevation (ft-CCB)	Length (ft)	Unbraced Length (ft)	Design Load (normal to the wall) (kips/ft)	Tributary Length (ft)	Angle B/N Strut and Wall (degrees)	Strut Size		Design Load (kips)	Jacking Load (kips)
							Diameter (in)	Wall Thickness (in)		
NW1-1	10	8.6	8.6	26	16.25	40.39	W14X90		555	0
NW1-2	10	40.8	40.8	26	24.25	40.4	36	0.38	828	414
NW1-3	10	76.6	38.3	26	24.25	40.4	36	0.38	828	414
NW1-4	10	114.7	57.4	26	25	40.4	36	0.38	853	427
NW2-1	-10	8.6	8.6	44	16.25	40.39	W14X120		939	0
NW2-2	-10	40.8	40.8	44	24.25	40.4	36	0.519	1401	700
NW2-3	-10	76.6	38.3	44	24.25	40.4	36	0.519	1401	700
NW2-4	-10	114.7	57.4	44	25	40.4	36	0.63	1444	722
SW1-1	10	7.8	7.8	26	16.25	45	W14X90		598	0
SW1-2	10	37.8	37.8	26	23.25	45	36	0.38	855	427
SW1-3	10	73.2	73.2	26	14.25	45	36	0.38	524	262
SW2-1	-10	7.8	7.8	44	16.25	45	W14X132		1011	0
SW2-2	-10	37.8	37.8	44	23.25	45	36	0.519	1447	723
SW2-3	-10	73.2	73.2	44	14.25	45	36	0.519	887	443
NE1-1	10	7.8	7.8	26	16.25	45	W14X90		598	0
NE1-2	10	37.8	37.8	26	25	45	36	0.38	919	460
NE1-3	10	73.2	36.6	26	25	45	36	0.38	919	460
NE1-4	10	108.5	54.3	26	25	45	36	0.38	919	460
NE2-1	-10	7.8	7.8	44	16.25	45	W14X132		1011	0
NE2-2	-10	37.8	37.8	44	25	45	36	0.519	1556	778
NE2-3	-10	73.2	36.6	44	25	45	36	0.519	1556	778
NE2-4	-10	108.5	54.3	44	25	45	36	0.63	1556	778
SE1-1	10	7.8	7.8	26	10.84	45	W14X90		398	0
SE1-2	10	20.2	20.2	26	19.59	48.09	36	0.38	720	360
SE1-3	10	55.5	55.5	26	25	46.32	36	0.38	919	460
SE1-4	10	90.9	45.5	26	23.25	45.84	36	0.38	855	427
SE1-5	10	121.3	60.7	26	14.25	45.95	36	0.38	524	262
SE2-1	-10	7.8	7.8	44	10.84	45	W14X90		674	0
SE2-2	-10	20.2	20.2	44	19.59	48.09	36	0.393	1219	609
SE2-3	-10	55.5	55.5	44	25	46.32	36	0.63	1556	778
SE2-4	-10	90.9	45.5	44	23.25	45.84	36	0.519	1447	723
SE2-5	-10	121.3	60.7	44	14.25	45.95	36	0.393	887	443

*NOTE: This is the location of the strut described, with NW1-1 meaning Northwest corner level one nearest brace to the corner.

Table 2-4: Details for Raker Supports at the MIT Stata Center (after Olsen, 2001)

Raker*	Elevation (@north wall) (ft-CCB)	Overall Length (ft)	Unbraced Length (ft)	Design Load (normal to the wall) (kips/ft)	Tributary Length (ft)	Angle B/N Raker and Wall (vertical) (degrees)	Angle B/N Raker and Wall (horizontal) (degrees)	Strut Size		Design Load (kips)	Jacking Load (kips)
								Diameter (in)	Wall Thickness (in)		
N1-1	10	88.6	88.6	26	25	16.61	91.53	36	0.519	678	339
N1-2	10	88.7	88.7	26	23.5	16.61	87.18	36	0.519	638	319
N1-3	10	89.5	89.5	26	23.5	16.61	81.61	36	0.519	644	322
N1-4	10	89	89	26	24	16.61	84.54	36	0.519	652	326
N1-5	10	88.6	88.6	26	24	16.61	91.53	36	0.519	650	325
N1-6	10	88.6	88.6	26	25	16.61	91.53	36	0.519	678	339
N1-7	10	88.6	88.6	26	25	16.61	91.53	36	0.519	678	339
N1-8	10	89.3	89.3	26	25	16.61	97.14	36	0.519	683	341
N2-1	-10	85.2	85.2	44	25	3.6	91.53	36	0.803	1103	551
N2-2	-10	85.6	85.6	44	23.5	3.6	84.18	36	0.803	1041	521
N2-3	-10	86.9	86.9	44	23.5	3.6	78.65	36	0.803	1057	528
N2-4	-10	86.2	86.2	44	24	3.6	81.06	36	0.803	1070	535
N2-5	-10	85.2	85.2	44	24	3.6	91.53	36	0.803	4057	529
N2-6	-10	85.2	85.2	44	25	3.6	91.53	36	0.803	1103	551
N2-7	-10	85.2	85.2	44	25	3.6	91.53	36	0.803	1103	551
N2-8	-10	85.4	85.4	44	25	3.6	94.14	36	0.803	1105	553

*NOTE: Raker Name is given as first: location, second: level, third: number from west to east(ie. N1-1 means North raker level one farthest west)

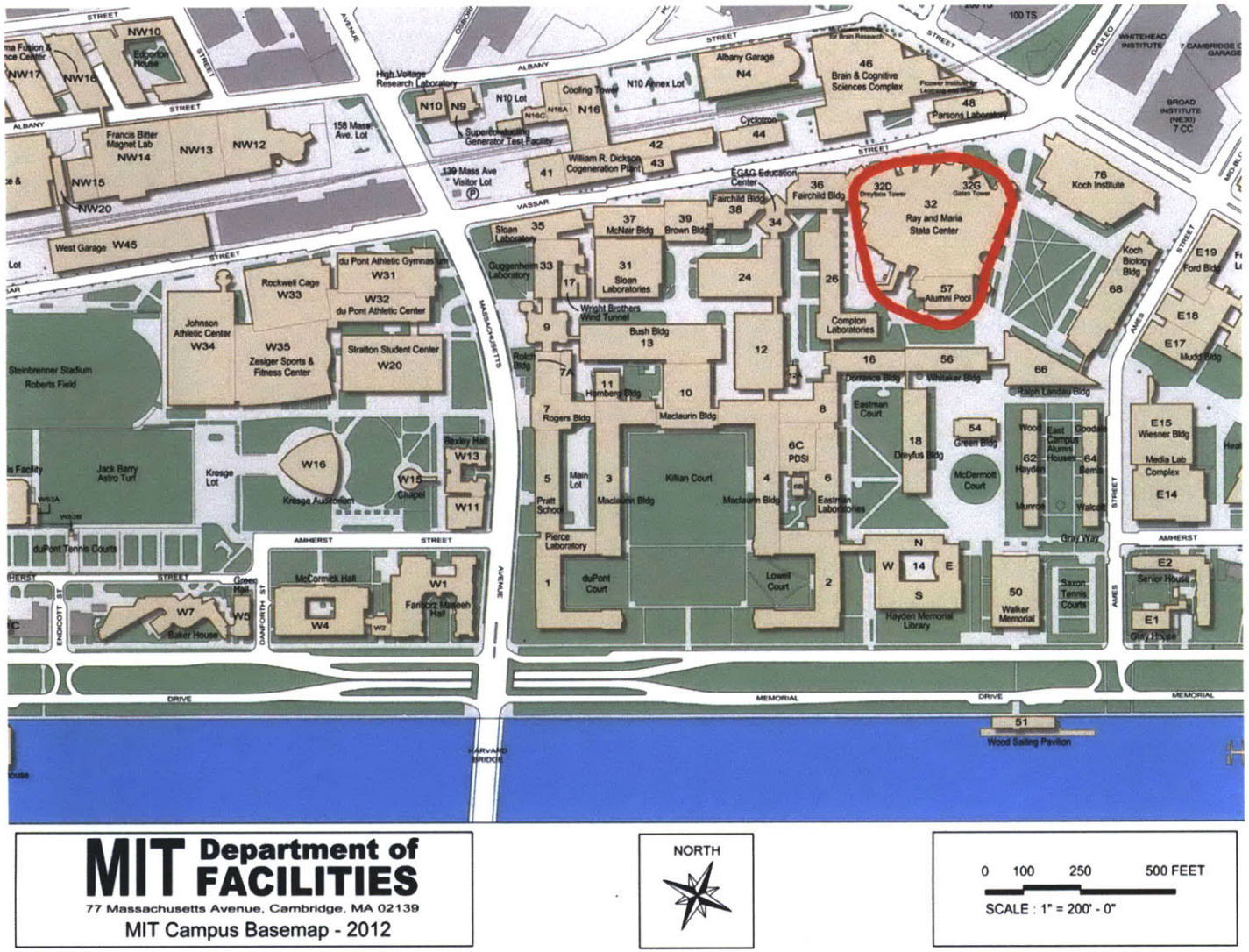

Figure 2-1: Map of MIT Campus showing the location of the Stata Center

Figure 2-2: View of MIT Stata Center building (photo courtesy Philip Greenspun)

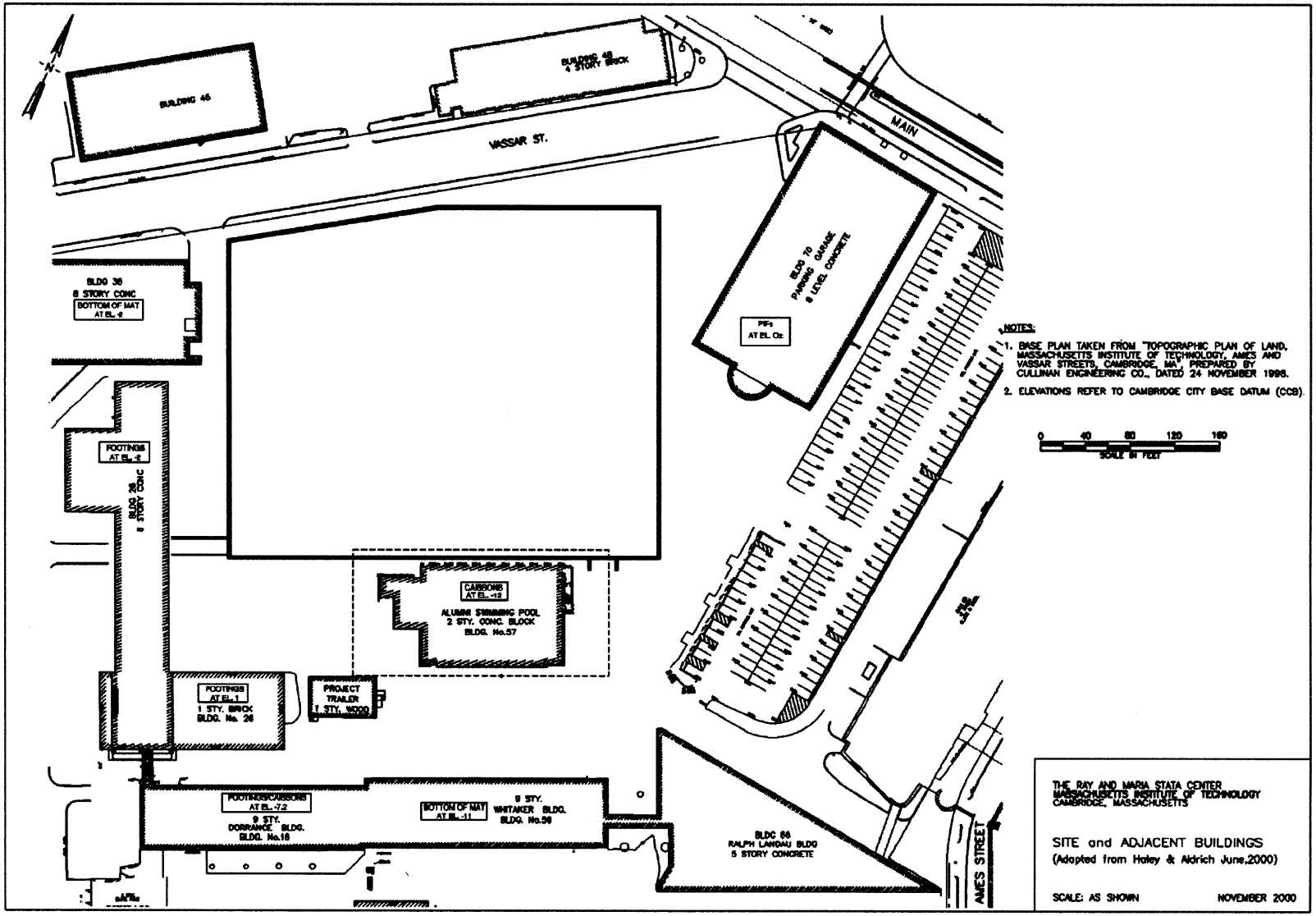

Figure 2-3: Project Plan and Adjacent Buildings Location

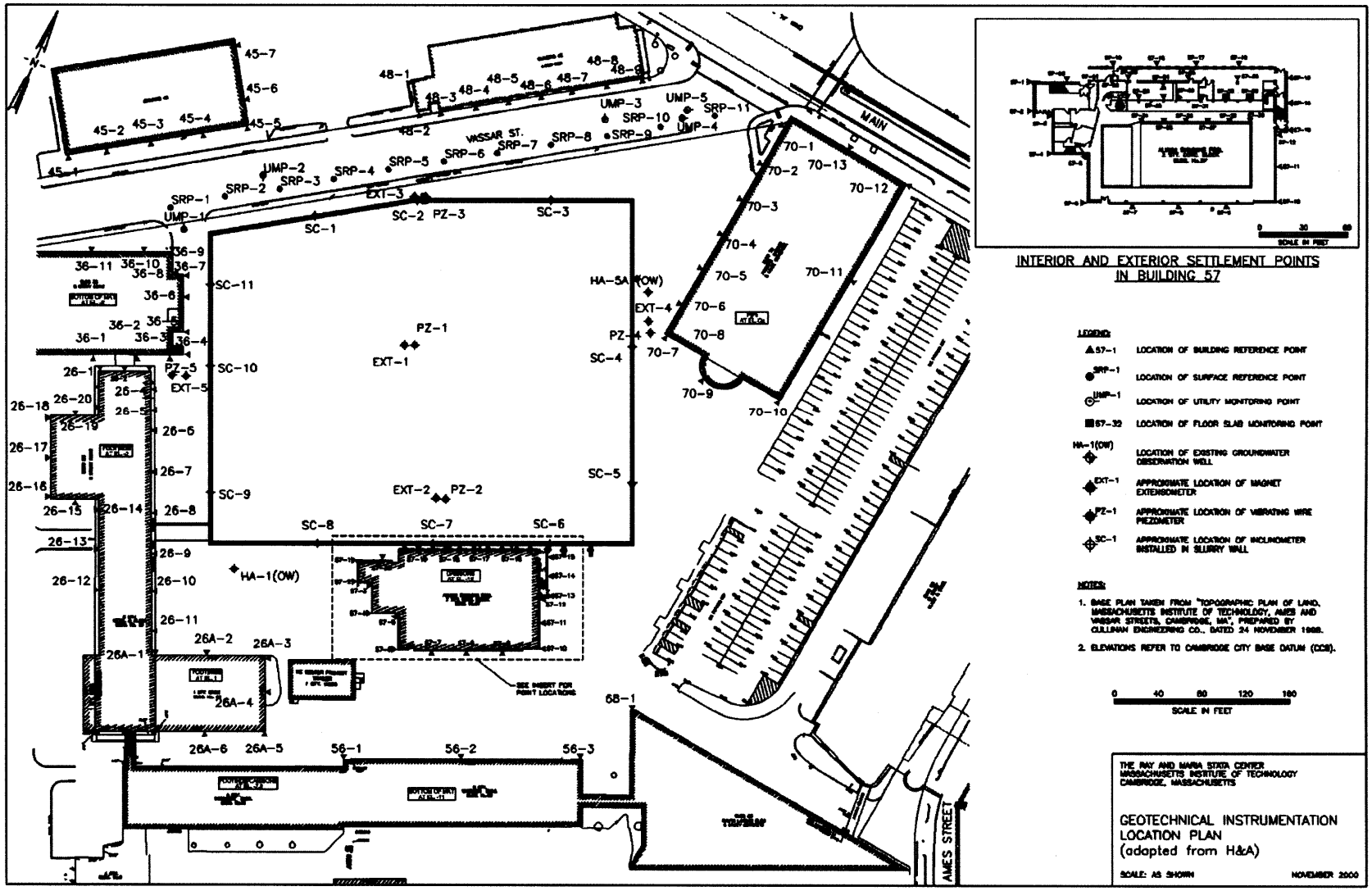

Figure 2-4: Geotechnical Instrumentation Location Plan

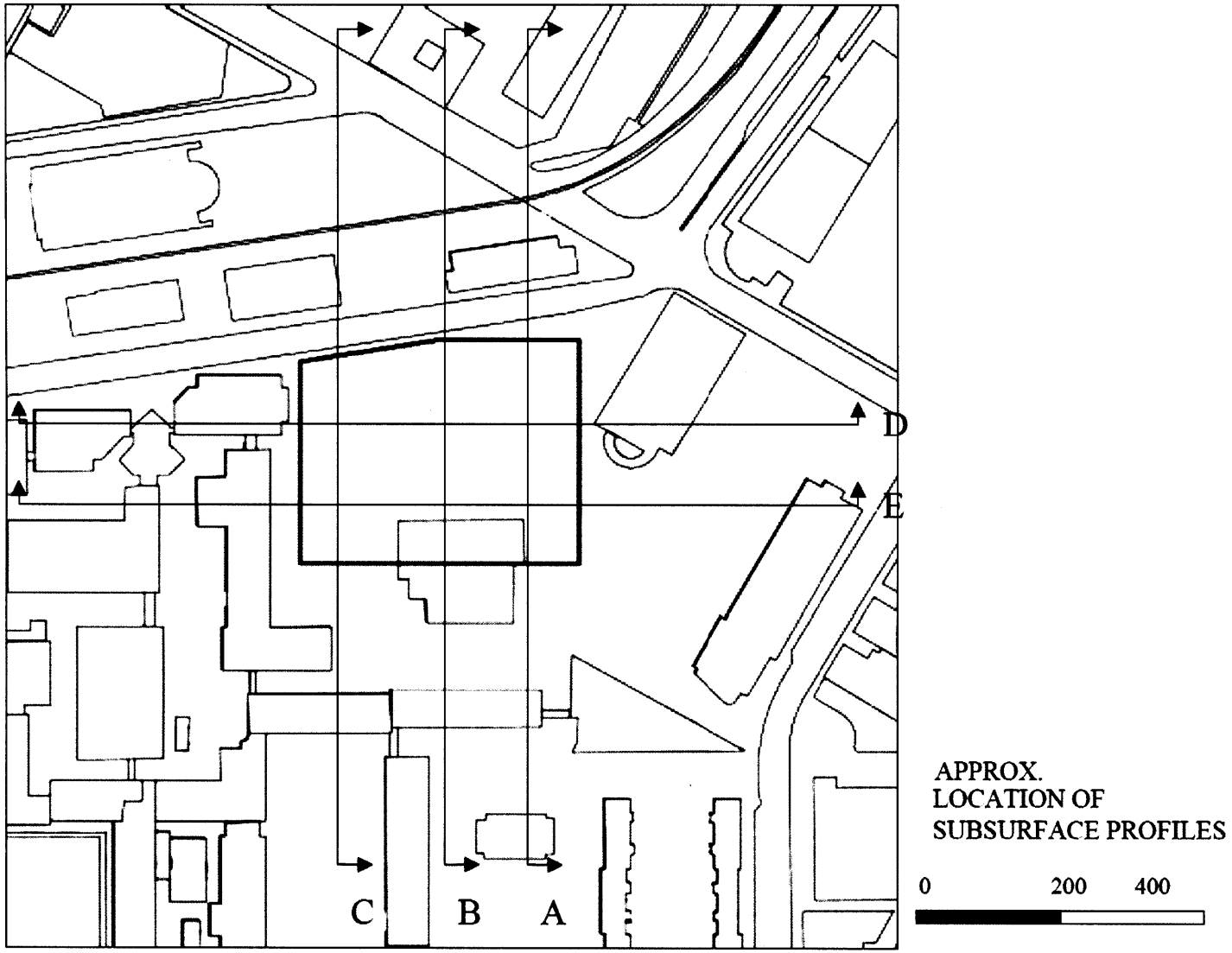

Figure 2-5: Subsurface Profiles Plan

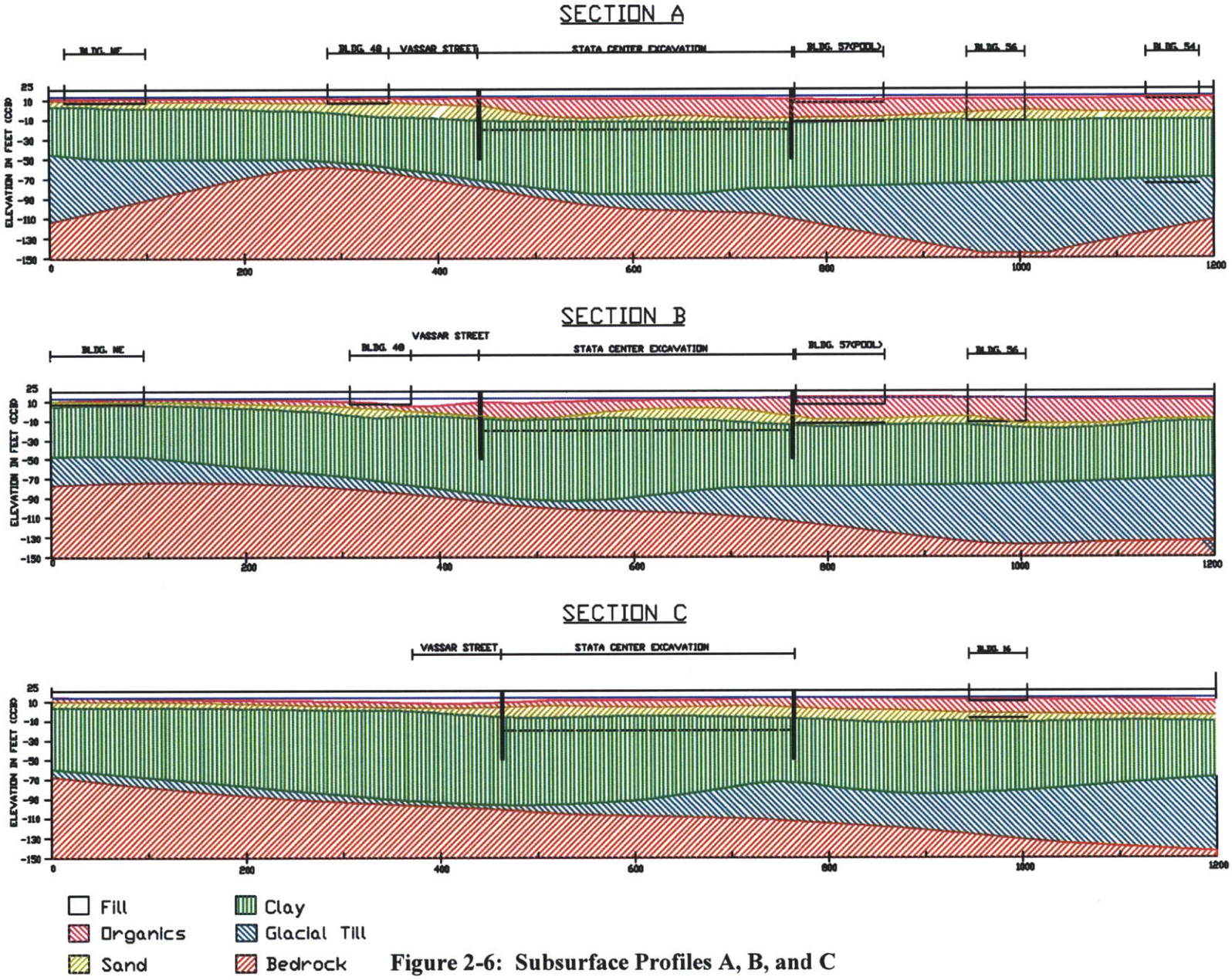

Figure 2-6: Subsurface Profiles A, B, and C

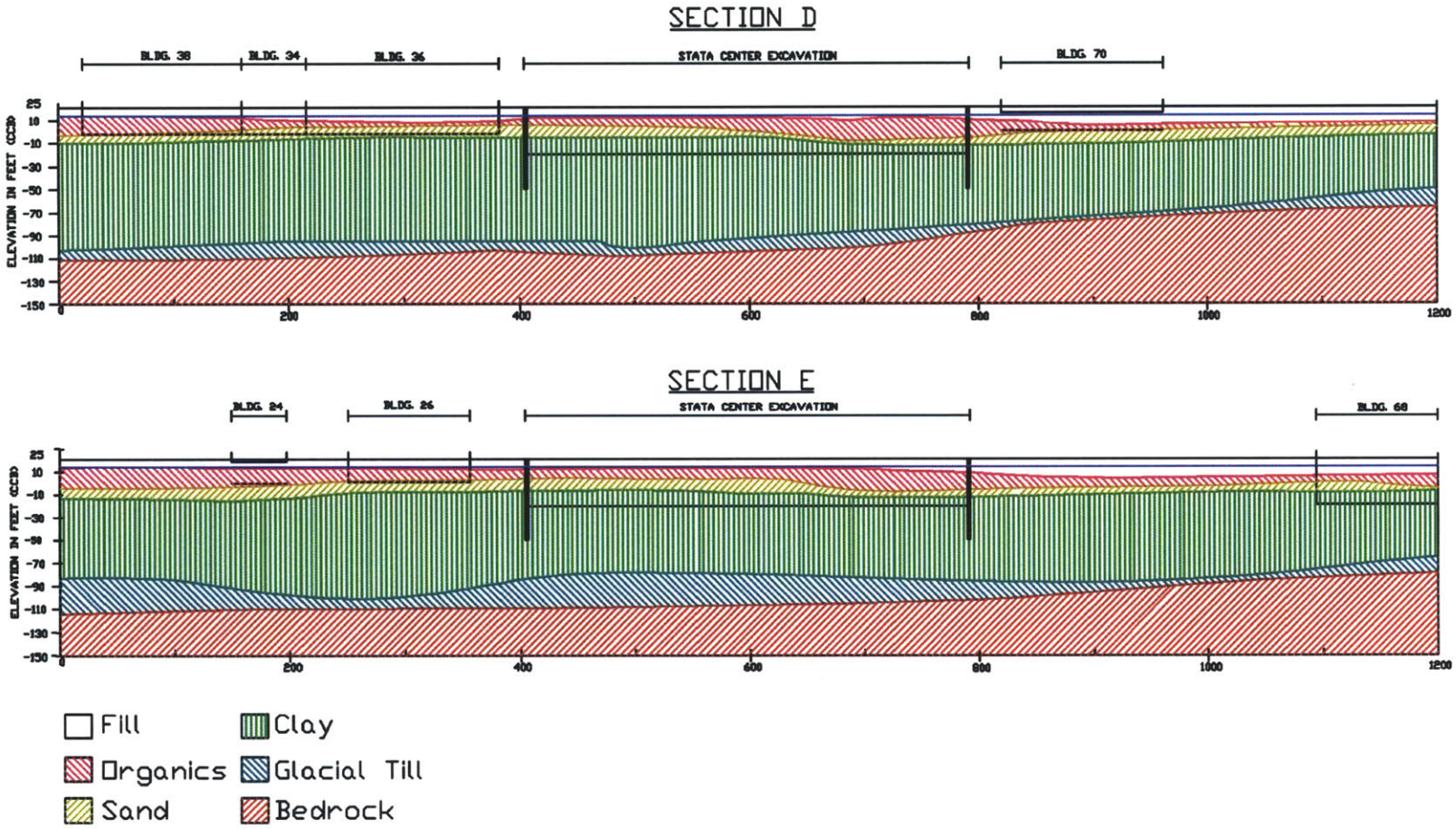

Figure 2-7: Subsurface Profiles D and E

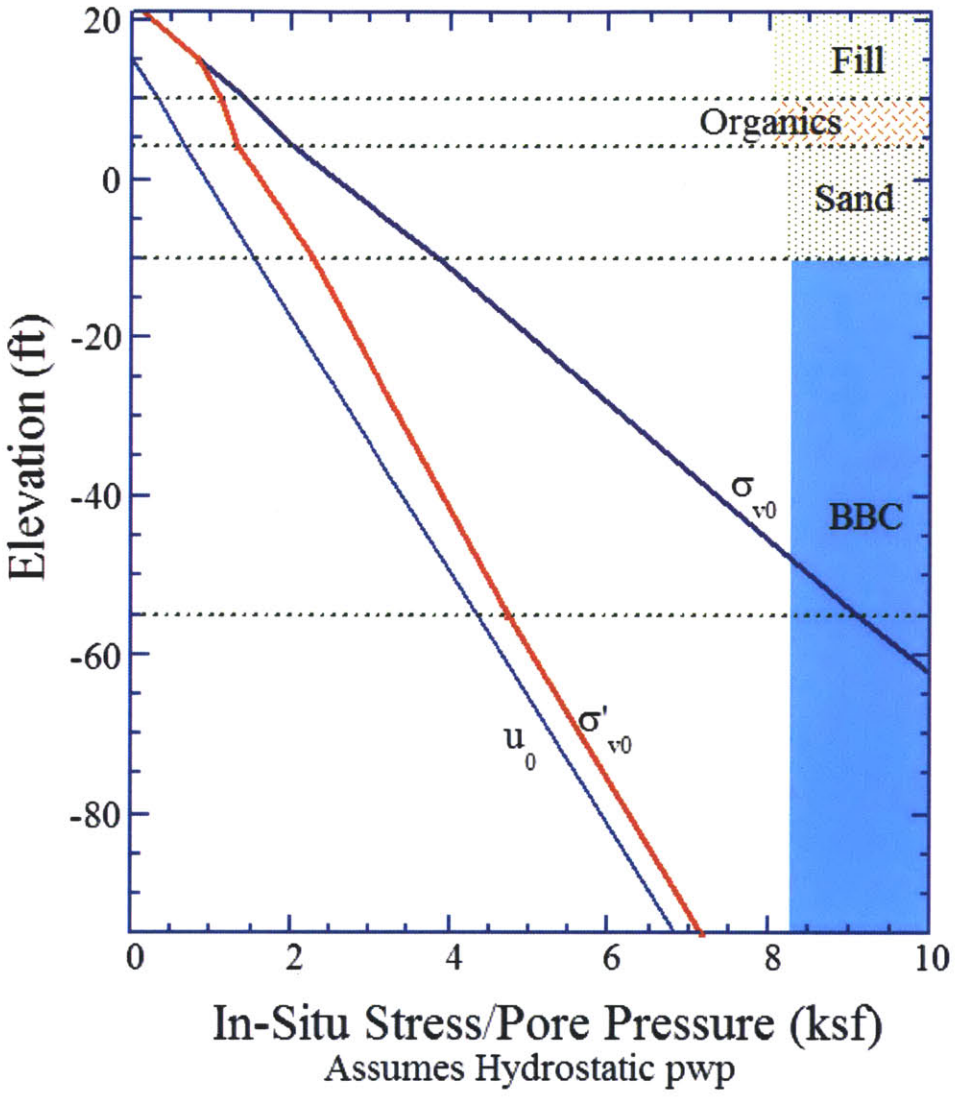

Figure 2-8: In-Site Stress and Pore Pressure vs. Elevation

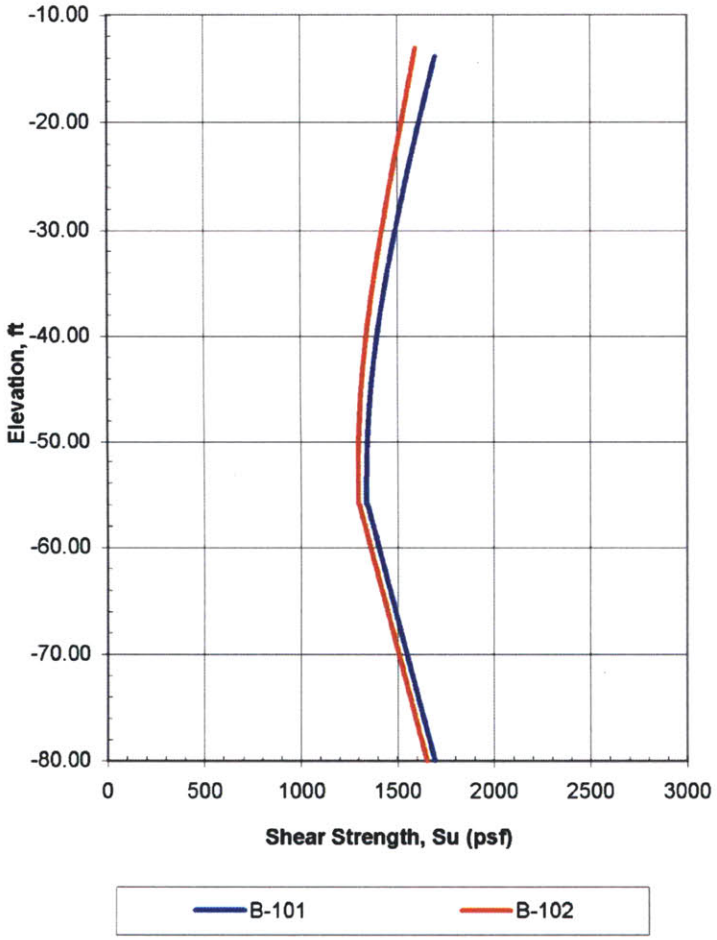

Profile computed using SHANSEP technique

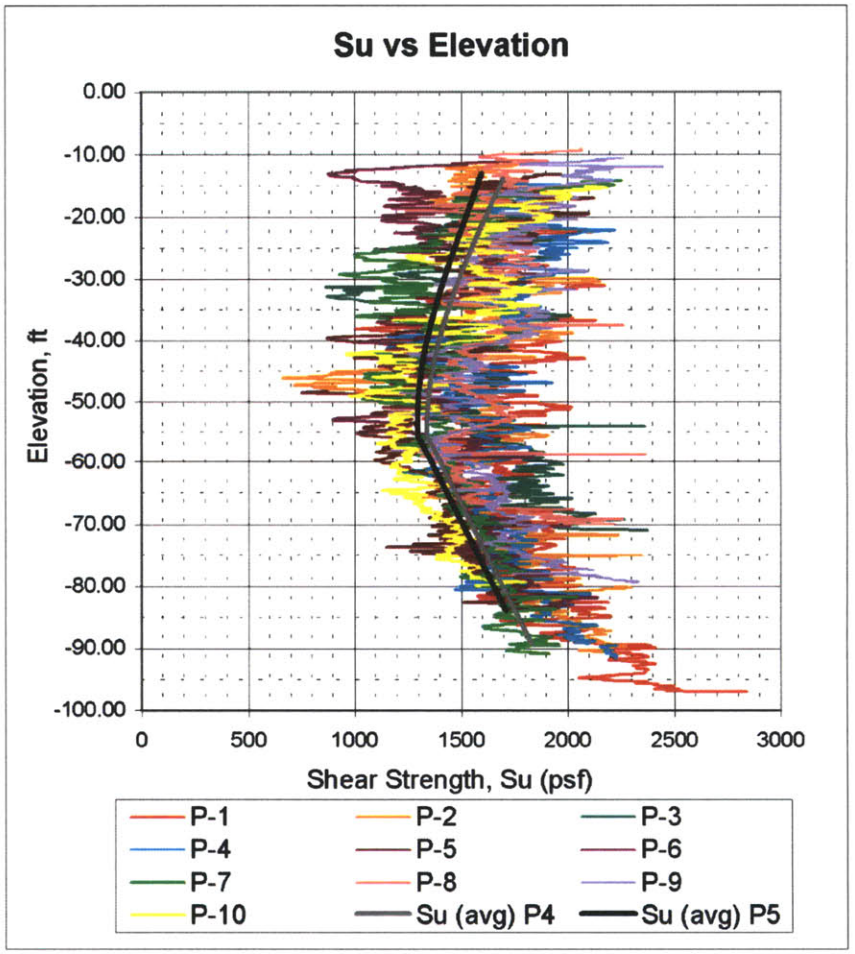

Combined data from Cone Penetration Tests P1 to P10

Figure 2-9: Undrained Shear Strength Profile (after Olsen, 2001)

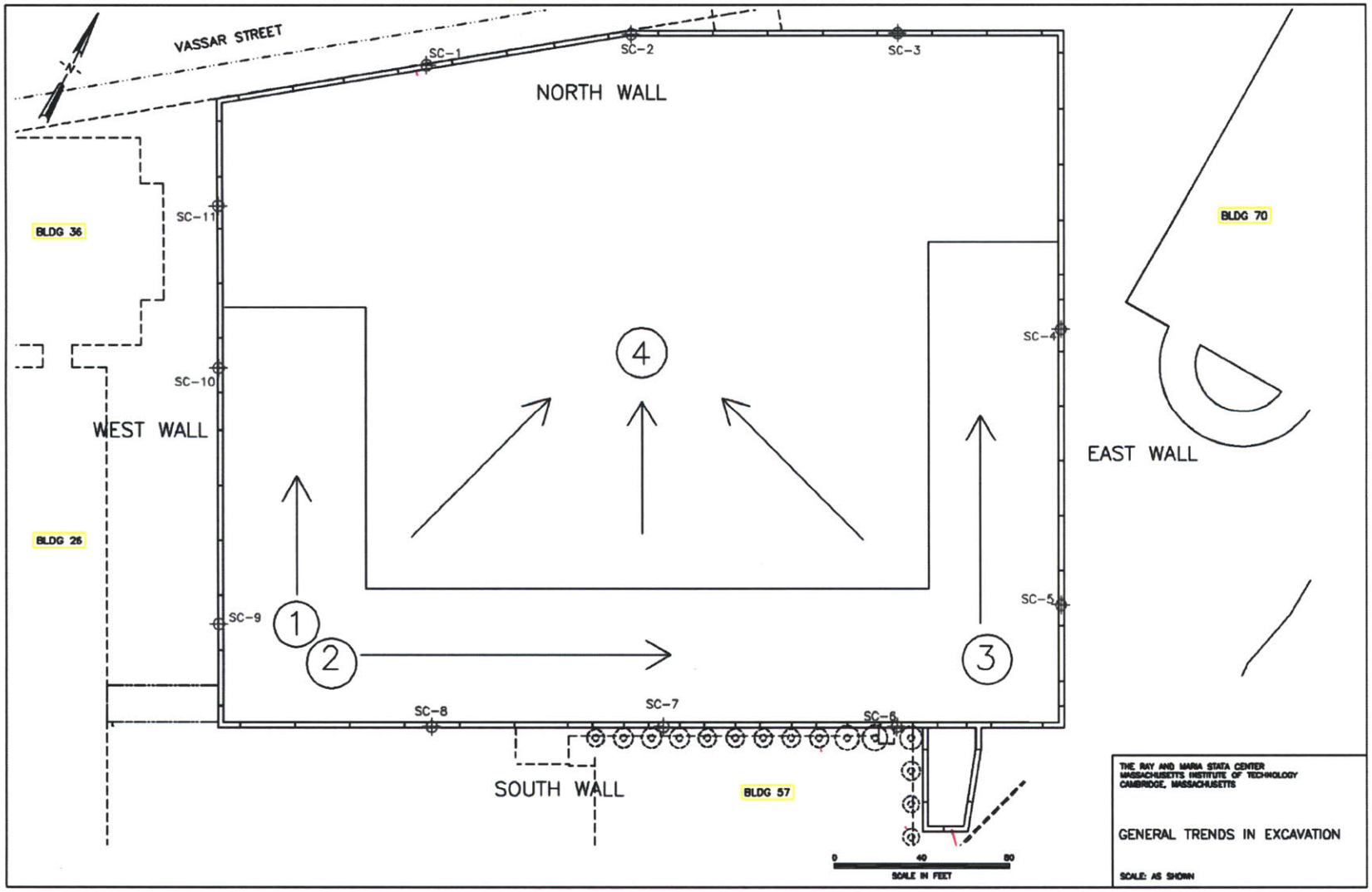

Figure 2-10: General Trends in Excavation

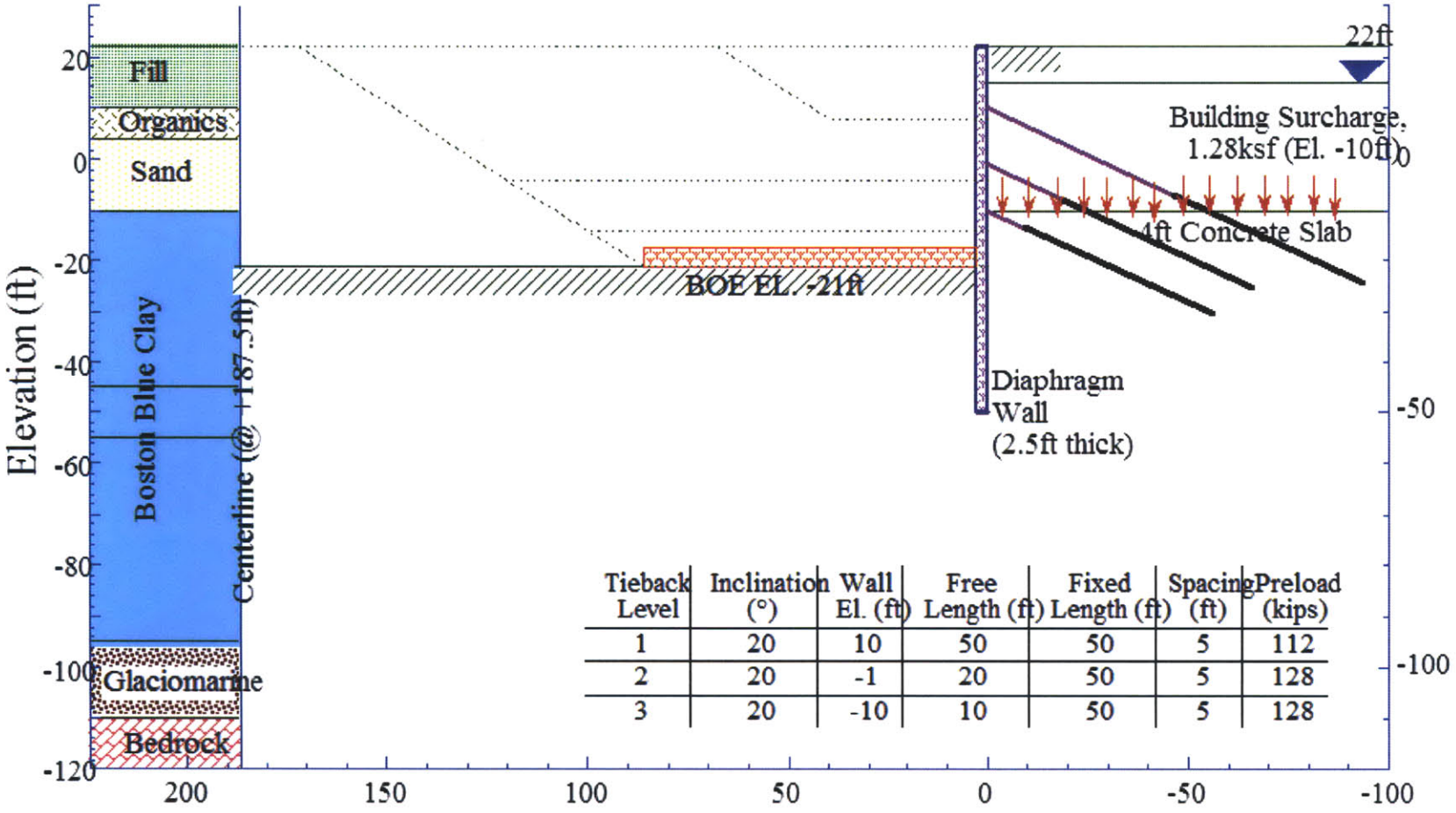

Tieback Level	Inclination (°)	Wall El. (ft)	Free Length (ft)	Fixed Length (ft)	Spacing (ft)	Preload (kips)
1	20	10	50	50	5	112
2	20	-1	20	50	5	128
3	20	-10	10	50	5	128

Figure 2-11: Typical Cross-Section of Tiebacks and Excavation (after Whittle, 2002)

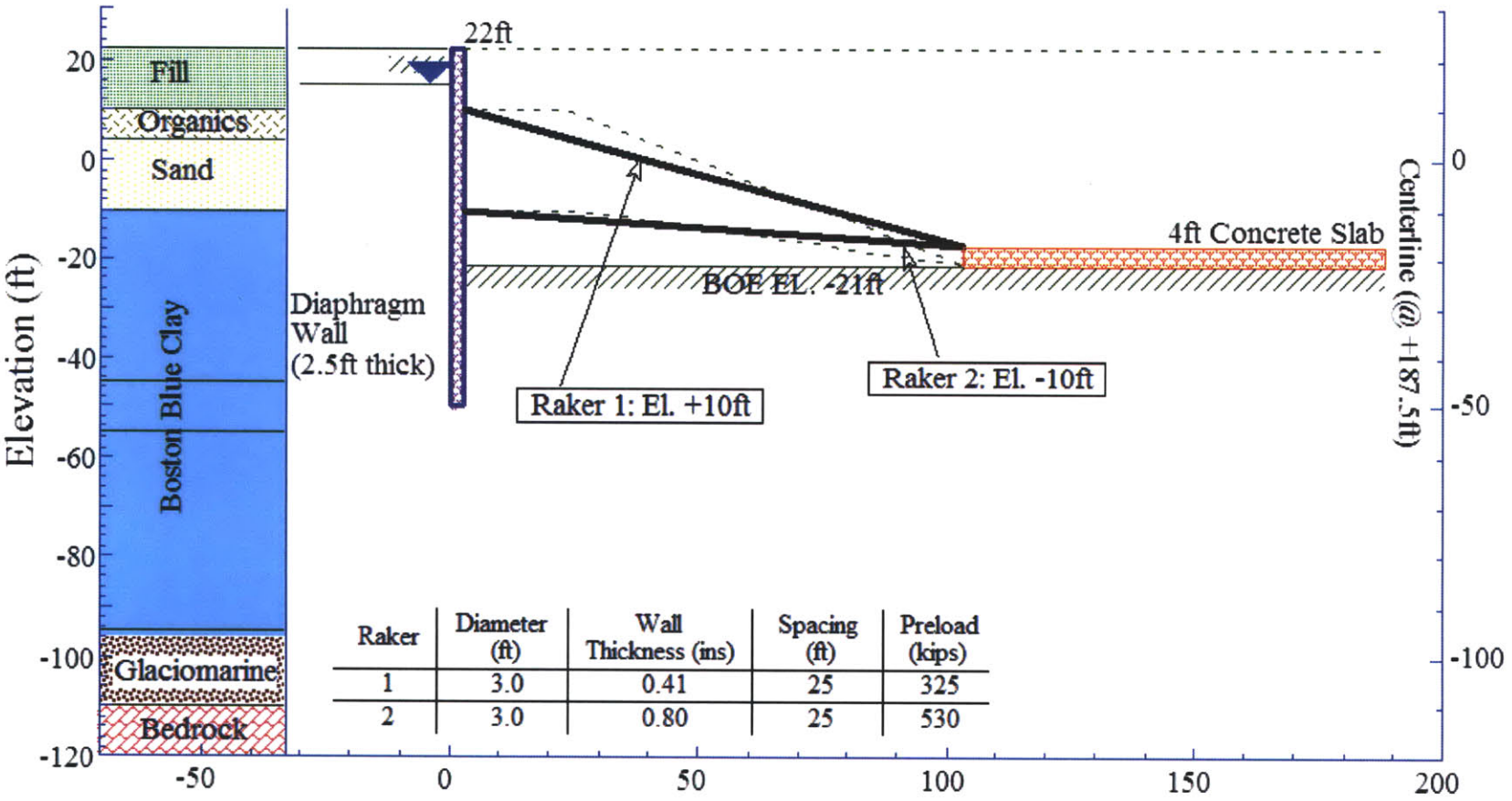

Figure 2-12: Typical Cross-Section of Rakers and Excavation (after Whittle, 2002)

3 THREE-DIMENSIONAL FINITE ELEMENT MODEL

3.1 Base Case Model Assumptions

3.1.1 Model Description

Comprehensive finite element analyses of soil-structure interaction offer a complete framework for interpreting the spatial and temporal behavior for complex excavation support systems (such as the Stata Center basement). These methods are based on calculation algorithms that solve the systems of partial differential equations and are functions of multiple variables such as stresses, strains, and constitutive model parameters (Potts et al., 2002). The Finite Element Method (FEM) is a technique to find the solution to these systems of equations taking into account a given geometry. The variables are combined into matrices and equilibrium is satisfied by the systems of equations using numerical procedures using a computer program. The Plaxis 3D 2011 program, a commercial special purpose finite element code, is used to build the three-dimensional model and perform the analysis for this project.

The excavation for the Stata Center has a complex geometry and variety of structural support systems which makes the project challenging to model (Figure 3-1). However, the uniqueness of this project is that the excavation process was very well documented - it was constantly photographed, monitored, and described in daily field logs, as well as recorded on webcams located around the construction site. Using these data, it is possible to create a precise three-dimensional numerical model of the actual excavation with respect to the time frame of construction sequence.

All available data were gathered and carefully analyzed. The information obtained from the project drawings (dimensions, structural elements location and coordinates) was used to create the initial model in a CAD (Computer-Aided Design) program, AutoDesk AutoCAD 2012 Educational Version. Figure 3-2 illustrates the CAD model of the support system in the actual scale. Using the exact dimensions, the full three-dimensional model of the diaphragm wall with associated support system was created in Plaxis 3D 2011.

The south-west corner was selected as a reference point, so the outer horizontal boundaries of the geometry model were X_{min}=-500 ft, X_{max}=881 ft, Y_{min}=-500 ft, Y_{max}=811 ft. The equal distance of 500 ft was measured from the each side of the diaphragm wall to the model boundaries. It has been verified by trial analyses that this distance was "far enough" and the model boundaries did not influence the results.

3.1.2 Soil Profile

The ground surface is approximately level at El. +21 ft, and the groundwater table is in the overlying fill at the depth of 6 ft. The soil profile of the model consists of 11 ft of fill, 6 ft of organics, 14 ft of sand, 85 ft of marine clay, and 15 ft of glacial till. The marine clay (Boston Blue Clay) is sub-divided into an upper overconsolidated clay crust and a lower normally consolidated unit. The clay has low hydraulic conductivity and is modeled as an Undrained Elastic-Plastic (EPP) material with the undrained shear strength profile which decreases from 1,600 psf to 1,300 psf at El. -55 ft, and then increases to a maximum of 1,900 psf at the bottom of the stratum. The other layers are also represented by the EPP (Mohr-Coulomb) model.

The EPP (linear elastic perfectly-plastic) Mohr-Coulomb constitutive model requires two stiffness and three strength parameters.

The stiffness parameters of the Mohr-Coulomb model are (based on soil sample tests):

- E' - Effective Young's modulus, kip/ft^2
- ν - Effective Poisson's ratio

The alternative stiffness parameters are (influences by E' and ν):

- G - Shear modulus, kip/ft^2

$$G = \frac{E'}{2(1+\nu)} \tag{3-1}$$

- E_{oed} - Oedometer modulus, kip/ft^2

$$E_{oed} = \frac{E'(1-\nu)}{(1+\nu)(1-2\nu)} \tag{3-2}$$

Stiffness varying with depth is defined by a value of E_{inc} which is the increment of stiffness per unit of depth. The stiffness is equal to E' for any z-coordinate above z_{ref}. For any z-coordinate below z_{ref} the stiffness is given by ($z < z_{ref}$):

$$E'(z) = E' + (z_{ref} - z)E_{inc} \tag{3-3}$$

The strength parameters of the Mohr-Coulomb model are (based on soil sample tests):

- Su - Undrained Shear Strength, kip/ft^2
- φ - Effective friction angle, °
- ψ - Dilatancy angle, °

Plaxis 3D 2011 also offers an advanced option for the input of clay layers in which the undrained shear strength, Su, changes with depth. In order to account for the increase/decrease of the undrained shear strength with depth the Su_{inc} value is used, which is Su per unit of depth

(expressed in the unit of stress per unit depth). For any z-coordinate below z_{ref} the stiffness is given by ($z < z_{ref}$):

$$Su(z) = Su + (z_{ref} - z)Su_{inc} \quad (3\text{-}4)$$

Table 3-1 summarizes the model parameters used to represent the soil profile based on the subsurface exploration program.

3.1.3 Groundwater Conditions

Since the site surface is assumed to be mainly horizontal, the stresses initialization is performed using Plaxis "K_0 procedure" with all soil clusters activated. The boundary conditions used in the model are the Plaxis standard boundary conditions with fixity in the horizontal plane at the basal boundary and zero prescribed lateral displacements along the corresponding axes at the borders. The hydraulic conditions include head-based groundwater flow boundary conditions (head = 15ft) at the bottom and the sides of the model. The groundwater table is specified at the elevation of 15 ft. The specific "water levels" inside the watertight diaphragm wall are introduced for each level of excavation to model the excavation dewatering. The current analysis assumes the steady-state groundwater seepage and uses groundwater flow calculation mode for each phase of the model.

3.1.4 Support Systems

The diaphragm wall panels and mat foundation were modeled as plate elements; rakers and corner bracers were represented as prestressed node-to-node anchors. The free lengths of tiebacks were modeled using node-to-node anchors, and the embedded pile elements represented

the grouted part. The input parameters for all structural elements and prestress values can be found in Tables 3-1 to 3-4.

3.1.4.1 Diaphragm Wall and Foundation Properties

The diaphragm wall is represented by three-dimensional elastic plate elements. The toe of the diaphragm wall does not extend into the underlying rock; therefore, it is free to move within the soil mass. The wall is 2.5 ft thick and consists of reinforced concrete. The mat foundation consists of a reinforced concrete slab that is 4.0 ft thick and is also modeled by the plate element.

Table 3-1 summarizes the input parameters for diaphragm wall and foundation represented as Plaxis plate elements.

3.1.4.2 Corner Bracers Properties

The corner bracing consists of 36 in diameter steel pipe struts installed at El. 10 ft and El. –10 ft. These were pre-loaded by jacking them in place at 50% of their design load. The details for each struts can be found in Table 2-3, including design loads, jacking loads, strut sizes, and angle formed between the braces and the wall. Figure 3-2 also illustrates the location of each corner bracing strut.

The wall thickness of the first level steel pipe struts is 0.38 in. The properties of the first level corner bracing support are estimated in the following way:

$$A_s = \frac{\pi}{4}(D^2 - (D^2 - 2t)^2) = 42.523 \text{ in}^2 = 0.295 \text{ ft}^2 \quad (3\text{-}5)$$

where:

A_s - cross-sectional area, in^2

D - diameter, in

t - wall thickness, in

$$E_s = 29\,000 \text{ ksi} = 4.176 \cdot 10^6 \text{ ksf} \quad (3\text{-}6)$$

$$EA = E_s A_s = 1.232 \cdot 10^6 \text{ kip} \quad (3\text{-}7)$$

where:

EA - axial stiffness, per anchor in the unit of force, kip

E_s - Young's modulus of steel, ksf

A_s - cross-sectional area, ft^2

The wall thickness of the second level steel pipe struts is 0.63 in. The properties of the second level corner bracing support are estimated in the following way:

$$A_s = \frac{\pi}{4}(D^2 - (D^2 - 2t)^2) = 70 \text{ in}^2 = 0.486 \text{ ft}^2 \quad (3\text{-}8)$$

where:

A_s - cross-sectional area, in^2

D - diameter, in

t - wall thickness, in

$$E_s = 29\,000 \text{ ksi} = 4.176 \cdot 10^6 \text{ ksf} \quad (3\text{-}9)$$

$$EA = E_s A_s = 2.030 \cdot 10^6 \text{ kip} \quad (3\text{-}10)$$

where:

EA - axial stiffness, per anchor in the unit of force, kip

E_s - Young's modulus of steel, ksf

A_s - cross-sectional area, ft^2

These input parameters for the corner bracing support which is represented as node-to-node anchors and their prestress values can be found in Table 3-2.

3.1.4.3 Rakers Properties

Each raker comprises a 36 in diameter steel pipe strut that supports the wall (at El. 10 ft and El. −10 ft) and is inclined downward to a kicker block cast into the foundation slab. All

rakers were pre-loaded to 50% of their design load. The details for raker support can be found in Table 2-4 and the locations for their installation is shown in Figures 2-1 and 2-2.

The properties of the first level raker support are estimated in the following way:

$$A_s = 0.32 \text{ ft}^2 \tag{3-11}$$

$$E_s = 30\,000 \text{ ksi} = 4.320 \cdot 10^6 \text{ ksf} \tag{3-12}$$

$$EA = E_s A_s = 1.382 \cdot 10^6 \text{ kip} \tag{3-13}$$

where:

EA - axial stiffness, per anchor in the unit of force, kip

E_s - Young's modulus of steel, ksf

A_s - cross-sectional area, ft^2

The properties of the second level raker support are estimated in the following way:

$$A_s = 0.63 \text{ ft}^2 \tag{3-14}$$

$$E_s = 30\,000 \text{ ksi} = 4.320 \cdot 10^6 \text{ ksf} \tag{3-15}$$

$$EA = E_s A_s = 2.722 \cdot 10^6 \text{ kip} \tag{3-16}$$

where:

EA - axial stiffness, per anchor in the unit of force, kip

E_s - Young's modulus of steel, ksf

A_s - cross-sectional area, ft^2

These input parameters for the raker support which is represented as node-to-node anchors and their prestress values can be found in Table 3-2.

3.1.4.4 Tieback Properties

Each tieback consists of 4, 0.6 in. diameter high strength steel tendons (270 ksi). The free length is sheathed with a polyethylene tube material to preclude bonding in that portion. The

grouted anchors consist of Type I/II Portland Cement and water. The water to cement ratio of 0.49 by weight and a minimum 28 day compressive strength of 4,000 psi.

The properties of the tieback support are estimated in the following way:

$$A_s = 4\left(\frac{\pi D^2}{4}\right) = 7.85 \cdot 10^{-3} \text{ ft}^2 \quad (3\text{-}17)$$

where:

A_s - cross-sectional area, ft^2

D - diameter, ft

$$E_s = 29\,000 \text{ ksi} = 4.176 \cdot 10^6 \text{ ksf} \quad (3\text{-}18)$$

$$EA = E_s A_s = 32.78 \cdot 10^3 \text{ kip} \quad (3\text{-}19)$$

where:

EA - axial stiffness, per anchor in the unit of force, kip

E_s - Young's modulus of steel, ksf

A_s - cross-sectional area, ft^2

The grouted part of the tieback support is represented as an embedded pile element. In case of failure, the first element that fails is the steel tendon. Therefore, the total bearing capacity of the embedded pile is:

$$N_{\text{embedded pile}} = \frac{1}{2} L_{pile}(T_{top,max} + T_{bot,max}) = 800 \text{ kip} \quad (3\text{-}20)$$

where:

$N_{\text{embedded pile}}$ - bearing capacity of the embedded pile element, kip

L_{pile} - embedded pile element length, ksf

$T_{top,max}$ - the skin resistance at the pile top, in force per unit pile length, kip/ft

$T_{bot,max}$ - the skin resistance at the pile bottom, in force per unit pile length, kip/ft

These input parameters for the tieback support which is represented as node-to-node anchors and embedded pile elements, as well as their prestress values can be found in Tables 3-2 and 3-3.

3.2 Development of the Three Dimensional Model in Plaxis 3D

3.2.1 Excavation Sequence and Phases

Although many projects can be easily sub-divided into discrete phases, the construction schedule of the Stata Center basement involved a number of concurrent activities occurring at different parts of the site at any given time. For example, a period of time could include excavation work, tieback installation, and corner bracing installation happening simultaneously. It is not a trivial task to correlate this whole construction process into the distinct stages over selected time intervals in an FE model. The first Plaxis models for this project included up to 60 phases in an attempt to correlate the complex schedule with the available data. However, after a more detailed interpretation of the calendar plan, the base case model with only 35 staged construction phases was chosen. Table 3-4 summarizes the actual construction phases with the start and end dates of each field activity based on daily field reports, together with the selected phases for the current Plaxis 3D model. The full list of Plaxis 3D phases with the time frame is presented in Table 3-5, and the details for each phase are shown in Table 3-6.

3.2.2 Complex Geometry Design

In order to capture the three-dimensional effects of the soil and support system responses from a non-uniform excavation process, the complex soil volumes were imported to Plaxis 3D from a CAD program where these shapes were extruded based on the photographs and excavation plans. Figures 3-3 and 3-4 depict the example summaries of excavation modeling for the Phase #3 and #30 - the CAD models of the excavation progress based on the field data corresponding to the appropriate time frame and the Plaxis 3D input/output for the same phases are shown.

Figures 3-5 to 3-10 present the process of geometry design for the simple case. First, an empty cluster is established in the CAD program (AutoDesk AutoCAD 2012 Educational Version) based on the input coordinates. Next, the three-dimensional soil volume for the excavation phase using the field data is created. This soil volume cluster is then subtracted from the empty cluster using standard commands. The obtained volume element is converted into the CAD mesh using the mesh tessellation options presented in Figure 3-8 and subdivided into distinct elements using the "explode" command. Finally, the converted soil cluster is directly imported into the Plaxis 3D 2011 and used in the model (Figure 3-11).

Figures 3-12 to 3-16 present the process of geometry design for the complex case when there is a need to take into account the previous excavation volumes. Figure 3-14 shows placing the existing soil cluster for Phase #13 into the next cluster phase. Then, both volumes are subtracted from each other in order to get the differentiated excavation volume. Next, all soil cluster volumes are directly imported into Plaxis 3D 2011 after several intermediate conversion steps described previously.

A great number of soil shapes and excavation sequences were created during this project. Some of them required extremely complicated meshes with a very large number of elements. The base case model for the current purposes uses an optimal version of the soil volume cluster configuration that generated a fine mesh with the total of 111 886 elements and 173 787 nodes.

Table 3-1: Summary of Plaxis 3D Materials Properties - Soils

Identification	Units	Fill	Organics	Sand	Upper Clay	Lower Clay	Glaciomarine
Identification number	#	1	2	3	4	5	6
Soil Model		MC	MC	MC	MC	MC	MC
Drainage type		Drained	Undrained (B)	Drained	Undrained (B)	Undrained (B)	Drained
Color							
Top Elevation	ft	21	10	4	-10	-55	-95
γ	kip/ft^3	0.1200	0.1000	0.1300	0.1170	0.1230	0.1400
E	kip/ft^2	200.0	400.0	600.0	420.0	920.0	7500
ν (nu)		0.3000	0.3000	0.3000	0.3000	0.3000	0.3000
G	kip/ft^2	76.92	153.8	230.8	161.5	353.8	2885
E_{oed}	kip/ft^2	269.2	538.5	807.7	565.4	1238	10.10E3
Su_{ref}	kip/ft^2	0.000	1.000	0.000	1.650	1.300	0.000
φ (phi)	°	35.00	0.000	37.00	0.000	0.000	45.00
V_s	ft/s	143.6	222.4	238.9	210.7	304.1	813.9
V_p	ft/s	268.6	416.1	446.9	394.2	569.0	1523
E_{inc}	$kip/ft^2/ft$	0.000	0.000	0.000	11.11	12.00	0.000
z_{ref}	ft	21.00	10.00	4.000	-10.00	-55.00	-95.00
Su_{inc}	$kip/ft^2/ft$	0.000	0.000	0.000	-7.800E-3	0.01500	0.000
K_0		0.5000	0.6000	0.5000	0.8000	0.6000	1.000
k	ft/day	3.000	0.3000	0.3000	7.000E-3	0.3000E-3	0.03000

Table 3-2: Summary of Plaxis 3D Materials Properties - Node-to-node Anchors

Identification	Units	CornerBracing1	CornerBracing2	Rakers1	Rakers2	Tiebacks
Identification number	#	1	2	3	4	5
Color		■	■	■	■	■
EA	kip	1.232E6	2.030E6	1.382E6	2.722E6	32.78E3 (per 5 ft) 65.56E3 (per 10 ft)
Prestress values	kip	See Table 2-3	See Table 2-3	See Table 2-4	See Table 2-4	See Table 2-2

Table 3-3: Summary of Plaxis 3D Materials Properties - Plates

Identification	Units	DiaphragmWall	Foundation
Identification number	#	1	2
Color		■	■
d	ft	2.500	4.000
γ	kip/ft^3	0.1500	0.1500
Linear		Yes	Yes
E_1	kip/ft^2	471.0E3	471.0E3
E_2	kip/ft^2	471.0E3	471.0E3
ν_{12}		0.1500	0.1500
G_{12}	kip/ft^2	204.8E3	204.8E3
G_{13}	kip/ft^2	204.8E3	204.8E3
G_{23}	kip/ft^2	204.8E3	204.8E3

Table 3-4: Summary of Plaxis 3D Materials Properties - Embedded piles

Identification	Units	Grout
Identification number	#	1
Color		
E	kip/ft^2	1.670E6
γ	kip/ft^3	0.1500
Pile type		Predefined
Predefined pile type		Massive circular pile
Diameter	ft	1.640
A	ft^2	2.112
I_3	ft^4	0.3551
I_2	ft^4	0.3551
Skin resistance		Linear
$T_{top, max}$	kip/ft	20.00
$T_{bot, max}$	kip/ft	20.00

Table 3-5: Calendar plan

Actual Project phases				Calendar plan
Description	Start Date	End Date	Duration	November / December / January / February / March / April / May / June
Diaphragm Wall installation	July, 2000	November, 2000	~150 days	
First Level of West Tiebacks	12/05/00	12/27/00	22 days	
First Level of South-West Bracing	12/06/00	12/13/00	7 days	
First Level of South Tiebacks	12/21/00	01/05/01	15 days	
First Level of South-East Bracing	12/18/00	01/05/01	18 days	
First Level of East Tiebacks	01/02/01	01/09/01	7 days	
First Level of North-West Bracing	01/08/01	01/17/01	9 days	
Second Level of West Tiebacks	01/02/01	01/18/01	16 days	
Second Level of South Tiebacks	01/12/01	01/23/01	11 days	
Second Level of East Tiebacks	01/23/01	02/01/01	9 days	
Second Level of South-West Bracing	01/22/01	01/29/01	7 days	
Third Level of West Tiebacks	01/29/01	02/09/01	11 days	
Third Level of South Tiebacks	02/02/01	02/20/01	18 days	
Second Level of South-East Bracing	02/02/01	02/16/01	14 days	
Third Level of East Tiebacks	02/21/01	03/26/01	33 days	
First Level of North-East Bracing	03/06/01	03/14/01	8 days	
Second Level of North-West Bracing	04/25/01	05/01/01	6 days	
Foundation slab at the center	03/03/01	04/25/01	53 days	
First Level of Raker support	04/06/01	05/15/01	39 days	
Second Level of Raker support	05/09/01	06/01/01	23 days	
Second Level of North-East Bracing	05/30/01	06/06/01	7 days	
Excavation process	11/14/00	06/19/01	~219 day	
Date				Nov 14 / Dec 5 / Dec 13 / Dec 19 / Dec 27 / Jan 6 / Jan 11 / Jan 17 / Jan 29 / Feb 2 / Feb 6 / Feb 13 / Feb 20 / Mar 14 / Mar 24 / Apr 6 / Apr 25 / May 1 / May 8 / May 17 / Jun 1 / Jun 6
Phase #				02 / 03 / 05 / 07 / 09 / 13 / 16 / 18 / 21 / 27 / 28 / 29 / 30 / 33 / 34 / 35

Table 3-6: Full list of Plaxis 3D phases with correlated duration time

Phases	Description	Date	Duration
0) Initial			
1) Surcharge			
2) Wall installation		14-Nov-00	153
3) Exc1	5-Dec-00	5-Dec-00	21
4) CornerSW1		13-Dec-00	8
5) Exc2	19-Dec-00	19-Dec-00	6
6) TiebacksW1		P	
7) Exc3	27-Dec-00	27-Dec-00	8
8) TiebacksS1_E1_Corner_SE1		P	
9) Exc4	11-Jan-01	11-Jan-01	15
10) CornerNW1		P	
11) Exc5		P	
12) TiebacksW2		P	
13) Exc6	17-Jan-01	17-Jan-01	6
14) CornerSW2		P	
15) TiebacksS2		P	
16) Exc7	29-Jan-01	29-Jan-01	12
17) TiebacksE2		P	
18) Exc8	6-Feb-01	6-Feb-01	8
19) TiebacksW3		P	
20) Exc9		10-Feb-01	4
21) Exc10	13-Feb-01	13-Feb-01	3
22) TiebacksS3		20-Feb-01	7
23) CornerSE2		P	
24) TiebacksE3		P	
25) Exc11	23-Feb-01	23-Feb-01	3
26) CornerNE1		P	
27) Exc12	14-Mar-01	14-Mar-01	19
28) Exc13		6-Apr-01	23
29) Foundation	25-Apr-01	25-Apr-01	19
30) RakersN1	8-May-01	8-May-01	13
31) Exc14		15-May-01	7
32) CornerNW2		P	
33) RakersN2	17-May-01	17-May-01	2
34) Exc15		1-Jun-01	15
35) CornerNE2		6-Jun-01	5

Table 3-7: Details of Plaxis 3D Model Phases

Available excavation data	Model Phase	Description
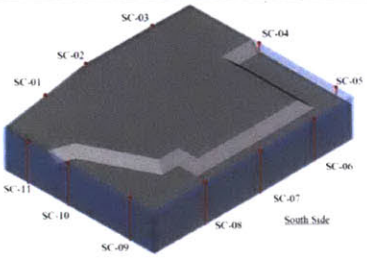	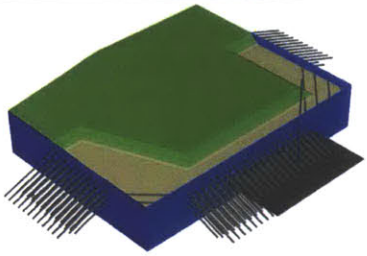	Date: December 5, 2000 Plaxis 3D phase: #3 Excavation clusters deactivated Maximum Excavated Elevation=8 ft
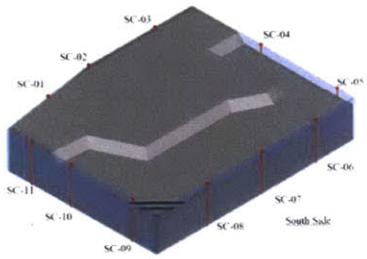	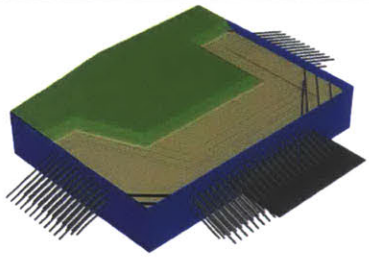	Date: December 19, 2000 Plaxis 3D phase: #5 Excavation clusters deactivated Maximum Excavated Elevation=8 ft First Level of South-West Bracing installed
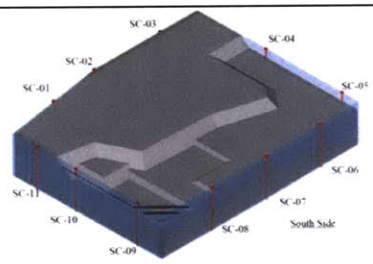	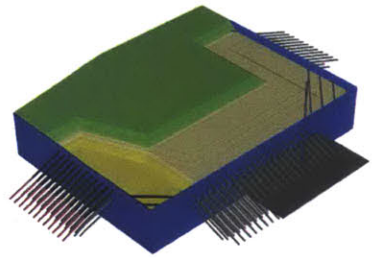	Date: December 27, 2000 Plaxis 3D phase: #7 Excavation clusters deactivated Maximum Excavated Elevation=-4 ft First Level of West Tiebacks installed
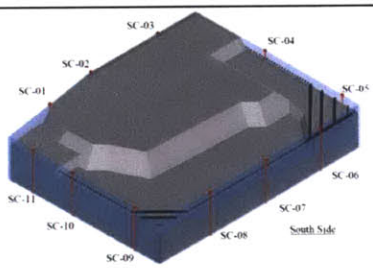	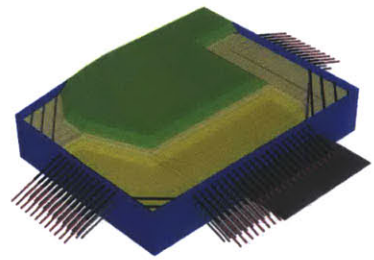	Date: January 11, 2001 Plaxis 3D phase: #9 Excavation clusters deactivated Maximum Excavated Elevation=-4 ft First Level of South and East Tiebacks installed First Level of South-East Bracing installed

Table 3-7: Details of Plaxis 3D Model Phases (continue)

Actual Phase	Model Phase	Description
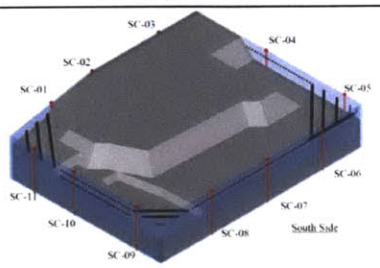	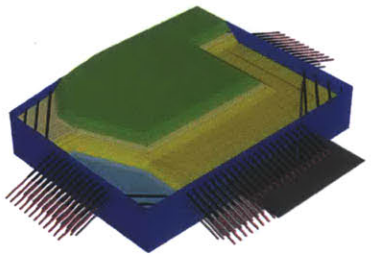	Date: January 17, 2001 Plaxis 3D phase: #13 Excavation clusters deactivated Maximum Excavated Elevation=-14 ft First Level of North-West Bracing installed Second Level of West Tiebacks installed
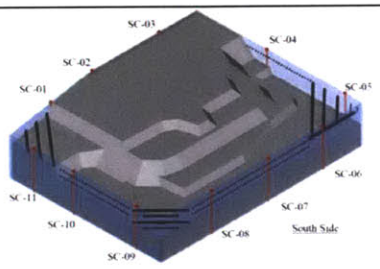	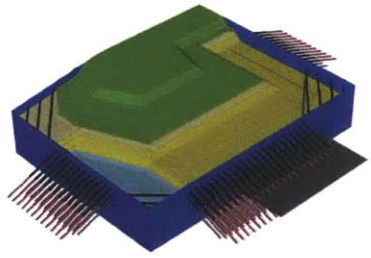	Date: January 29, 2001 Plaxis 3D phase: #16 Excavation clusters deactivated Maximum Excavated Elevation=-14 ft Second Level of South Tiebacks installed
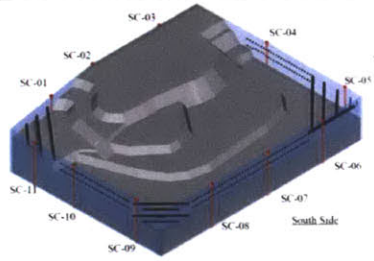	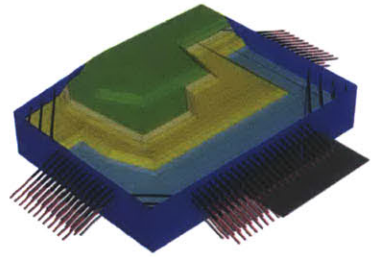	Date: February 6, 2001 Plaxis 3D phase: #18 Excavation clusters deactivated Maximum Excavated Elevation=-14 ft Second Level of East Tiebacks installed Second Level of South-West Bracing installed
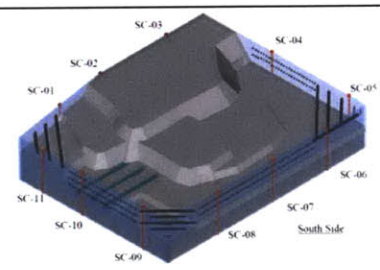	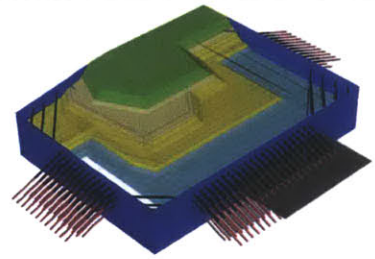	Date: February 13, 2001 Plaxis 3D phase: #21 Excavation clusters deactivated Maximum Excavated Elevation=-21 ft Third Level of West Tiebacks

Table 3-7: Details of Plaxis 3D Model Phases (continue)

Actual Phase	Model Phase	Description
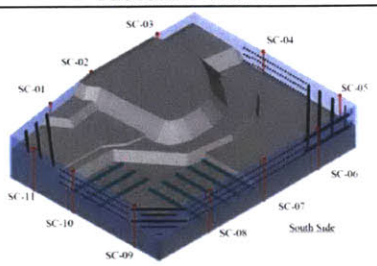	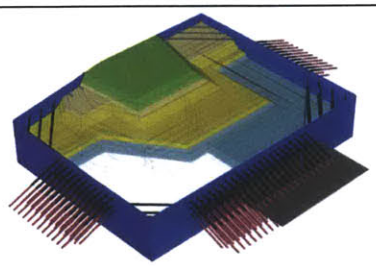	Date: February 23, 2001 Plaxis 3D phase: #25 Excavation clusters deactivated Third Level of South and East Tiebacks installed Second Level of South-East Bracing installed
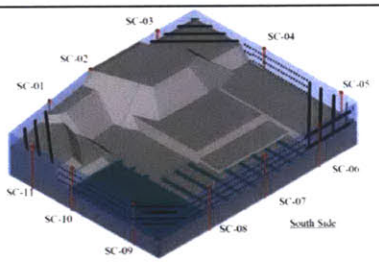	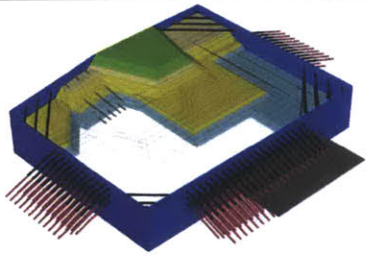	Date: March 14, 2001 Plaxis 3D phase: #27 Excavation clusters deactivated First Level of North-East Bracing installed
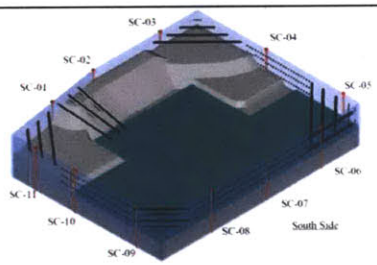	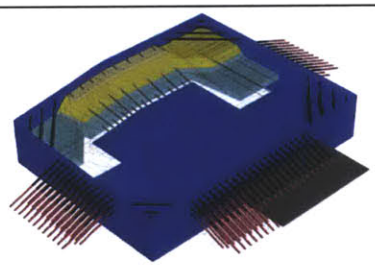	Date: April 25, 2001 Plaxis 3D phase: #29 Excavation clusters deactivated Foundation slab installed
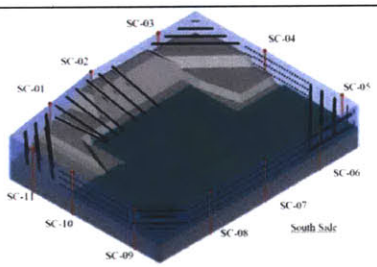	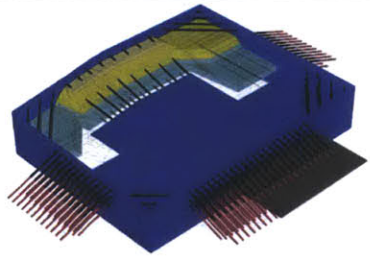	Date: May 8, 2001 Plaxis 3D phase: #30 Excavation clusters deactivated First Level of Raker support installed
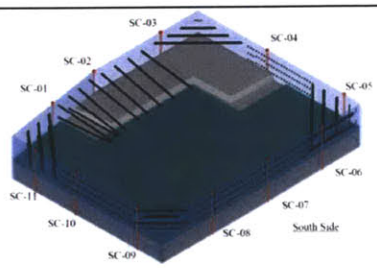	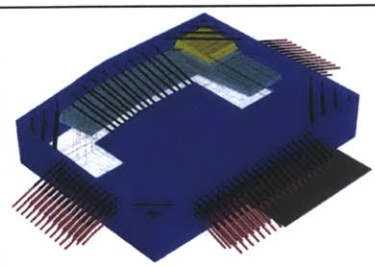	Date: May 17, 2001 Plaxis 3D phase: #33 Excavation clusters deactivated Second Level of North-West Bracing installed Second Level of Raker support installed

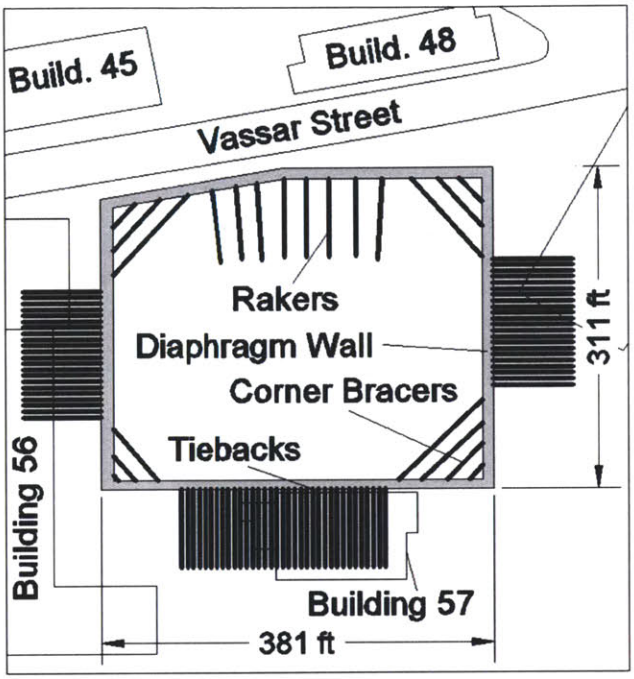

Figure 3-1: Schematic plan of structural support system with dimensions

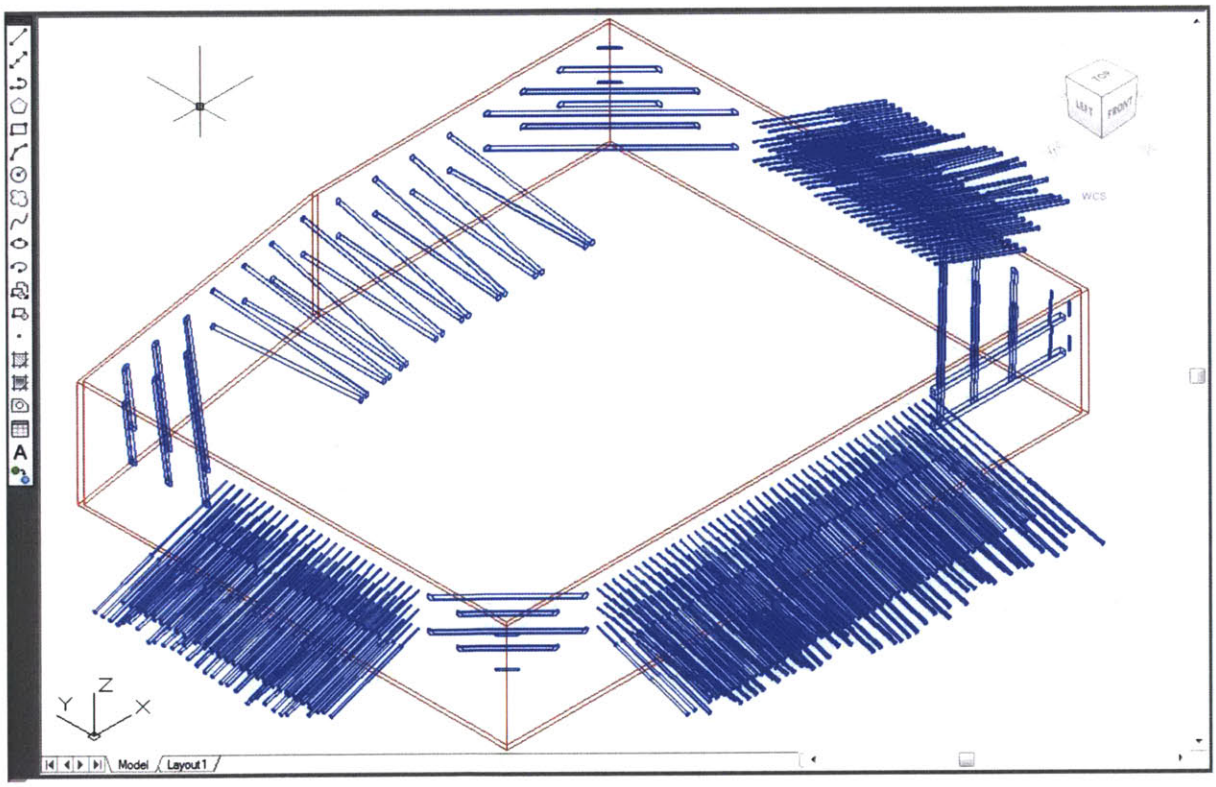

Figure 3-2: CAD model of the support system

Photo of excavation progress on 11/28/2000

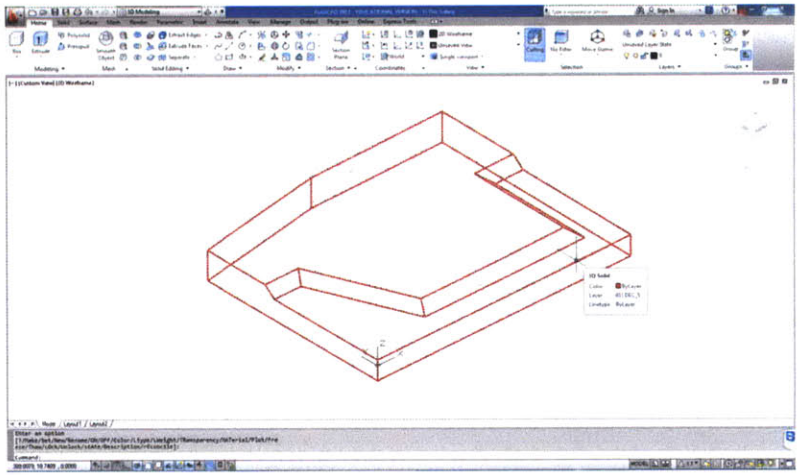

CAD model of excavation progress on 12/05/2001

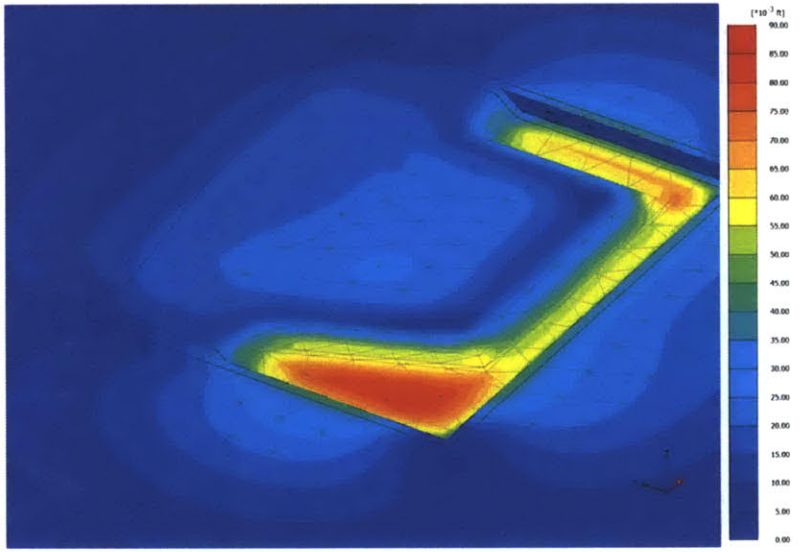

Plaxis 3D output - total ground deformations (Phase #3)

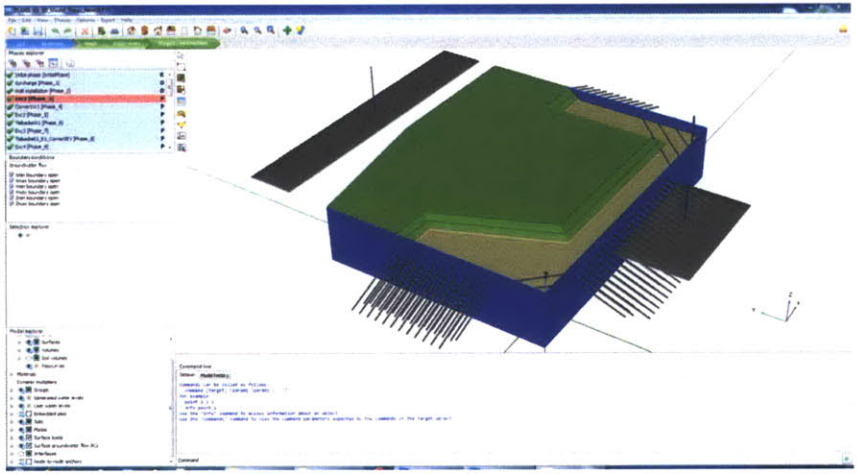

Plaxis 3D input model (Phase #3)

Figure 3-3: Example of excavation modeling - Phase #3 (12/05/2001)

Photo of excavation progress on 5/04/2001

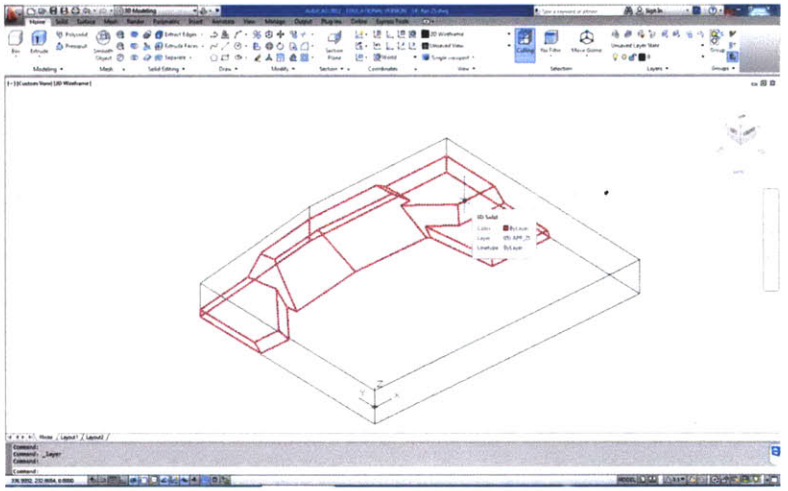

CAD model of excavation progress on 5/08/2001

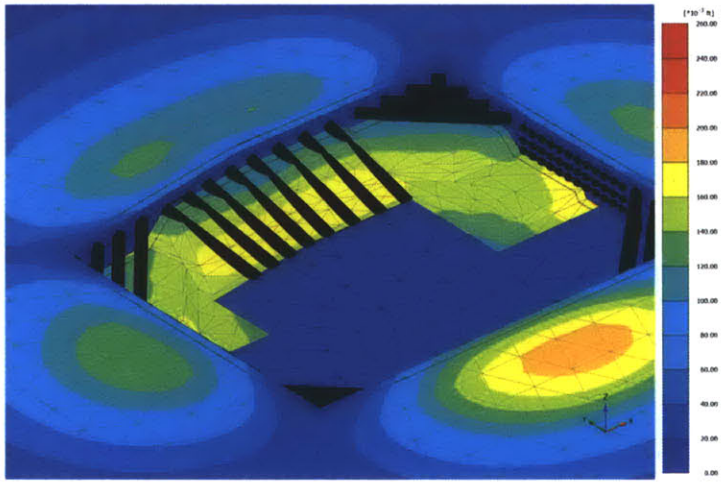

Plaxis 3D output - total ground deformations (Phase #30)

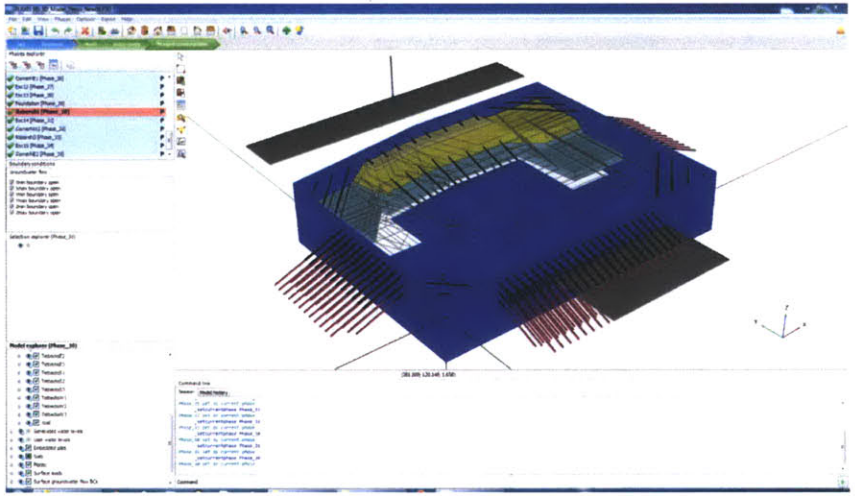

Plaxis 3D input model (Phase #30)

Figure 3-4: Example of excavation modeling - Phase #30 (5/08/2001)

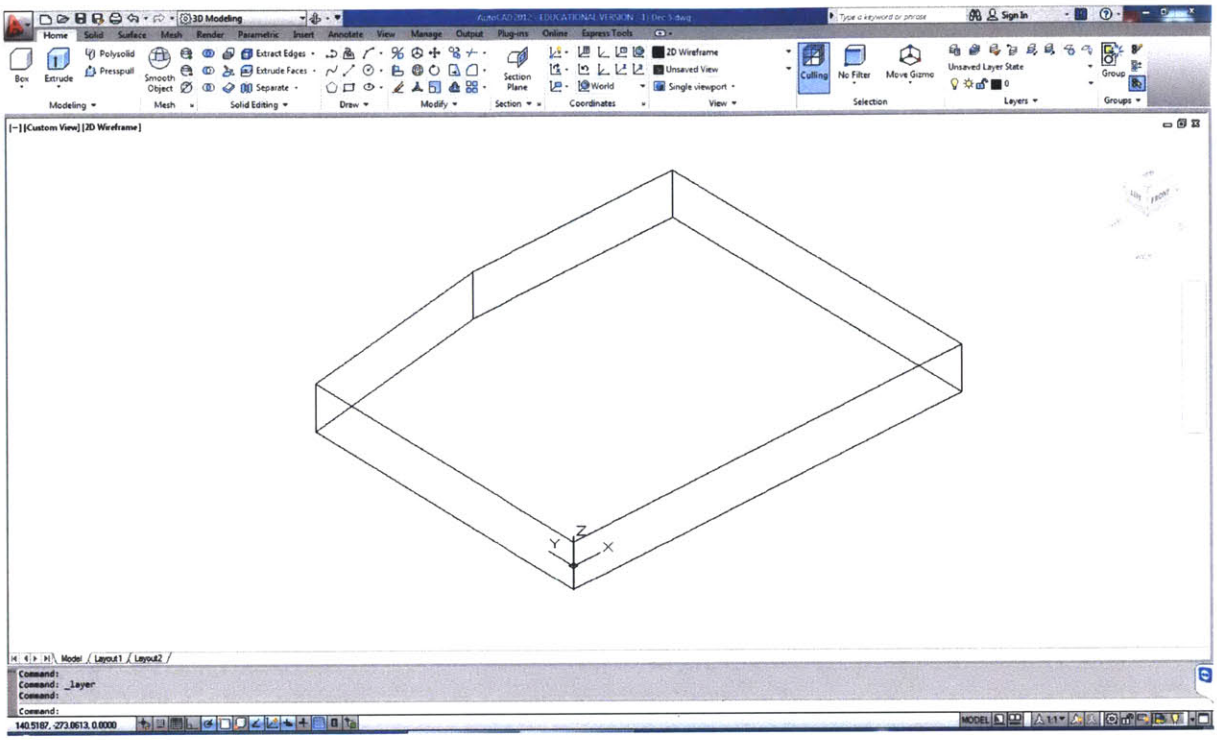

Figure 3-5: CAD Model (simple case) - creation of full cluster

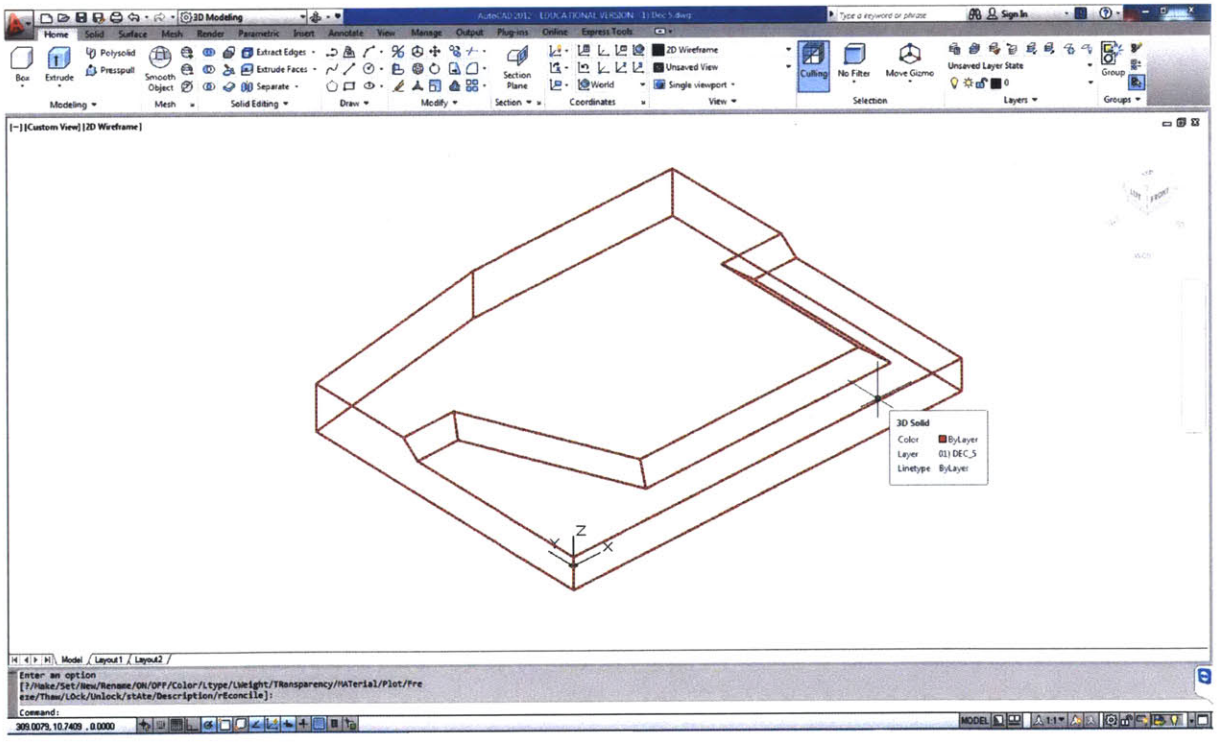

Figure 3-6: CAD Model (simple case) - creation of input cluster based on available information

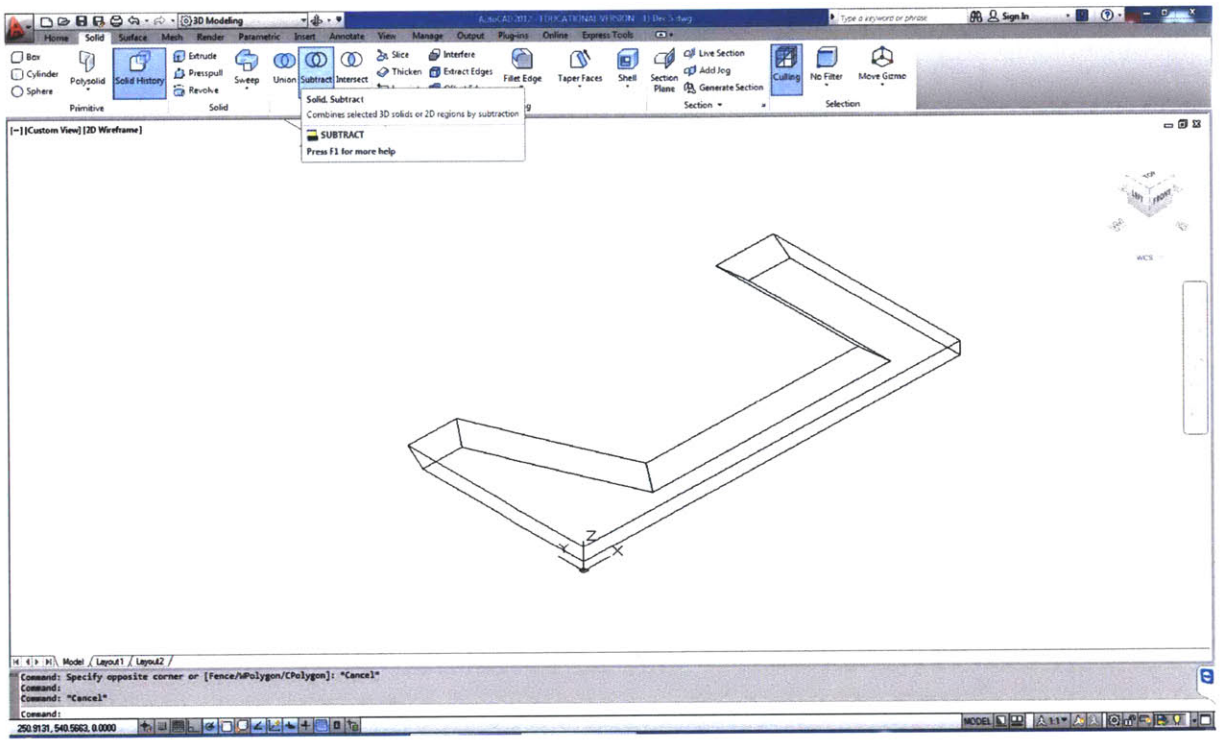

Figure 3-7: CAD Model (simple case) - subtracting input cluster from full cluster

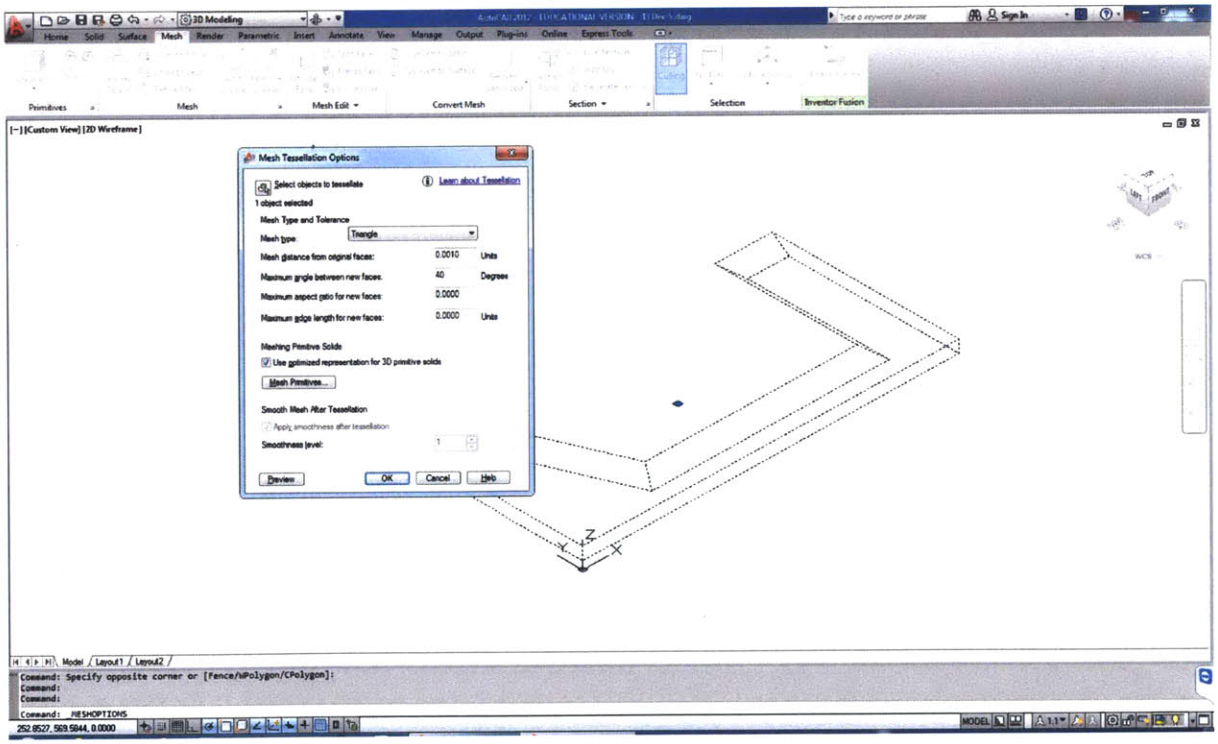

Figure 3-8: CAD Model (simple case) - mesh tessellation settings for cluster conversion

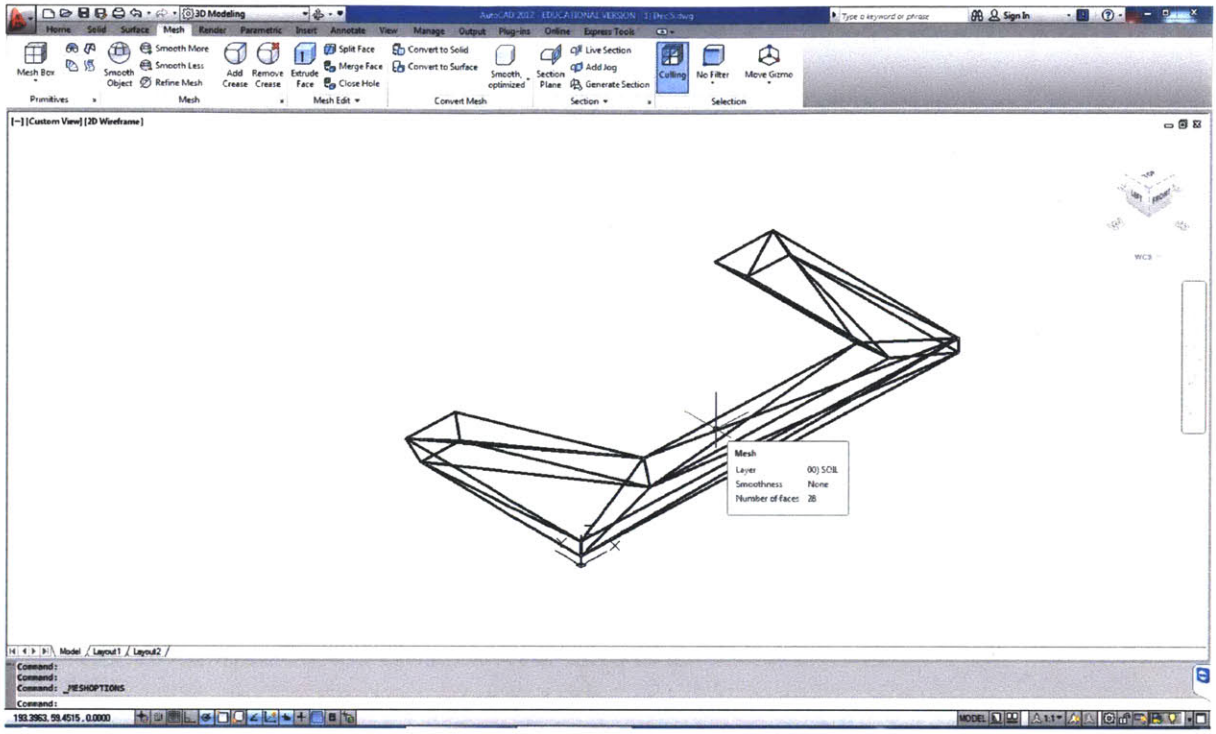

Figure 3-9: CAD Model (simple case) - converted cluster

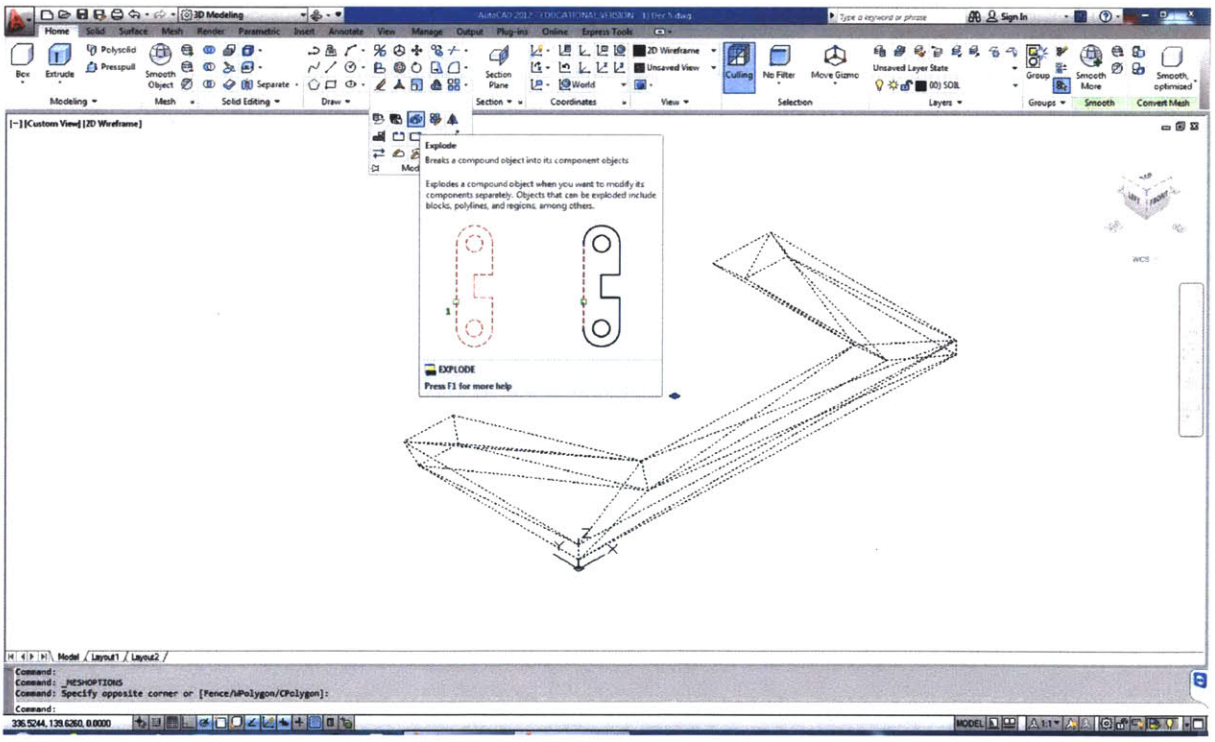

Figure 3-10: CAD Model (simple case) - converted cluster preparation

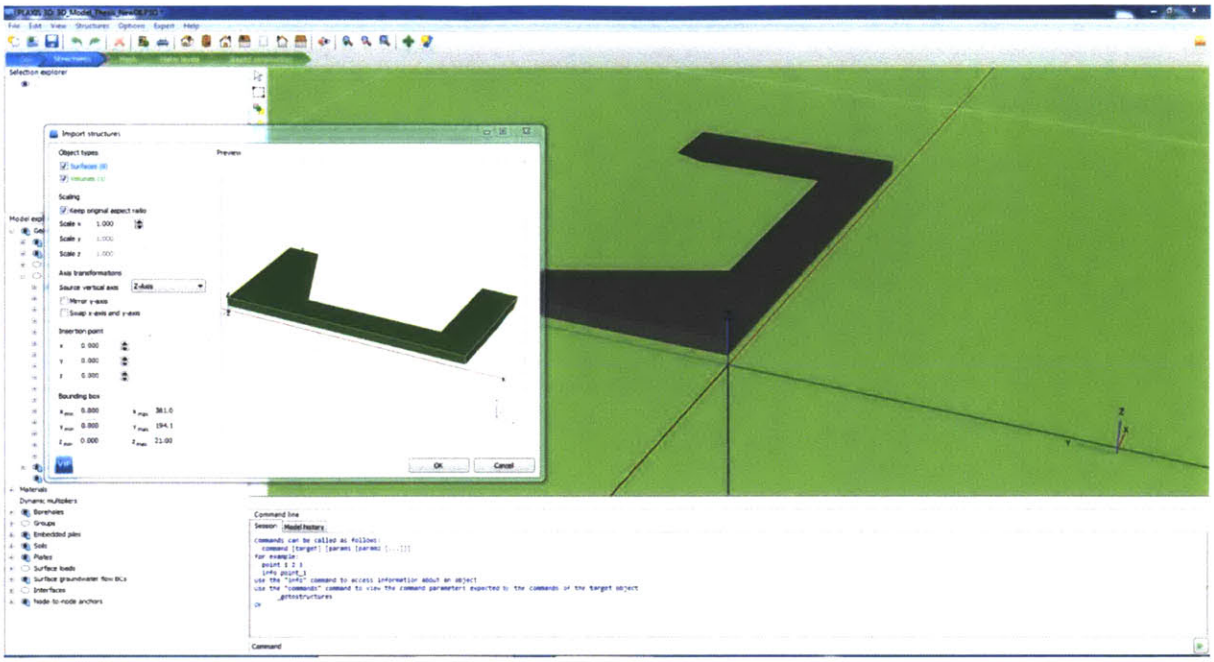

Figure 3-11: Importing prepared soil cluster into the Plaxis 3D model

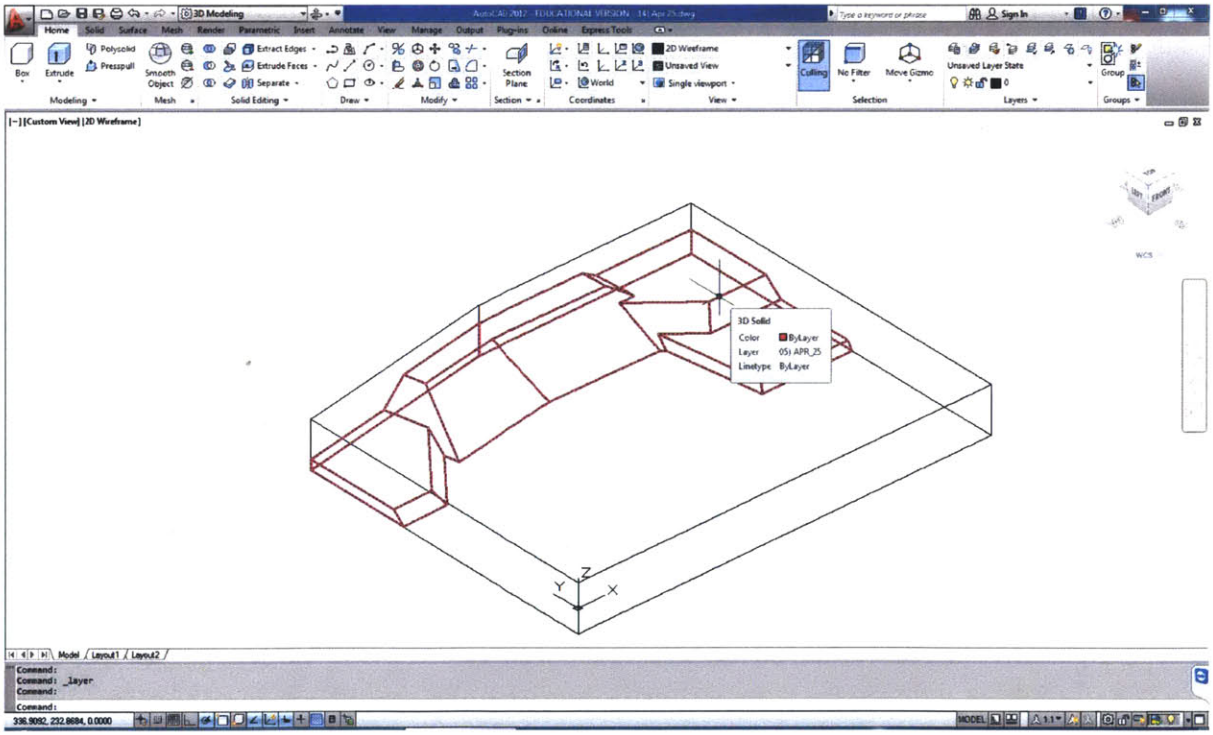

Figure 3-12: CAD Model (complex case) - input cluster based on available information

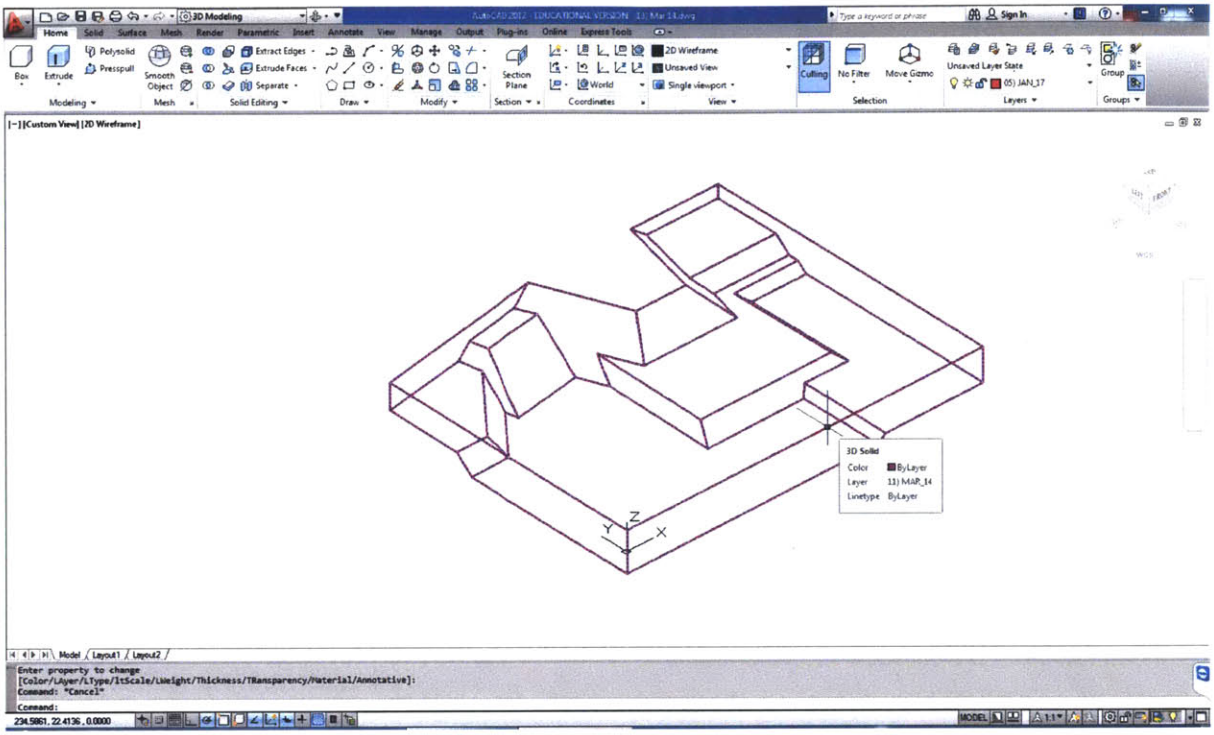

Figure 3-13: CAD Model (complex case) - inversion of input cluster

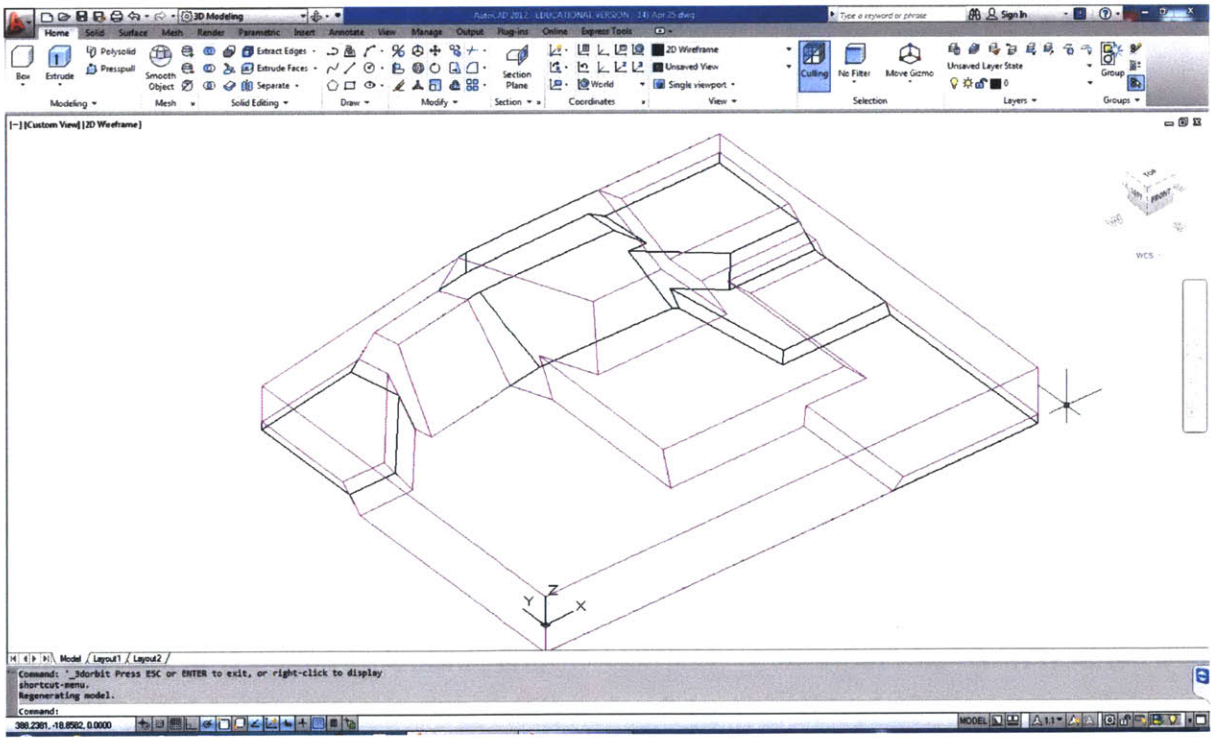

Figure 3-14: CAD Model (complex case) - subtracting new input cluster from previous phase cluster

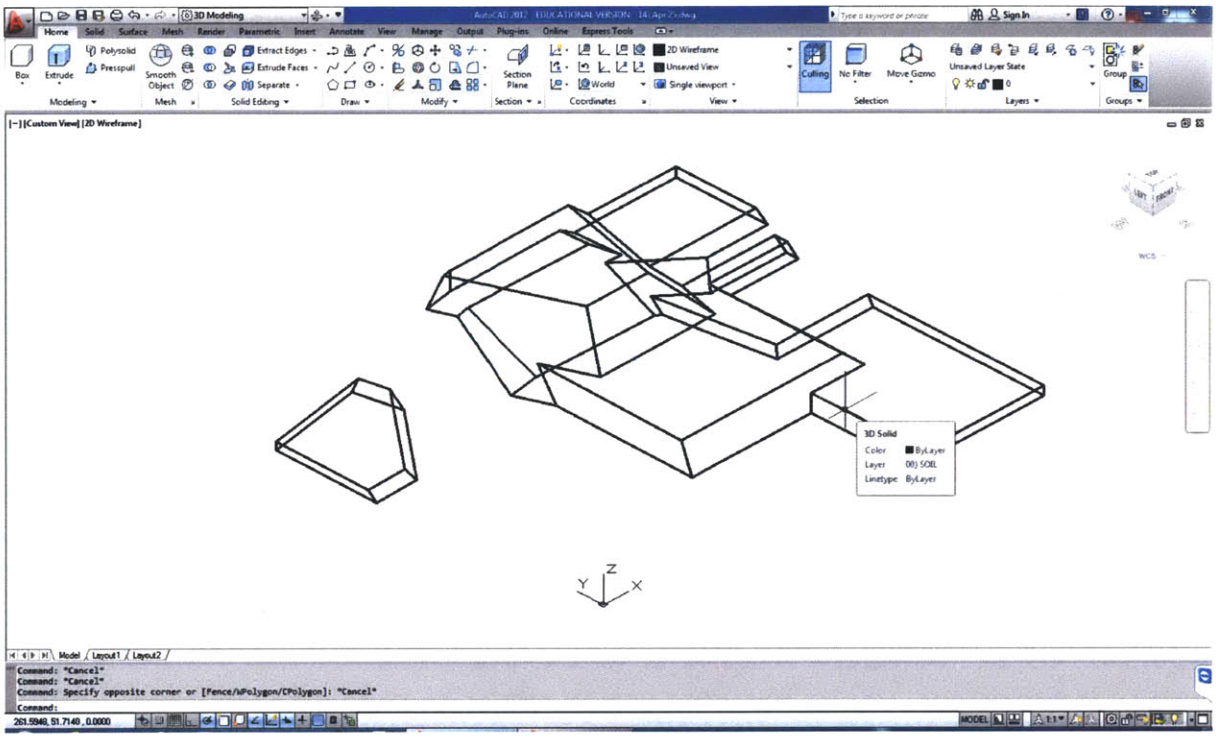

Figure 3-15: CAD Model (complex case) - input cluster differentiated

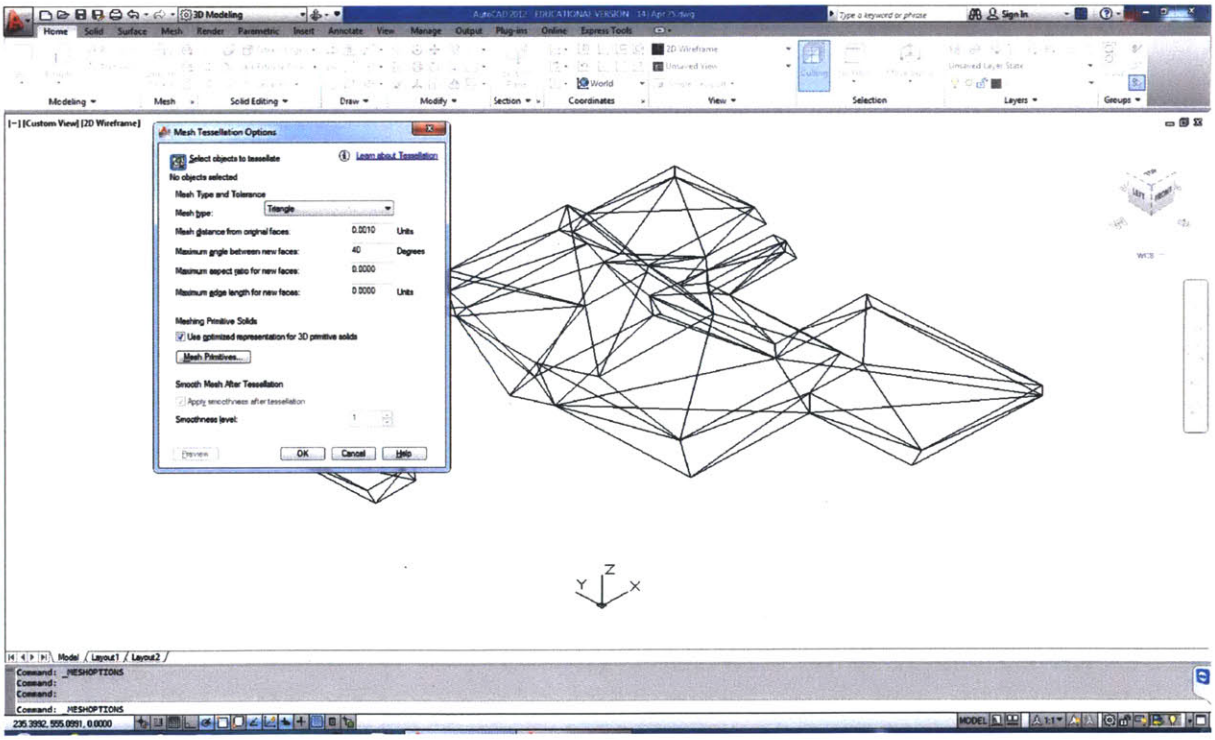

Figure 3-16: CAD Model (complex case) - mesh tessellation settings for cluster conversion

4 RESULTS AND INTERPRETATION

This chapter compares the field measurements with the model predictions of wall deflections, ground deformations, and pore pressures obtained from the three dimensional finite element Base Case (A) analysis using MC soil model assuming undrained conditions within the clay layer. The results are presented and interpreted. The effects of partial drainage (Case B analysis, which incorporated the actual construction time from the calendar plan) on wall deflections are discussed. A "curve integration" method for evaluating the results is also presented.

4.1 Wall Deflections

Figures 4-1 through 4-4 compare the lateral wall deflections at different stages of the excavation for the North, East, South, and West walls at the actual location of vertical inclinometers in the field. The inclinometers SC-01 through SC-03 are located along the North wall. The movements of the East wall are measured by the inclinometers SC-04 and SC-05. In addition, the inclinometers SC-06 through SC-08 are installed along the South wall, and the rest of inclinometers, SC-09 though SC-11, measure the lateral wall deflections of the West wall. Each predicted phase correspond to a specific date according to the construction sequence and calendar plan (Table 3-5).

A general pattern of measured movements at the center of a wall typically correspond to an initial cantilever movements of about 0.4-0.75 in during the excavation to the first tieback support level, as well as 1.25 in before the first level of raker support. The movement was fully recovered (except the North Wall) and the wall moved back during pre-stressing the first level of bracing. After the installation of the first level support, the wall rotated at the brace during the

excavation progress. At the subsequent bracing, the wall kept moving laterally below the brace location. The maximum movements (June, 2001) measured in the inclinometers range from 2.0-2.5 in at SC-02 (North), SC-04 (East), and SC-10 (West) to about 3.2 in at SC-07 (South). The greatest movements were observed within the middle of a tieback supported wall while the smallest movements were recorded by the inclinometers located closer to the corners. This is a well-known three-dimensional effect attributed to the increased rigidity of the corner braces combined with corner effects (Finno et al., 2005). In contrast, the North wall, supported by the raker support, showed an opposite pattern with the smallest movements occurring at the center. However, this observation could be attributed in part to the fact that the plan geometry of the North wall consisted of two planes that intersect at the wall center (Figure 3-1).

Figure 4-1 summarizes wall deflections measured by two inclinometers located along the East wall versus the predictions from the Base Case (A) analysis at the corresponding location and time. The location of inclinometers on the site plan with dimensions is also shown. For the inclinometer SC-04 located in the middle of the wall, the analysis shows a reasonable agreement with the measured wall deflections, except the initial cantilever movement which is underestimated by 0.5 in possibly due to the simplifications in the initial excavation geometry. At the Phase #29, which corresponds to the installation of the foundation slab, the analysis underestimates the maximum wall deflections by 0.35 in. The final maximum movement is underestimated by 0.25 in during the last phase #35 corresponding to the date of 6/16/2001. The model predictions show more movement of the top of the wall than the field measurement with the maximum difference of 0.4 in. For the inclinometer SC-05 located close to the south-east corner, the mode shape of deformation is an agreement with the measured data and shows the effects of corner bracing support (the movements of the top of the wall are minimal and the

maximum deflections are less than those in the middle of the wall). The maximum wall deflection at the Phase #21 (02/06/2001) is the same as in the measured data, but the toe movement is overestimated by 0.5 in. The final maximum wall deflection at the last phase is also underestimated by 0.5 in.

Figure 4-2 presents the comparison of wall deflections measured by inclinometers located along the South wall and the model predictions. The MIT Alumni swimming pool building is located 5 ft from the edge of the excavation at this location and is simulated as a three-dimensional surface surcharge (1.28 ksf) at the level of the pile tip (El. -10 ft). The inclinometer SC-07 located in the middle of the wall recorded the maximum wall deflection of 3.2 inches; the phase #35 predictions for the same location show 2.9 in. The predictions for the inclinometer SC-06 show a very good agreement with the measured data until the "installation of foundation slab" phase. The field data indicate the further movement of 0.5 in at that location. The maximum wall deflections at the location of inclinometer SC-08 are slightly overestimated by 0.2 in and the movements of the top of the wall are overestimated by 0.35 in.

Wall deflections measured by inclinometers SC-09 through SC-11 along the West wall versus three-dimensional finite element analysis predictions are summarized in Figure 4-3. The general wall behavior is similar to that of the east wall. The noticeable three-dimensional effects that cause the induced ground deformations to be smaller near the corner of an excavation wall than near its center (Finno et al., 2005) were also observed in the measured data and captured by the analysis. The inclinometers SC-09 and SC-11 show an excellent agreement between measured and predicted movements. The maximum wall deflections match perfectly, but the top and toe movements are overestimated by 0.3-0.6 in. The predicted maximum wall deflections in the middle of the wall are reasonably consistent with the data.

Figure 4-4 presents the results for the North wall supported by the raker support system. The measured data in inclinometers SC-01, SC-02, and SC-03 show perfect correlation with the predicted data when small movements at the toe of the wall were observed at the early phases of the analysis. However, the analysis greatly underestimates wall deflections as soon as the only narrow soil berm was left in place before the first level raker brace installation along the north wall. The predictions overestimate toe movements of wall by 0.5-0.6 in while underestimating the maximum wall deflection by the same amount at the corner locations. The values of maximum wall deflection in the middle of the North wall are 2.0 in for both measured and predicted data.

Figures 4-5 through 4-17 show the view of excavation progress with corresponding Plaxis model, three-dimensional wall deflections, and total ground deformations during each of the construction phases. The three-dimensional effects of corner bracing support and effects of the North Wall geometry can be seen from the total three-dimensional deformations of the wall.

In order to quantitatively assess the obtained predictions from the Base Case (A) model and consistently compare them with the field data, a "curve integration" method was used. The idea of this method is to obtain and compare the areas under each curves on the "elevation vs. wall deflection" plots (Bolton, et al., 2010). Inclusive areas (areas broken by missing values) are used to compare the bending moments. The total area ratio is used as a general comparison criteria which takes into account discrepancies in both the mode shape of the wall (magnitudes of bending) and movements of top and bottom. Figures 4-18 to 4-21 summarize the results of this wall deflections comparison technique for the centers of the North, East, South, and West walls of the MIT Stata Center project. It is clear that the Base Case (A) analysis underestimates the

magnitudes of wall bending and slightly overestimates the toe movements during the final phases of excavation. These results can be attributed to the following possible factors:

1. The Base Case analysis assumes a constant height of the diaphragm wall with the top at the ground surface (El. +21 ft) while the actual top elevation varied from El. 15.4 ft to El. 19.0 ft.
2. The material properties of the diaphragm wall are assumed to be linear-isotropic.
3. The soil layers in geological profile are assumed to be horizontal. A simple elastic-perfectly plastic constitutive soil model is used.
4. The groundwater table is assumed to be at El. +15 ft around the excavation site and is lowered inside the impermeable diaphragm wall each time to match the current maximum level of excavation and produce steady-state seepage.
5. The adjacent Building 57 is simulated only as a surcharge load at the tip of the caissons.

Nevertheless, the results show on average 93% in total and 76% in inclusive areas agreement with the measured data (integrated wall deflection curves). This is a reasonably good agreement taking into account the usage of a relatively simple soil model.

4.2 Pore Pressures

Figure 4-22 summarizes the predicted piezometric elevations at the coordinates of the field piezometer PZ-1 located at the center of the excavation. The excavation progress level according to the project time frame is also present in the figure. The predicted piezometric heads at the El. -30 ft and El. -50 ft (clay layers) show a reasonable agreement with the measured data. However, unlike the measured data, the predicted piezometric elevation within El. -98 remain

almost constant throughout the time frame of excavation. This can be explained by the fact that the model assumes undrained conditions in the lower clay adjacent to a highly permeable material (glacial till, drained).

Figure 4-23 presents piezometric elevations measured by the piezometer PZ-2 located at the South wall versus the Base Case (A) analysis predictions. The predictions for El. -30 are in reasonably good agreement with the observed piezometric head. For the next elevation at El. -50, the analysis overestimates the change in piezometric elevation. In contrast, at El. -90, the predictions underestimate the change in piezometric elevations. One of the possible causes of this discrepancy could be the fact that the MIT Alumni pool building is located at this exact location which is modeled as a surcharge load.

The predictions of piezometric elevations at the location of the piezometer PZ-3 near the North wall and measured values are compared in Figure 4-24. The predicted results for El. -50 are in very good agreement with the measured data. Nonetheless, the measured piezometric elevation at El. -95 remain approximately constant throughout the time frame of excavation, but the predicted values show significant changes in pore pressures at the later excavation stages. The measured constant piezometric head can be attributed to the existence of a highly permeable glacial till layer below the Boston Blue Clay at the corresponding elevation. Therefore, the discrepancy in the piezometric heads can be explained by the fact that the Base Case model assumes the bottom elevation of the clay layer still to be at El. -95 ft.

Figures 4-25 and 4-26 present the predicted and measured values of piezometric elevations at the vicinity of the East and West walls. The predicted changes in pore pressure well

correspond to the excavation progress. Overall, the changes in pore pressure at these locations are in reasonably good agreement with the field measurements.

4.3 Excavation Heave

The vertical movements of the ground and the excavation heave were monitored at several locations during the excavation using the borehole magnet extensometers (EXT-1 to EXT-5) located every 10 to 20 feet vertically within the marine clay stratum. A summary of the predicted and observed vertical ground movements are shown in Figures 4-26 to 4-36.

The extensometers EXT-1 and EXT-2 were located within the excavation at the center and 40 ft apart from the south wall. The total observed heave recorded at the extensometer EXT-2 during the period from the start of excavation to mat foundation placement was about 1.4 in (at El. -31). The model prediction shows approximately the same heave at the location of EXT-2 (Figures 4-30 and 4-31). The heave value of around 0.7-1.0 in was measured by the extensometer EXT-1 located at the center of excavation. The analysis results are also in a relatively good agreement with this data (Figures 4-27 and 4-28). It was reported that the observed heave within the Boston Blue clay stratum decreased with depth below the base of the excavation and practically stopped after mat placement. This behavior was also well captured by the model predictions.

The magnet extensometers EXT-3, EXT-4, and EXT-5 were installed outside of the excavation perimeter adjacent to the North, East, and West walls, respectively. The predictions for the extensometer EXT-3 at El. +10, 0, and -20 underestimate vertical movements by 0.5 to 1.2 in. However, for the lower elevations, the numerical predictions were in agreement with the measured values (Figure 4-32). The results for the location of the extensometers EXT-4 and

EXT-5 are similar and reasonably consistent with the field measurements, as can be seen in Figures 4-33 to 4-36. The discrepancies can be explained by the usage of simplified soil stratigraphy and limitations of the used simple soil model.

4.4 Surface Settlements

The settlements of adjacent buildings were monitored as the excavation progressed using survey reference points (SRPs) which were attached to the buildings and installed on the Vassar Street (behind the North Wall). Approximately 125 settlement points were optically surveyed during the excavation work. These data were compiled into contour maps of the surface settlement (Olsen, 2001) for each of the four sides of the excavation and compared with the Base Case (A) model predictions (Figures 4-41 to 4-44). The largest movements on each side were measured near the middle of each wall, where the three-dimensional model predicted the largest wall deflections.

Figures 4-37 through 4-40 present the three-dimensional finite element analysis predictions (Base Case A) of surface settlements behind the center of the West, East, South, and North walls versus field measurements on June 1, 2001.

The maximum settlements at the East wall were in the order of 0.8 in, while the West wall settlements were up to 0.9 in. These values are reasonably consistent with the results obtained from the Base Case (A) analysis. The measured settlements at the South Wall of the adjacent building ranged from 0.3 in to 1.8 in, and the maximum surface settlements on the North side were about to 2 in. The analysis results underestimated the surface settlements at these locations.

The Base Case (A) model also produced some amount of unrealistic heave directly behind the selected part of the wall (Figures 4-37 to 4-40). These effects can be attributed to the limitations of the simple constitutive model that was used in the Base Case analysis (linear elastic perfectly-plastic Mohr Coulomb soil model).

4.5 Structural Loads

Figure 4-45 summarizes the Base Case (A) analysis predictions of tieback loads with time along the East wall. The black color represents the first level of tieback support, the red color symbolizes the second level of support, and the third level of tieback support is coded by the blue color.

The error bars illustrate the standard deviation in the tieback load at a selected period of time. Figure 4-46 presents the results for the West wall, and the tieback loads for the South wall can be found in Figure 4-47.

4.6 Effects of Partial Drainage

The Case B consolidation analysis, which incorporated the actual construction time from the calendar plan, was performed. Figure 4-48 summarizes the effects of partial drainage on wall deflections in the middle of North, East, West, and South walls.

In terms of wall deflections, partial drainage caused a very small increase in the initial cantilever wall deflections. During the subsequent phases, partial drainage caused a 0.2-0.5 in reduction in the wall deflections. As the excavation progressed, the deflected mode shapes of the North, East, and West walls were almost identical to the undrained analyses. However, at the South wall location, the partial drainage analysis produced not only a reduction in the maximum

wall deflection, but also a reduction in the toe movement which produced more bending of the wall. The difference between the final maximum wall deflections from the partial drainage and the undrained analyses was about 0.5 in (Figure 4-48).

These results show that partial drainage effects do not substantially alter the excavation performance in Boston Blue Clay, but can control the maximum wall deflections and, in some cases, the toe movements of the diaphragm wall. Nonetheless, a partial drainage analysis requires detailed information on permeability properties, drainage conditions, and time history of the construction.

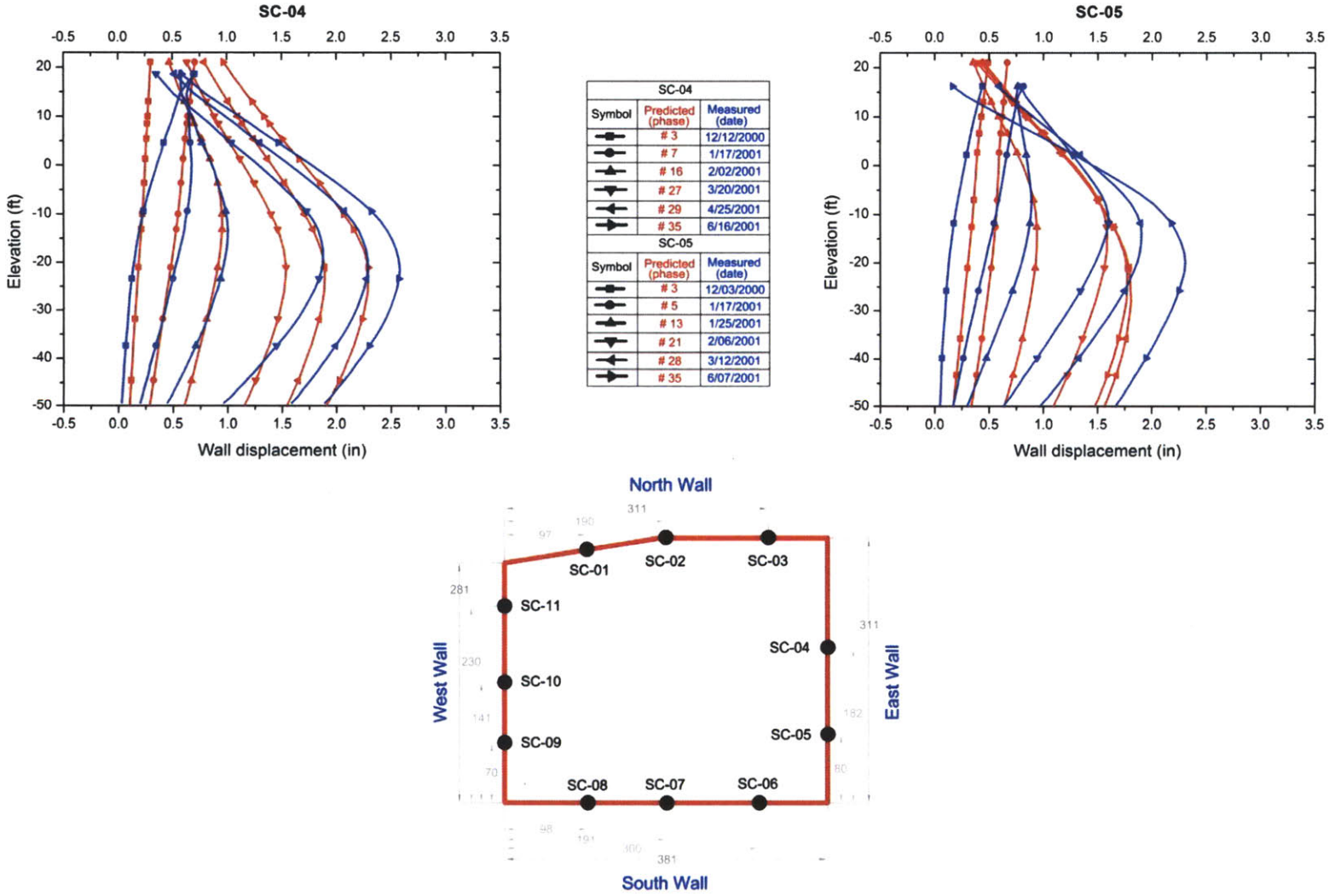

Figure 4-1: Wall deflections measured by inclinometers SC-04 and SC-05 along the East Wall vs. 3D Finite Element Analysis predictions (Base Case A)

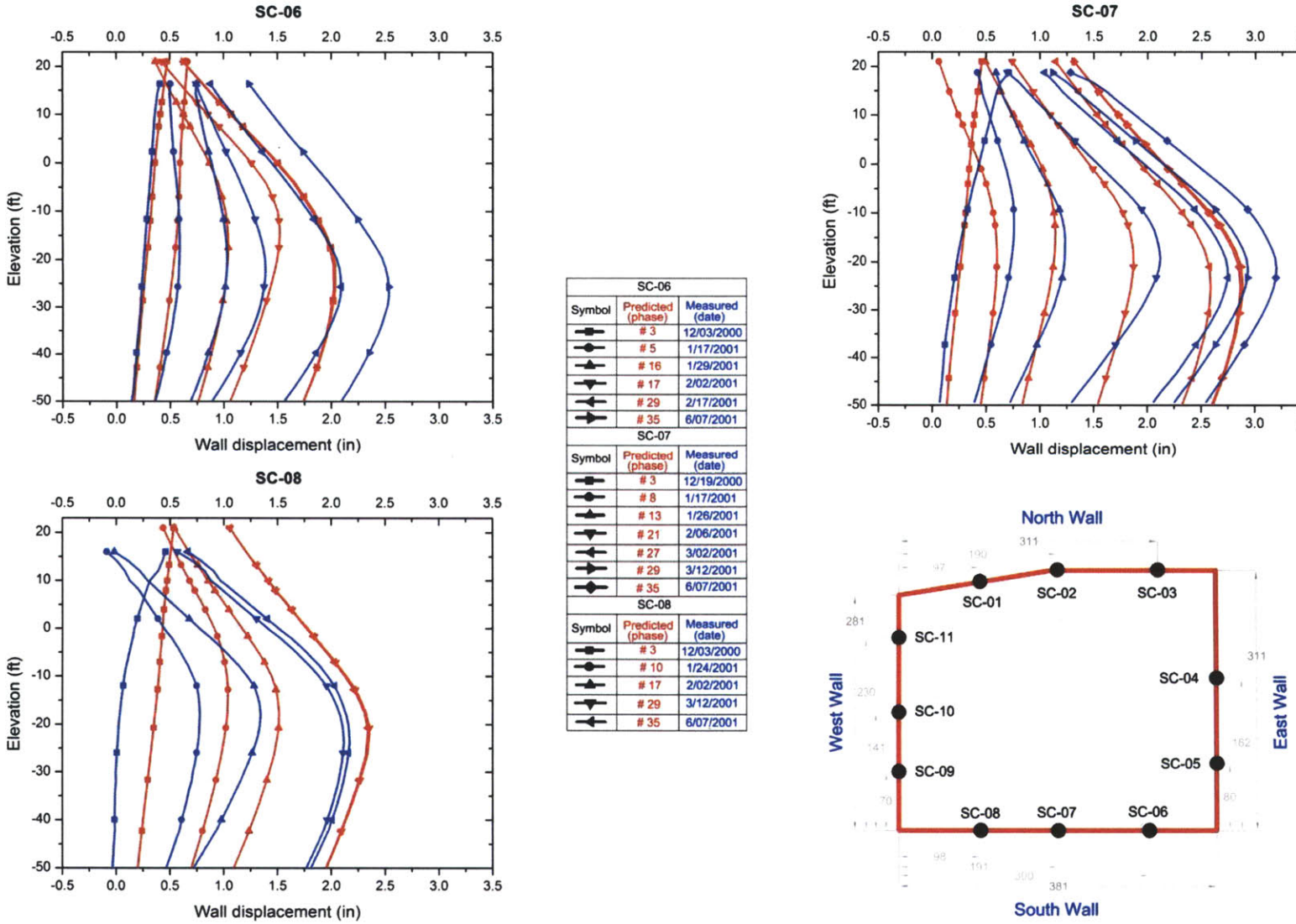

Figure 4-2: Wall deflections measured by inclinometers SC-06 through SC-08 along the South Wall vs. 3D Finite Element Analysis predictions (Base Case A)

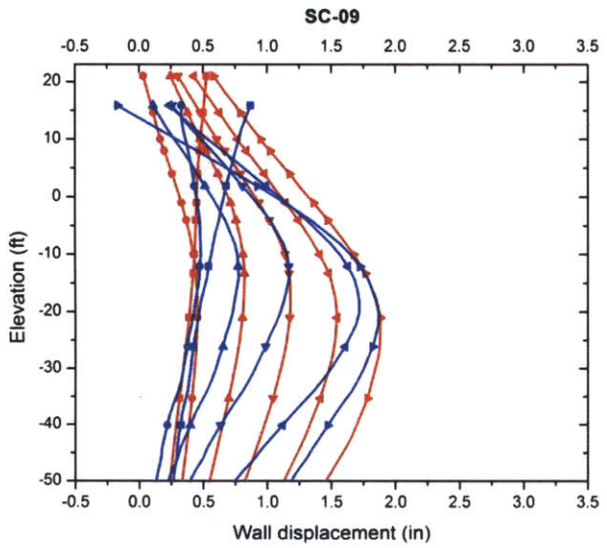

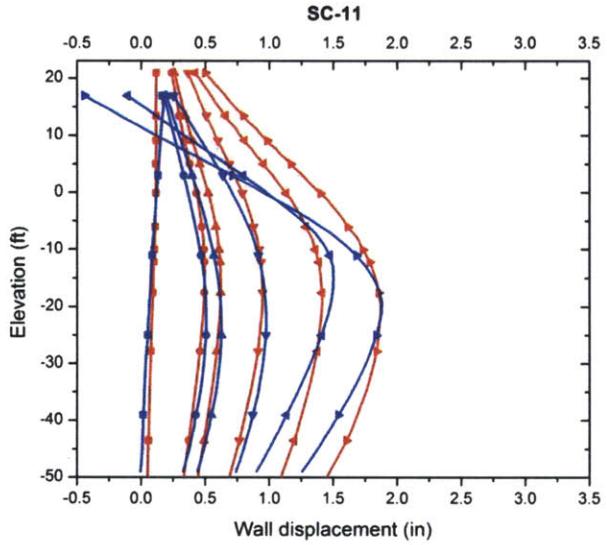

SC-09		
Symbol	Predicted (phase)	Measured (date)
	# 3	12/03/2000
	# 6	1/05/2001
	# 7	1/17/2001
	# 14	1/24/2001
	# 21	2/12/2001
	# 35	6/07/2001
SC-10		
Symbol	Predicted (phase)	Measured (date)
	# 3	12/12/2000
	# 7	1/17/2001
	# 16	1/24/2001
	# 25	2/16/2001
	# 29	3/02/2001
SC-11		
Symbol	Predicted (phase)	Measured (date)
	# 3	12/19/2000
	# 13	2/20/2001
	# 16	2/27/2001
	# 21	4/19/2001
	# 27	4/25/2001
	# 34	5/18/2001

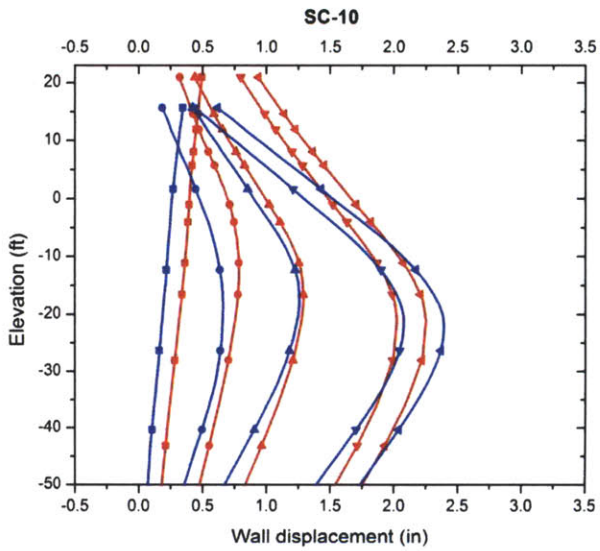

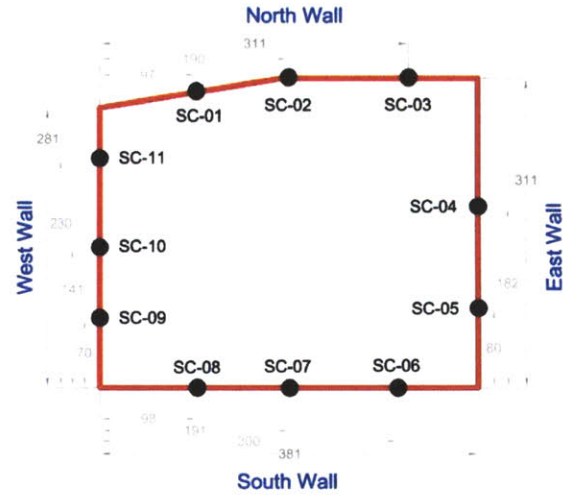

Figure 4-3: Wall deflections measured by inclinometers SC-09 through SC-11 along the West Wall vs. 3D Finite Element Analysis predictions (Base Case A)

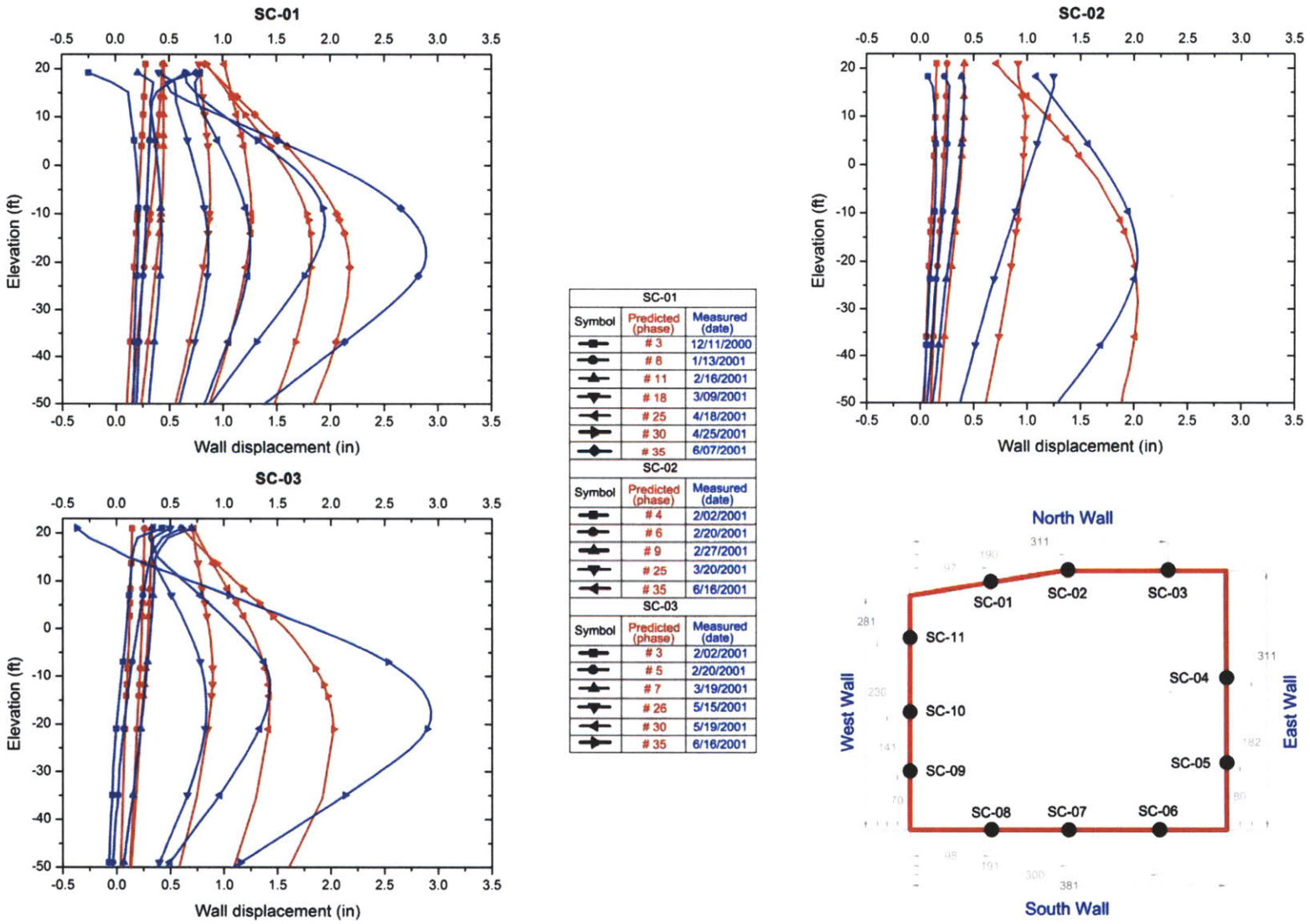

Figure 4-4: Wall deflections measured by inclinometers SC-01 through SC-03 along the North Wall vs. 3D Finite Element Analysis predictions (Base Case A)

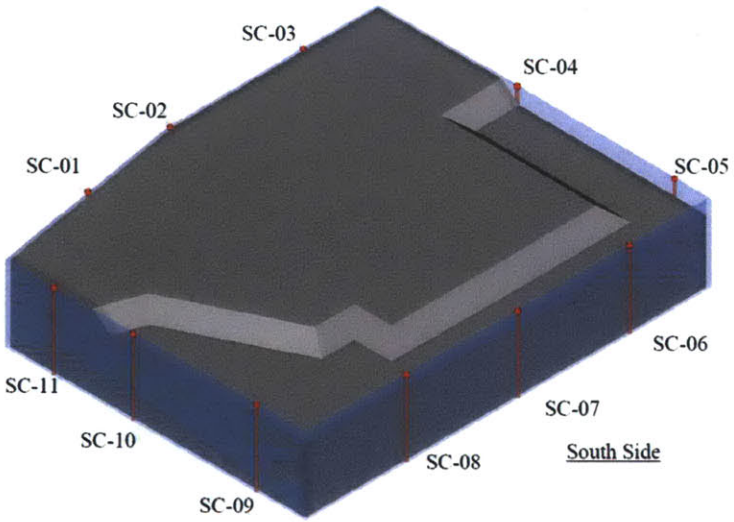

Excavation Progress Data - December 5, 2000

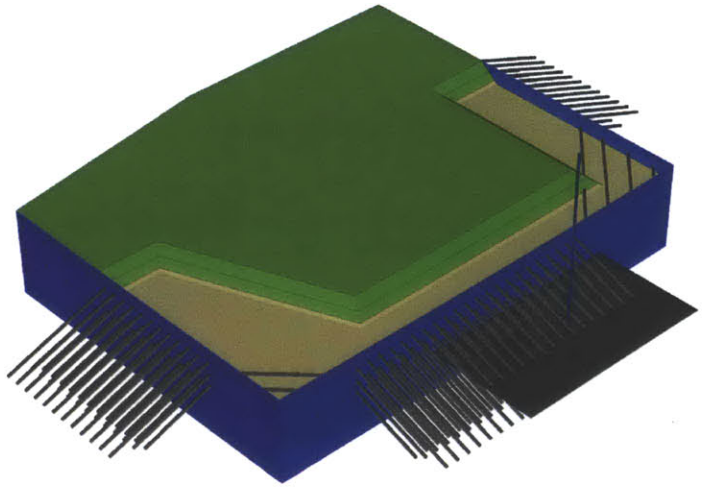

Plaxis 3D Model - Phase #3

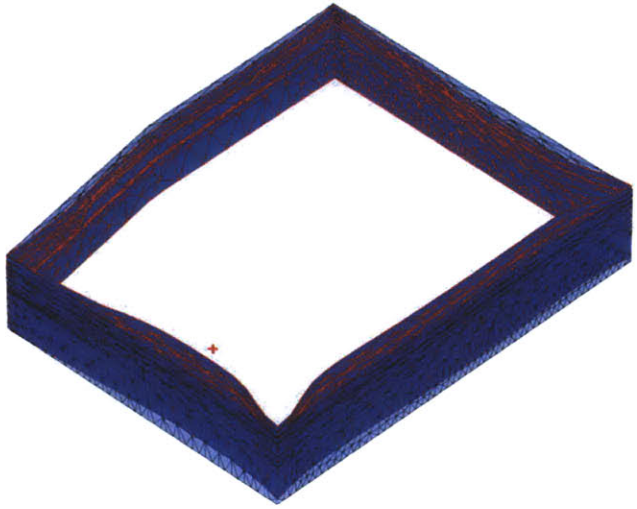

3D Wall Deflections

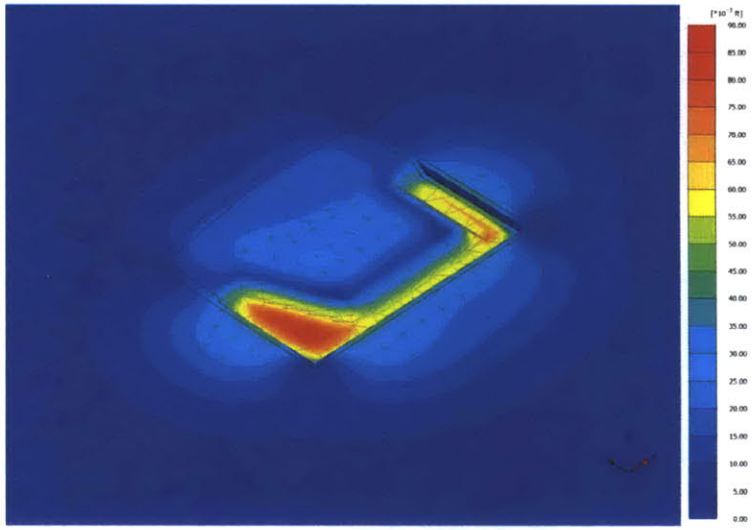

Total Ground Deformations

Figure 4-5: Excavation Progress on December 5, 2000 and 3D Finite Element Analysis Predictions (Base Case A)

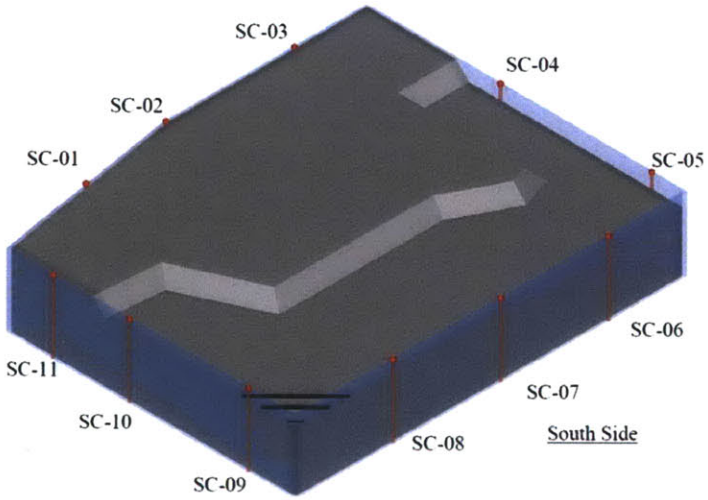

Excavation Progress Data - December 19, 2000

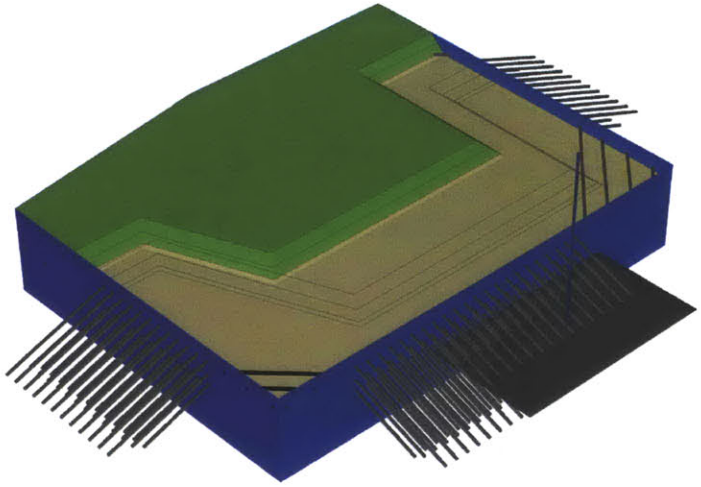

Plaxis 3D Model - Phase #5

3D Wall Deflections

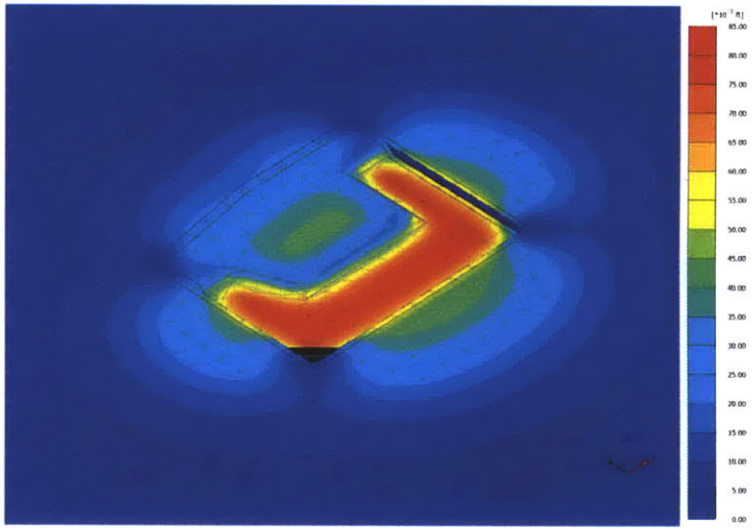

Total ground deformations

Figure 4-6: Excavation Progress on December 19, 2000 and 3D Finite Element Analysis Predictions (Base Case A)

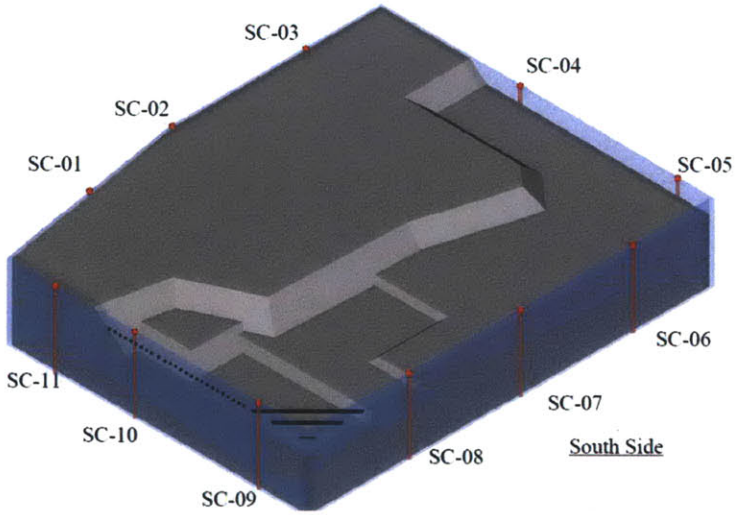

Excavation Progress Data - December 27, 2000

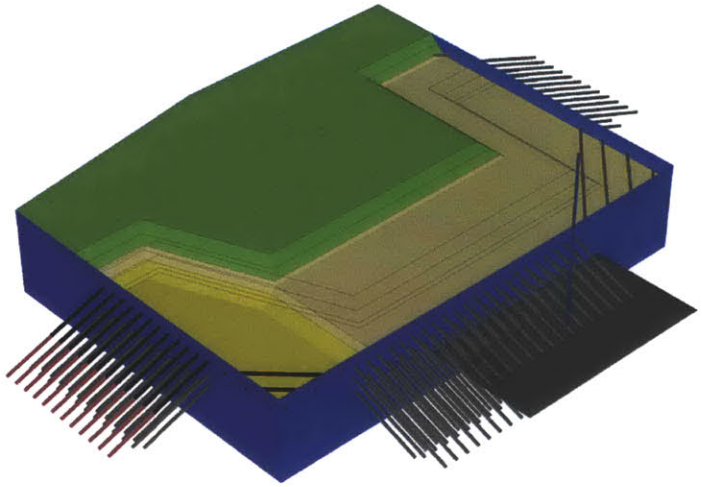

Plaxis 3D Model - Phase #7

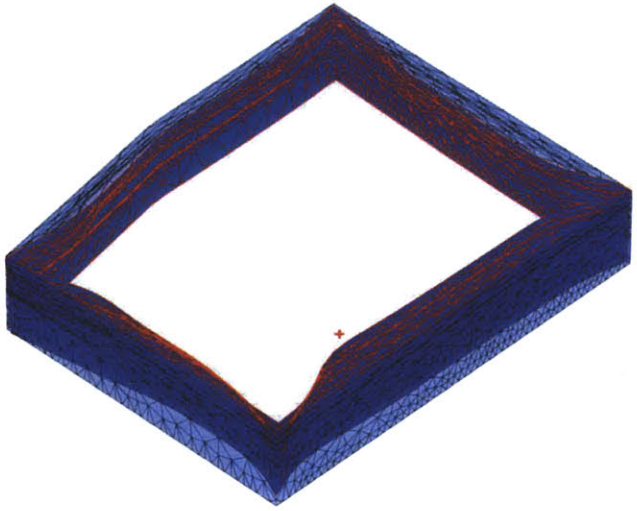

3D Wall Deflections

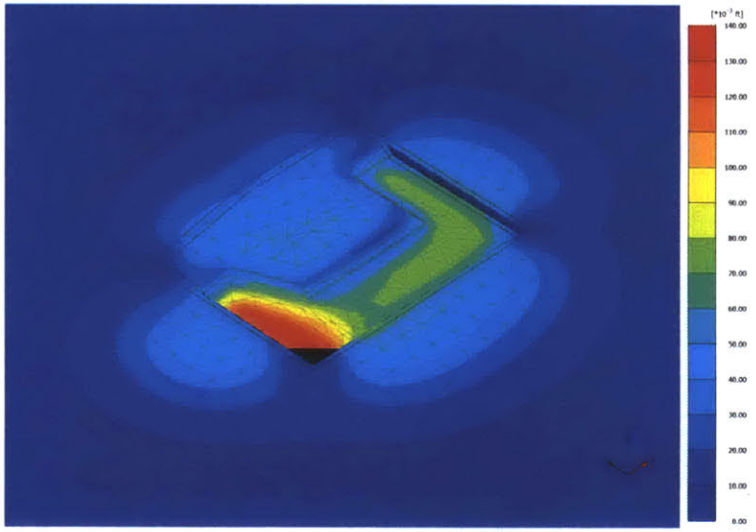

Total ground deformations

Figure 4-7: Excavation Progress on December 27, 2000 and 3D Finite Element Analysis Predictions (Base Case A)

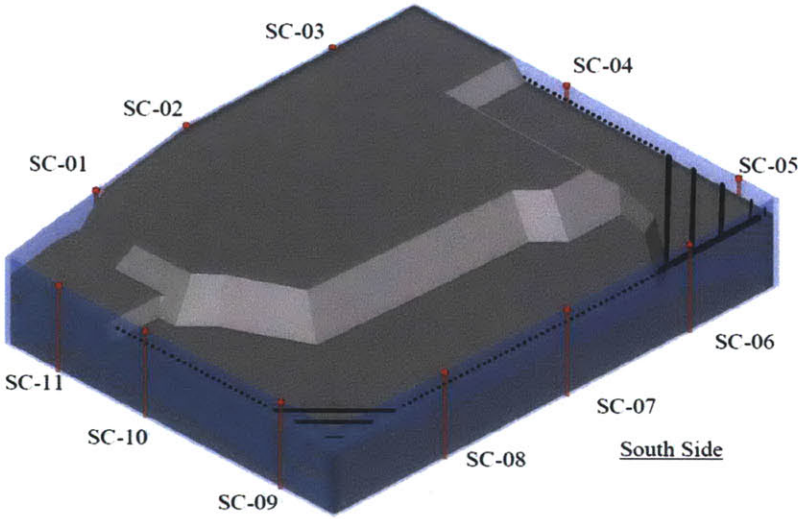

Excavation Progress Data - January 11, 2001

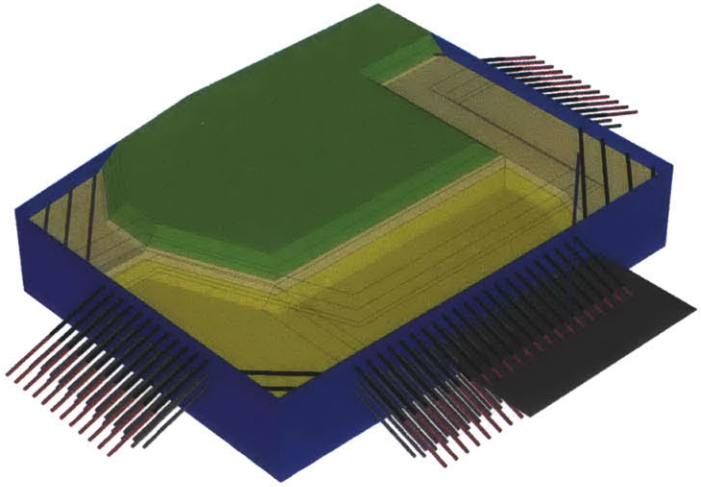

Plaxis 3D Model - Phase #9

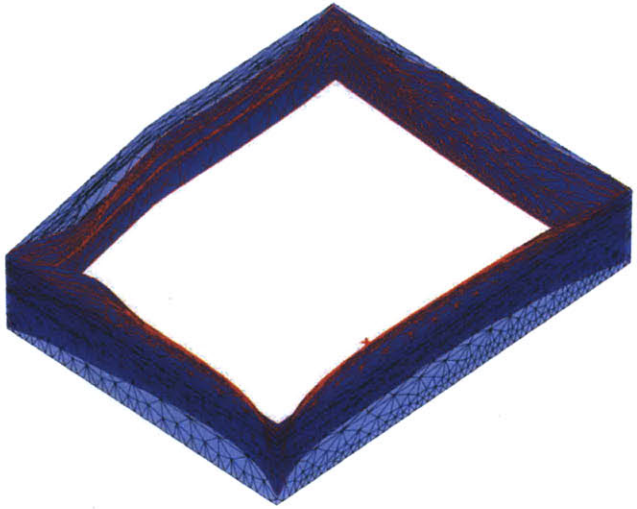

3D Wall Deflections

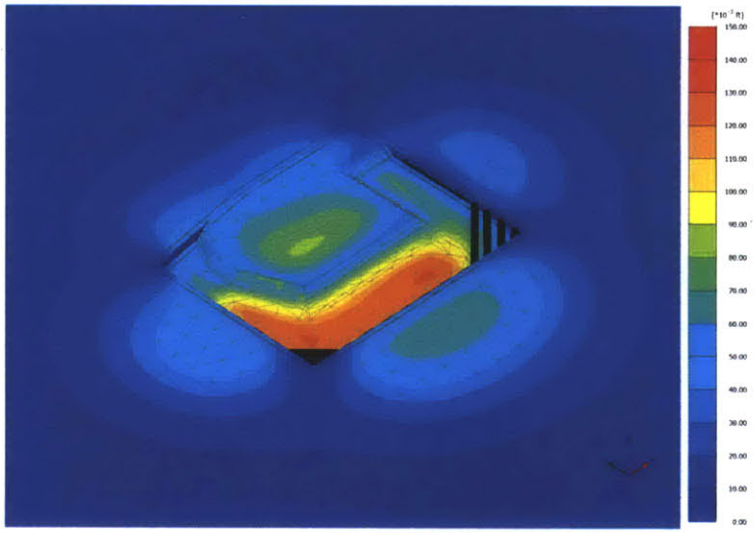

Total ground deformations

Figure 4-8: Excavation Progress on January 11, 2001 and 3D Finite Element Analysis Predictions (Base Case A)

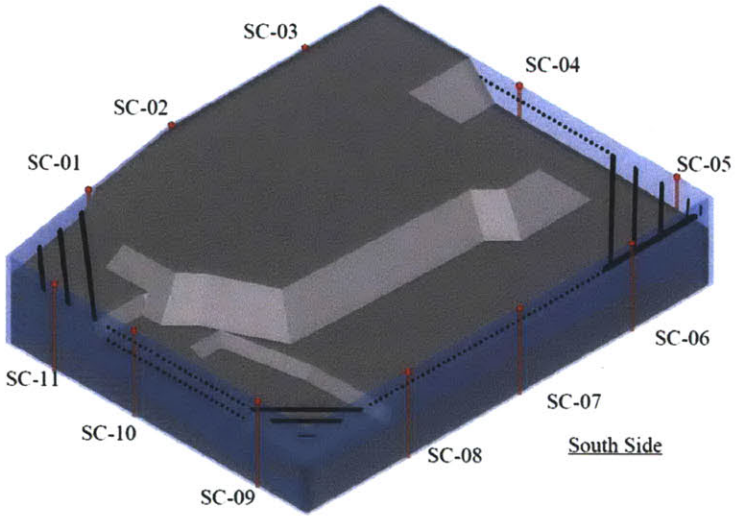

Excavation Progress Data - January 17, 2001

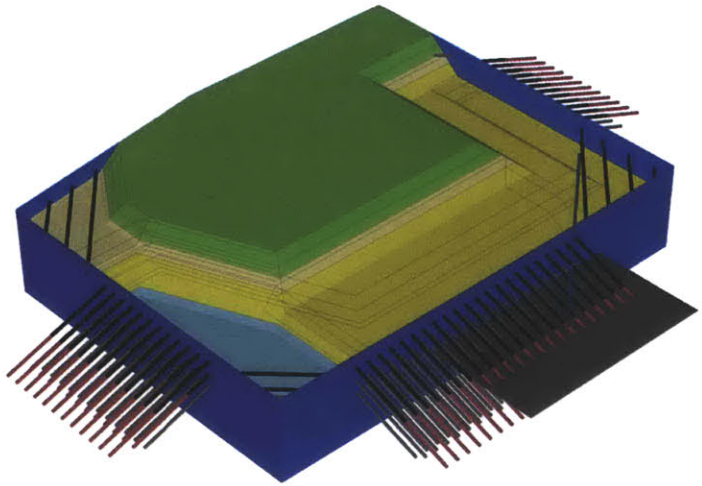

Plaxis 3D Model - Phase #13

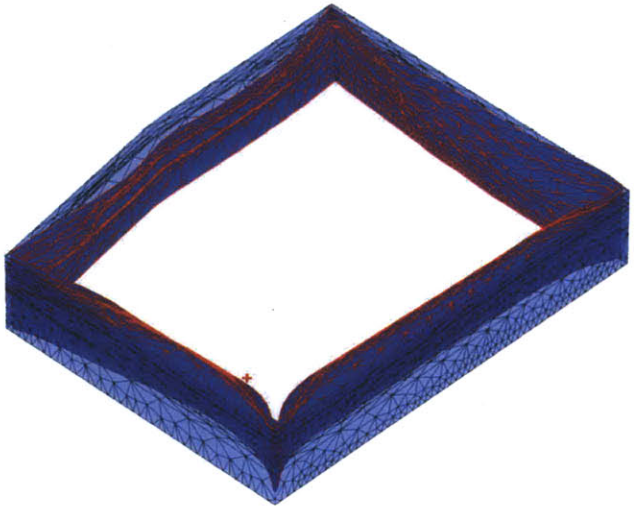

3D Wall Deflections

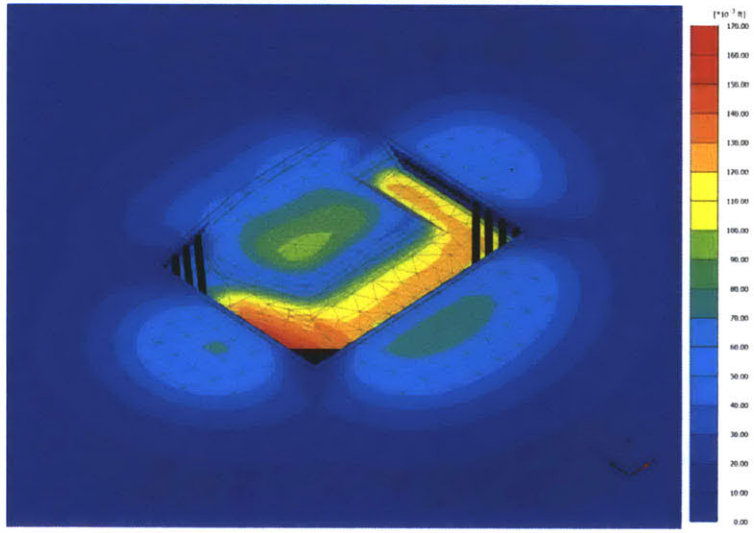

Total ground deformations

Figure 4-9: Excavation Progress on January 17, 2001 and 3D Finite Element Analysis Predictions (Base Case A)

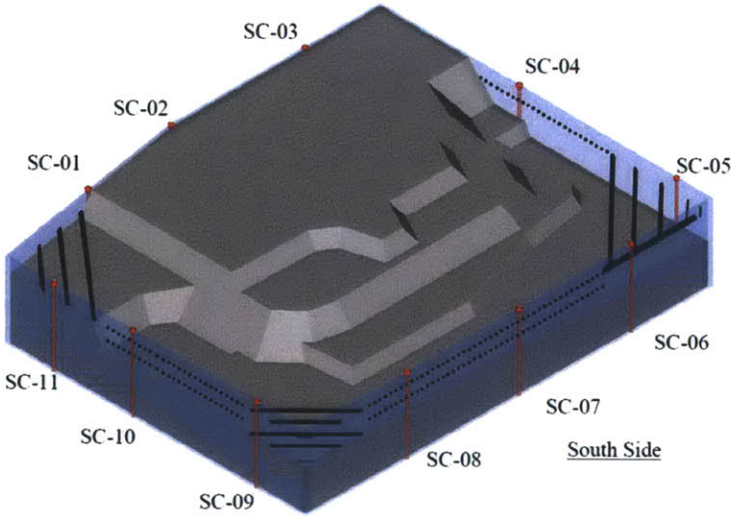

Excavation Progress Data - January 29, 2001

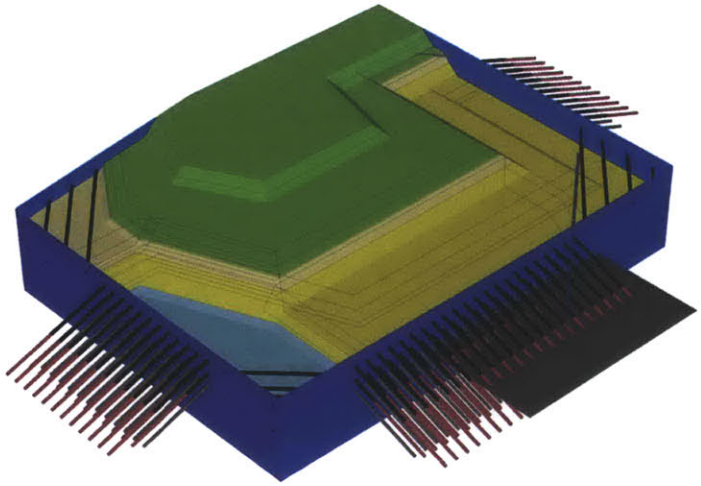

Plaxis 3D Model - Phase #16

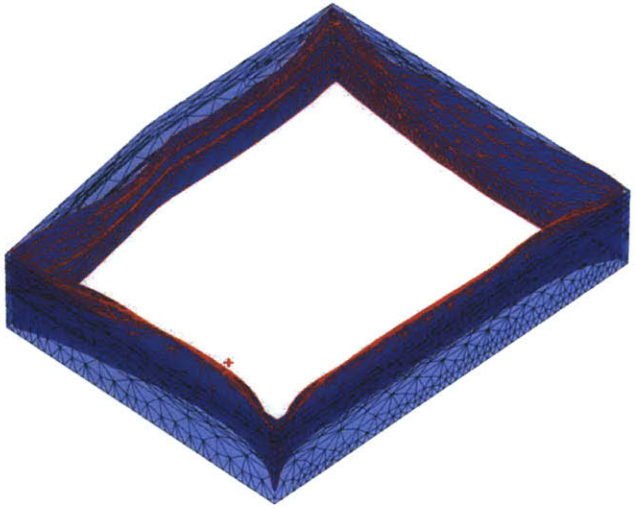

3D Wall Deflections

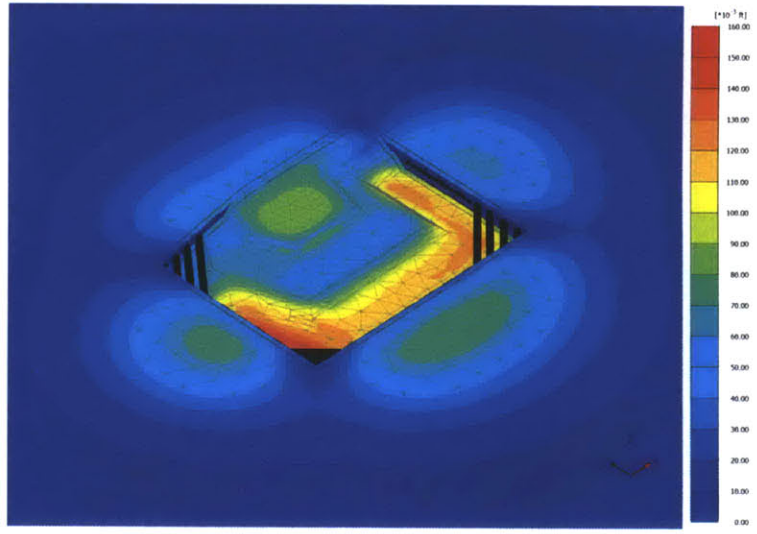

Total ground deformations

Figure 4-10: Excavation Progress on January 29, 2001 and 3D Finite Element Analysis Predictions (Base Case A)

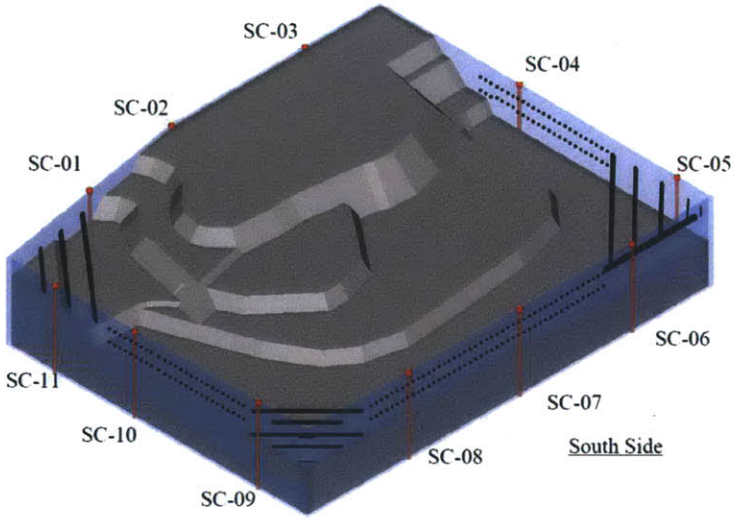

Excavation Progress Data - February 6, 2001

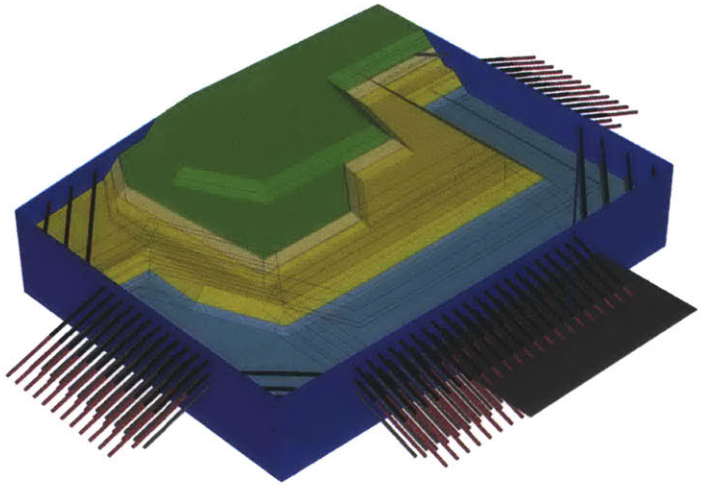

Plaxis 3D Model - Phase #18

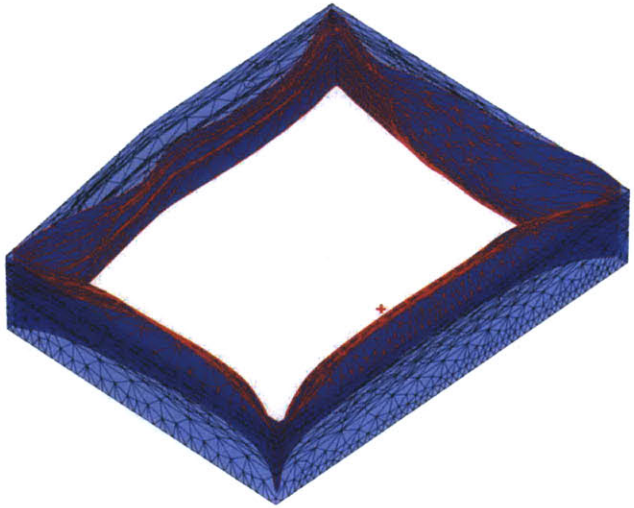

3D Wall Deflections

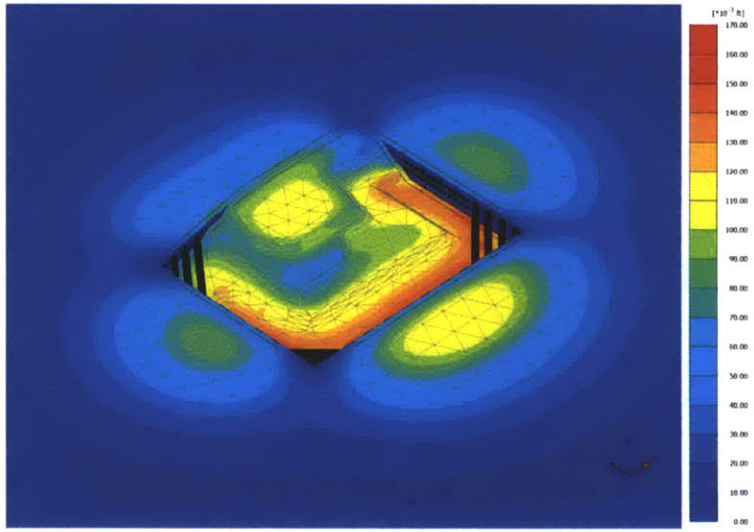

Total ground deformations

Figure 4-11: Excavation Progress on February 6, 2001 and 3D Finite Element Analysis Predictions (Base Case A)

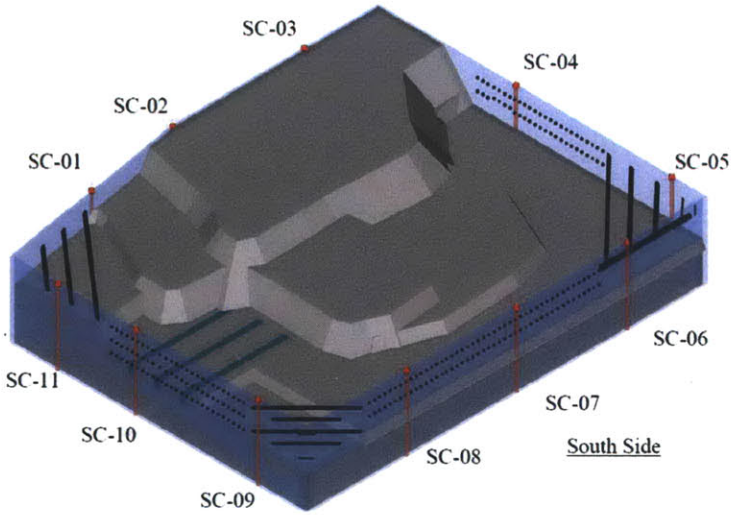

Excavation Progress Data - February 13, 2001

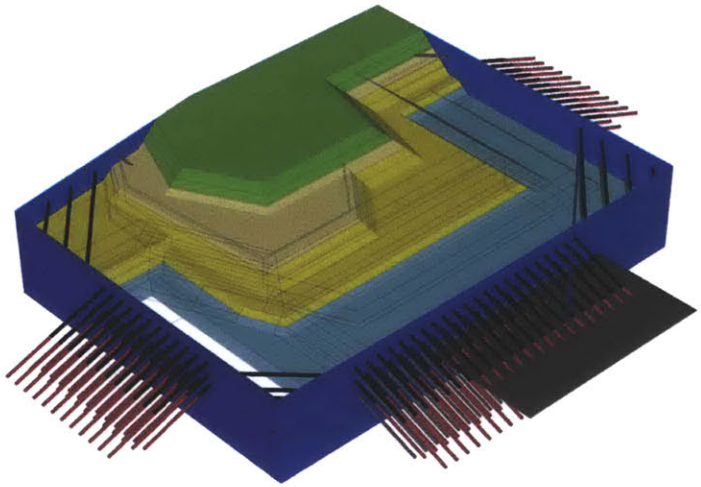

Plaxis 3D Model - Phase #21

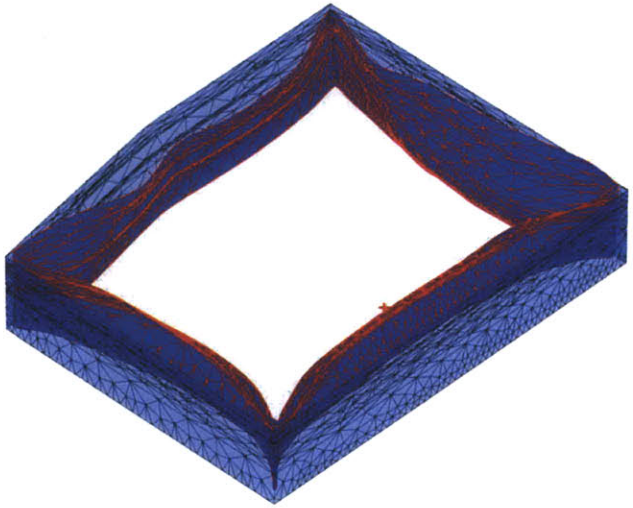

3D Wall Deflections

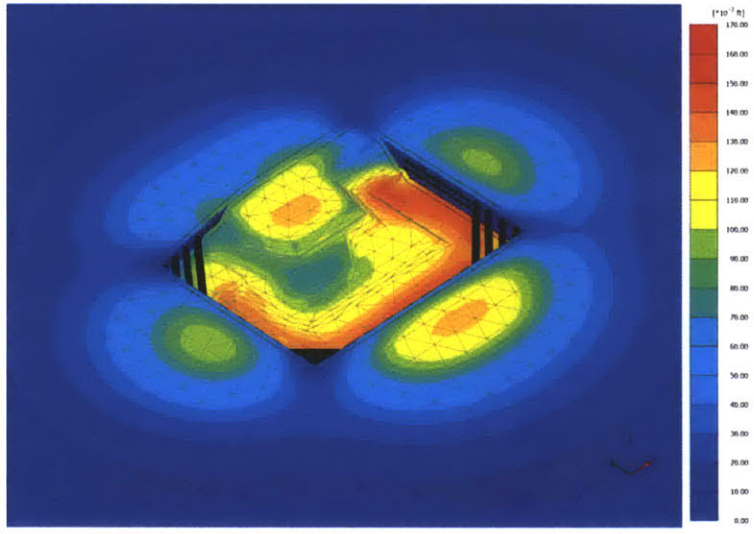

Total ground deformations

Figure 4-12: Excavation Progress on February 13, 2001 and 3D Finite Element Analysis Predictions (Base Case A)

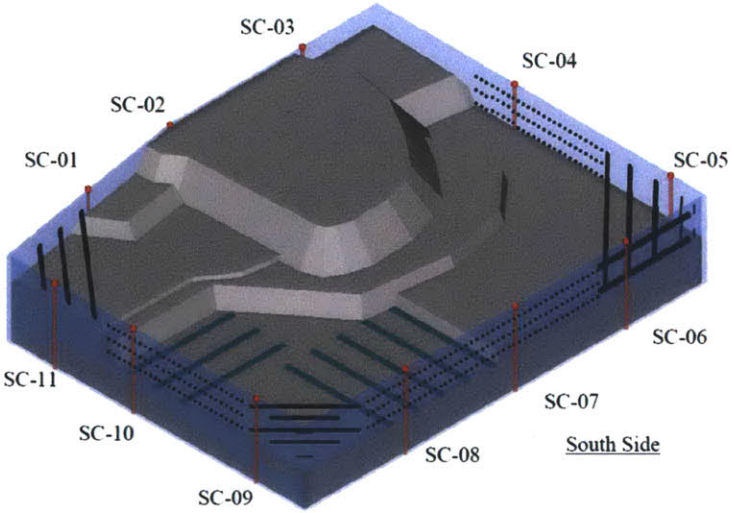

Excavation Progress Data - February 23, 2001

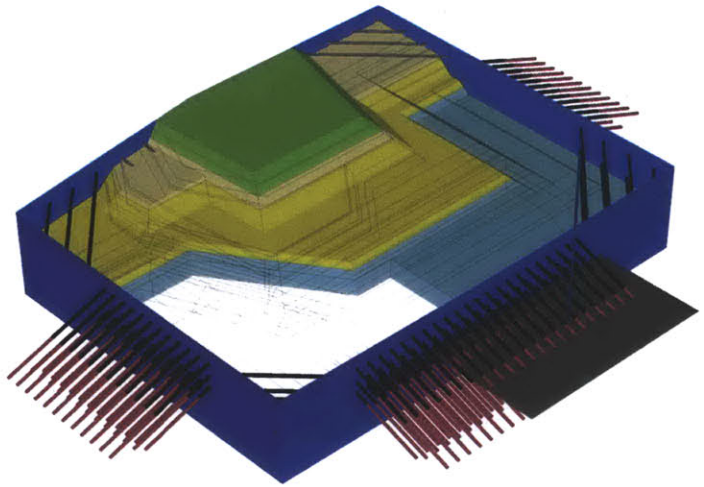

Plaxis 3D Model - Phase #25

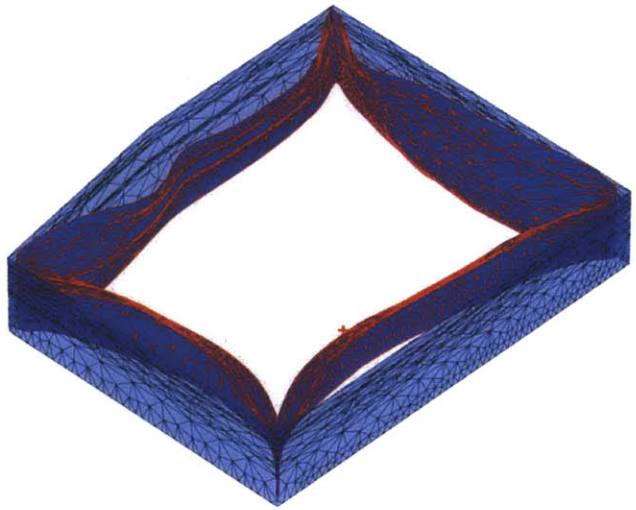

3D Wall Deflections

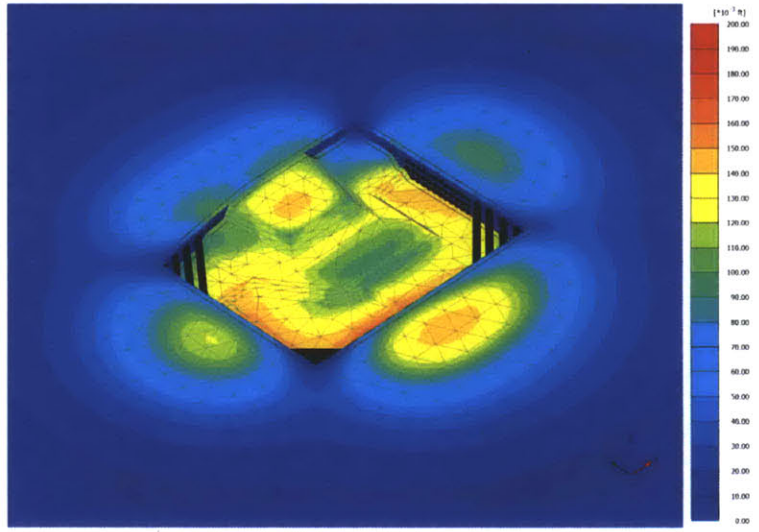

Total ground deformations

Figure 4-13: Excavation Progress on February 23, 2001 and 3D Finite Element Analysis Predictions (Base Case A)

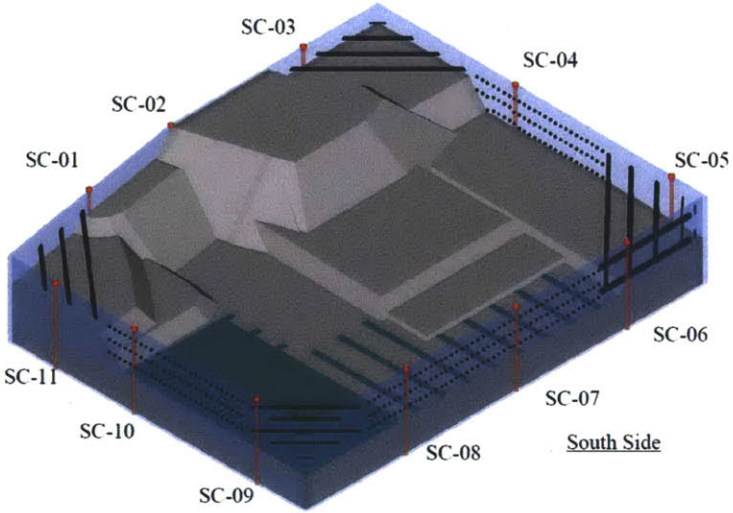

Excavation Progress Data - March 14, 2001

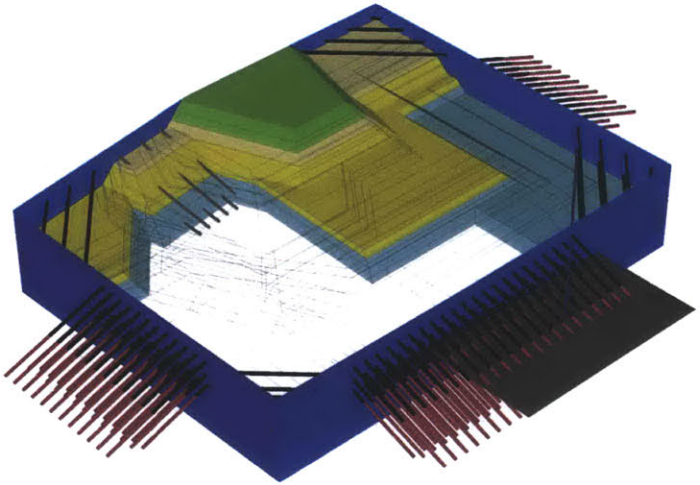

Plaxis 3D Model - Phase #27

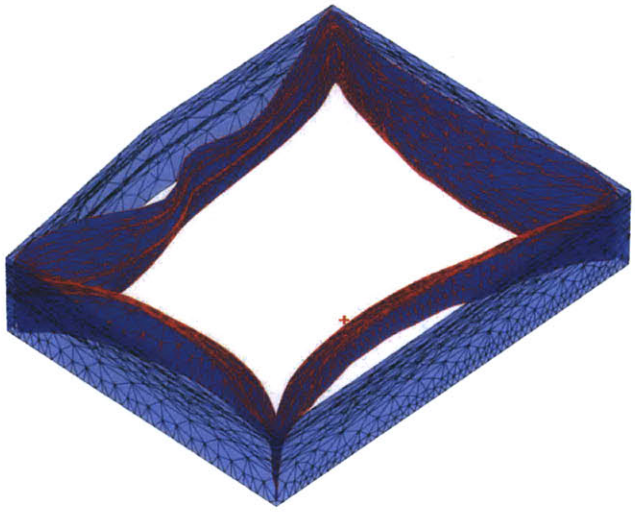

3D Wall Deflections

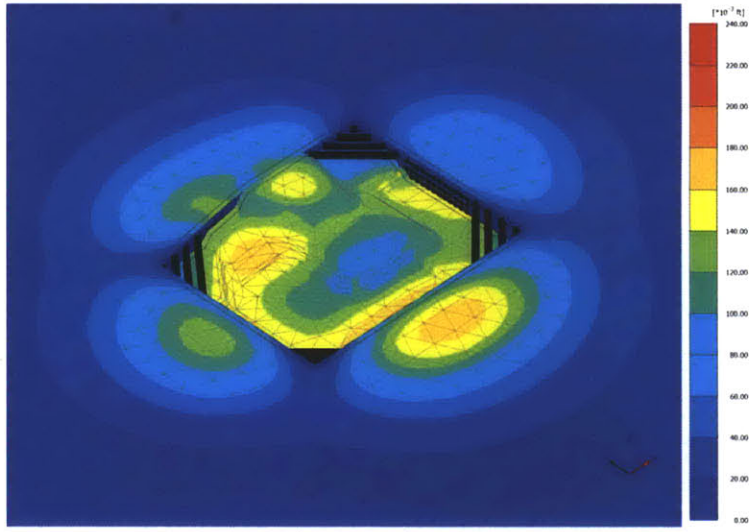

Total ground deformations

Figure 4-14: Excavation Progress on March 14, 2001 and 3D Finite Element Analysis Predictions (Base Case A)

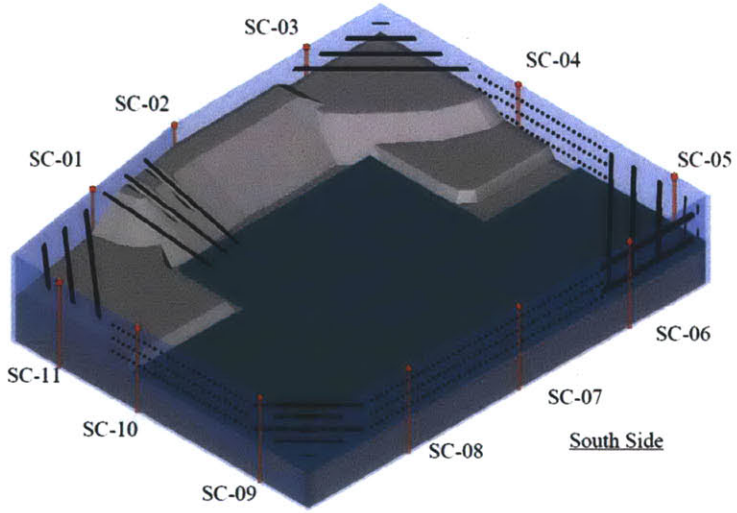

Excavation Progress Data - April 25, 2001

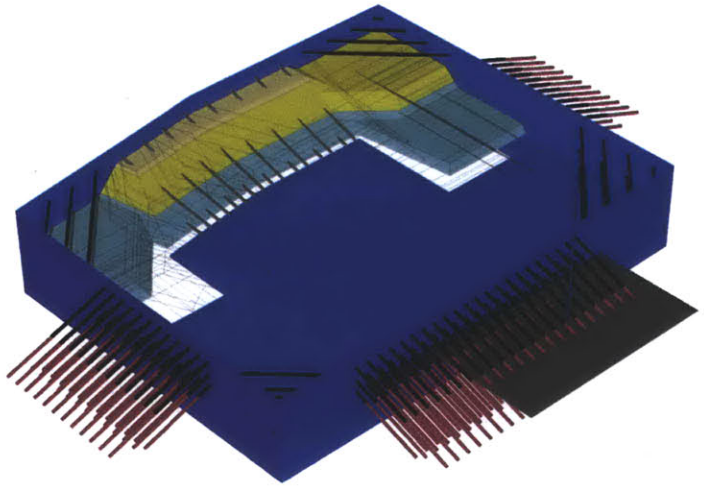

Plaxis 3D Model - Phase #29

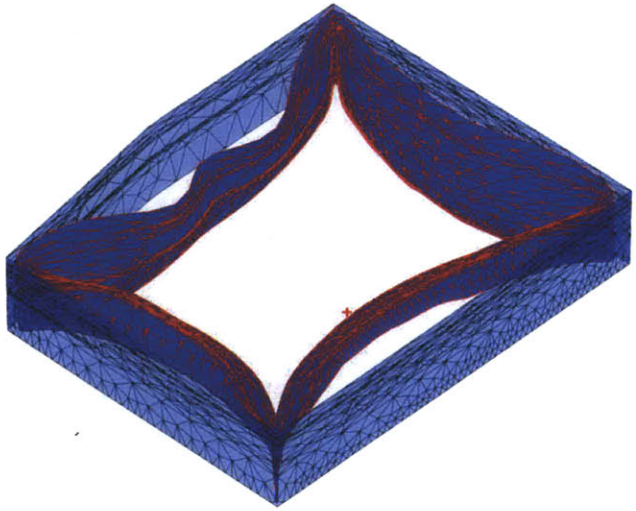

3D Wall Deflections

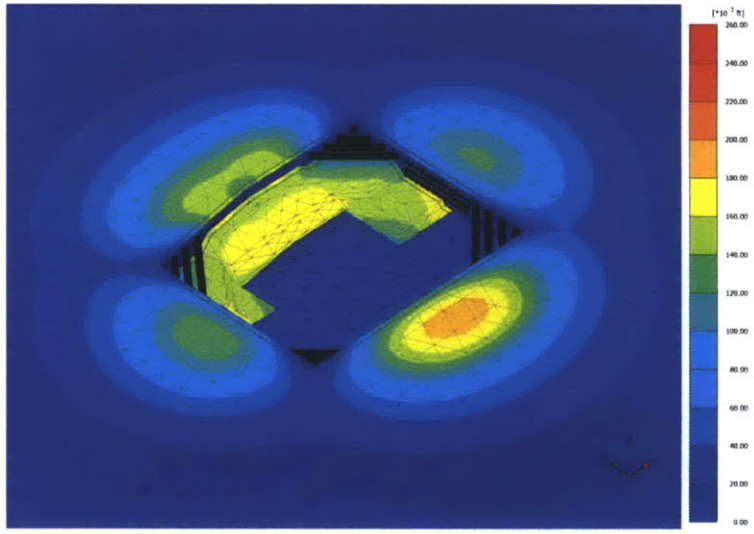

Total ground deformations

Figure 4-15: Excavation Progress on April 25, 2001 and 3D Finite Element Analysis Predictions (Base Case A)

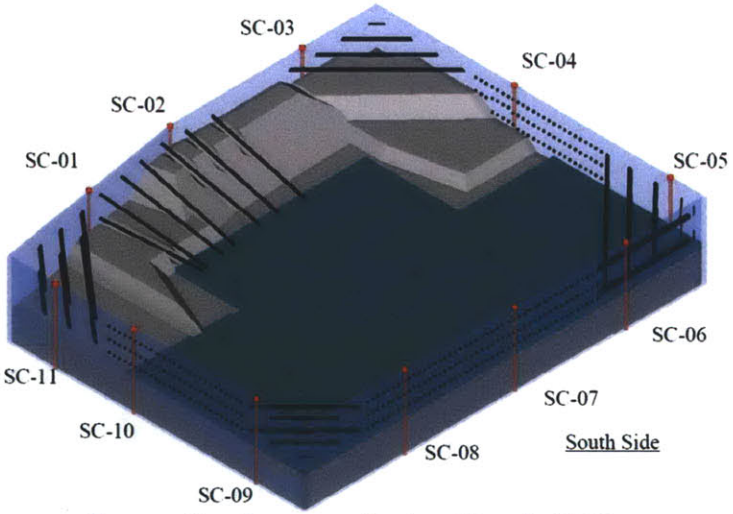

Excavation Progress Data - May 8, 2001

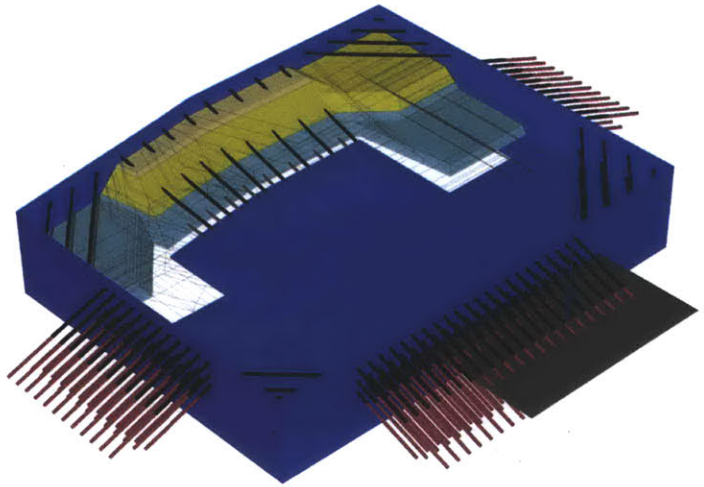

Plaxis 3D Model - Phase #30

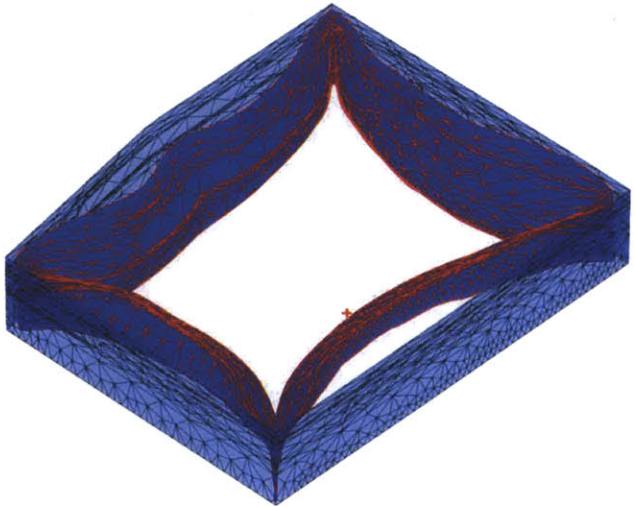

3D Wall Deflections

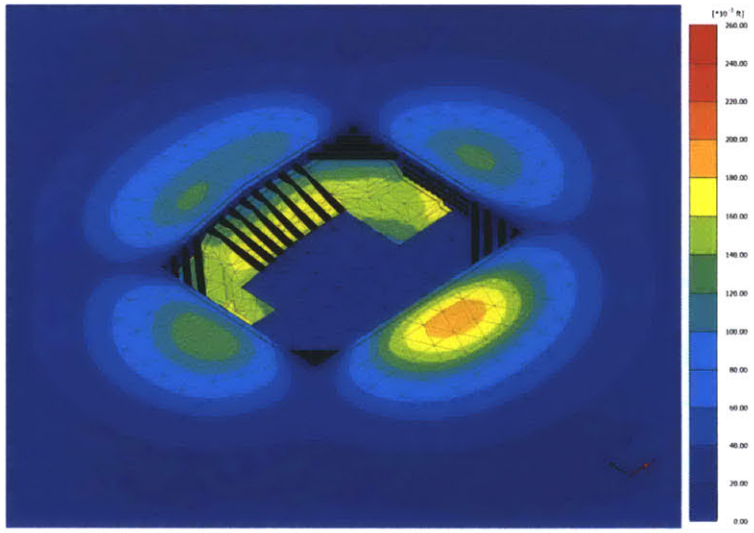

Total ground deformations

Figure 4-16: Excavation Progress on May 8, 2001 and 3D Finite Element Analysis Predictions (Base Case A)

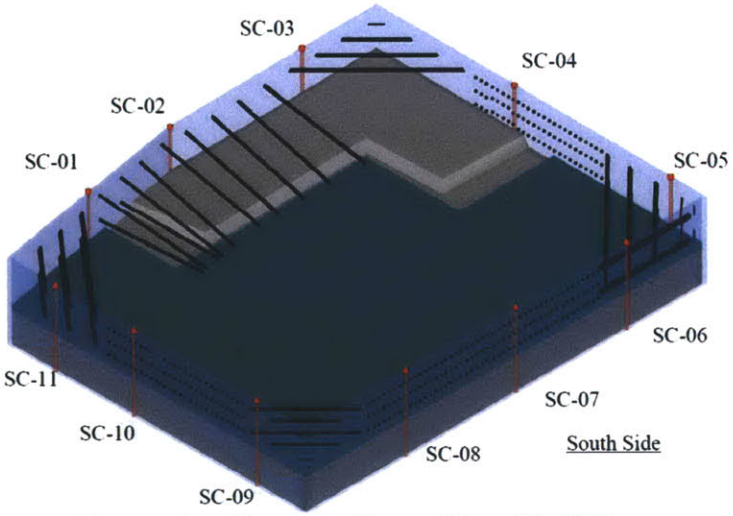

Excavation Progress Data - May 17, 2001

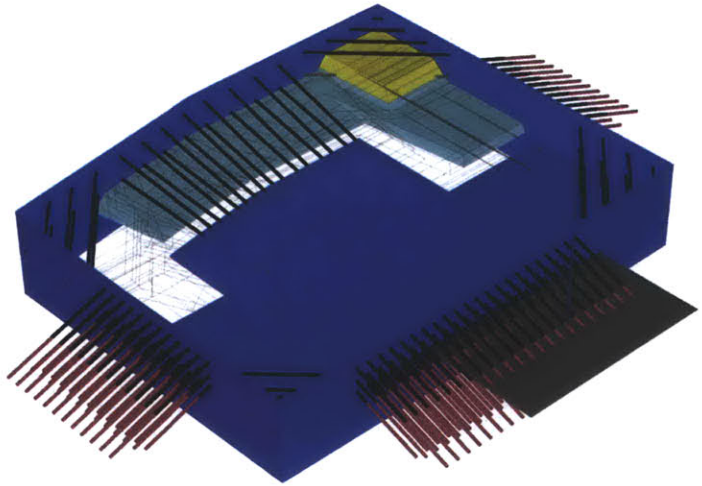

Plaxis 3D Model - Phase #33

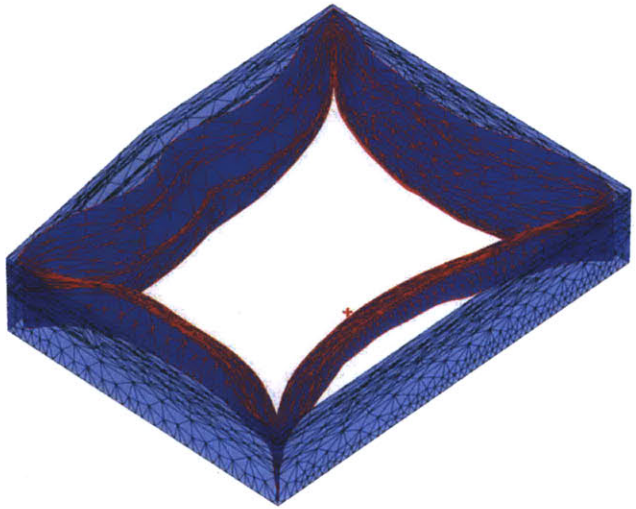

3D Wall Deflections

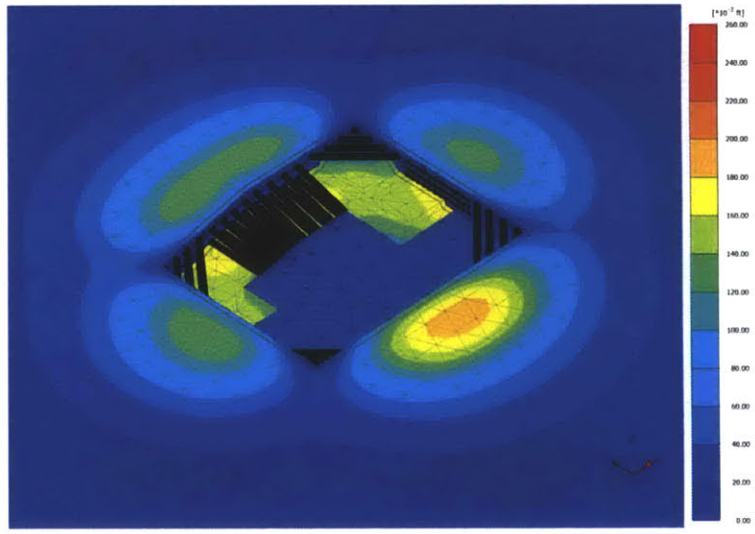

Total ground deformations

Figure 4-17: Excavation Progress on May 17, 2001 and 3D Finite Element Analysis Predictions (Base Case A)

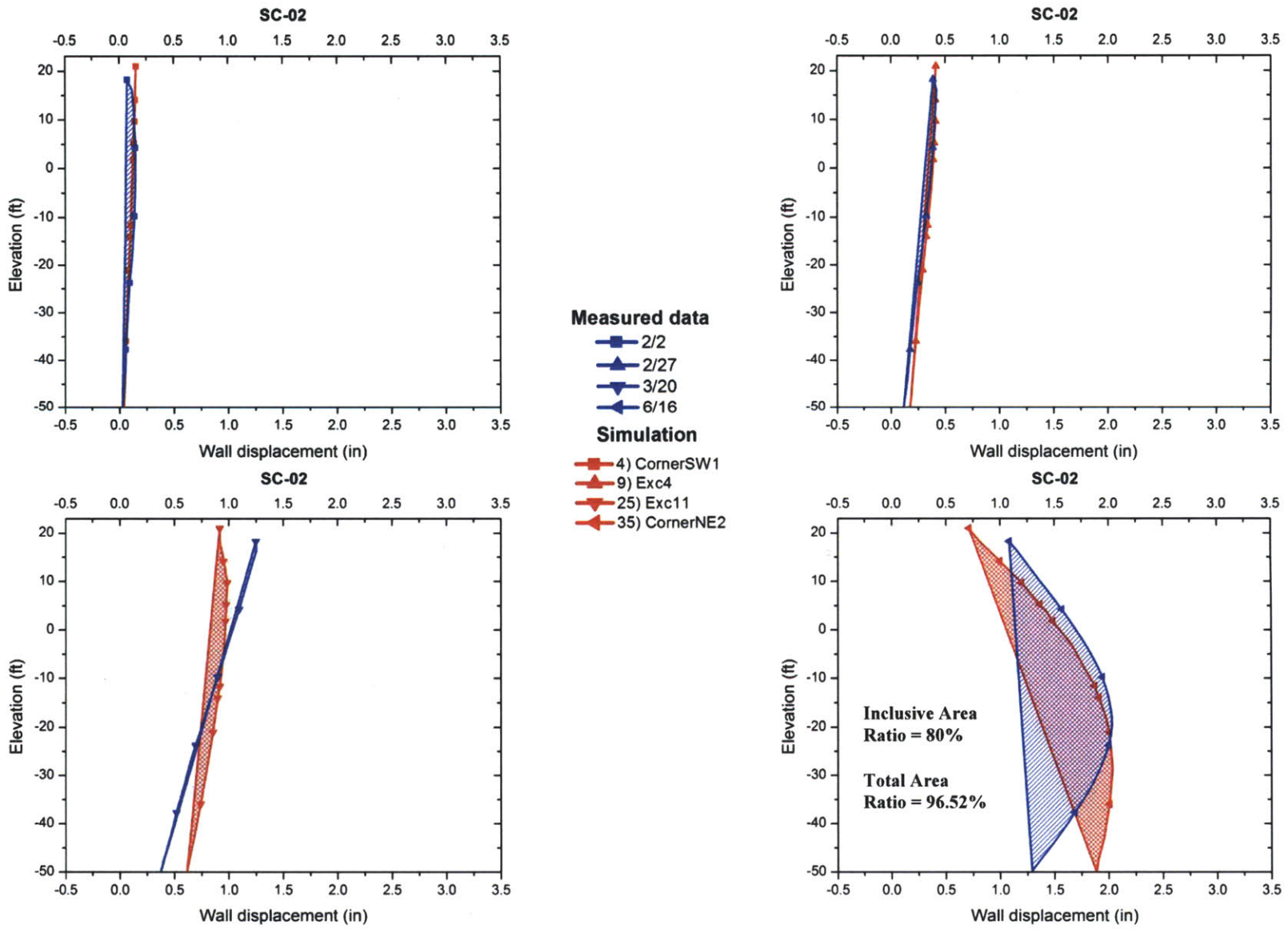

Figure 4-18: Wall Deflections Comparison Technique for the North Wall - Measured Data vs. Simulation (Base Case A)

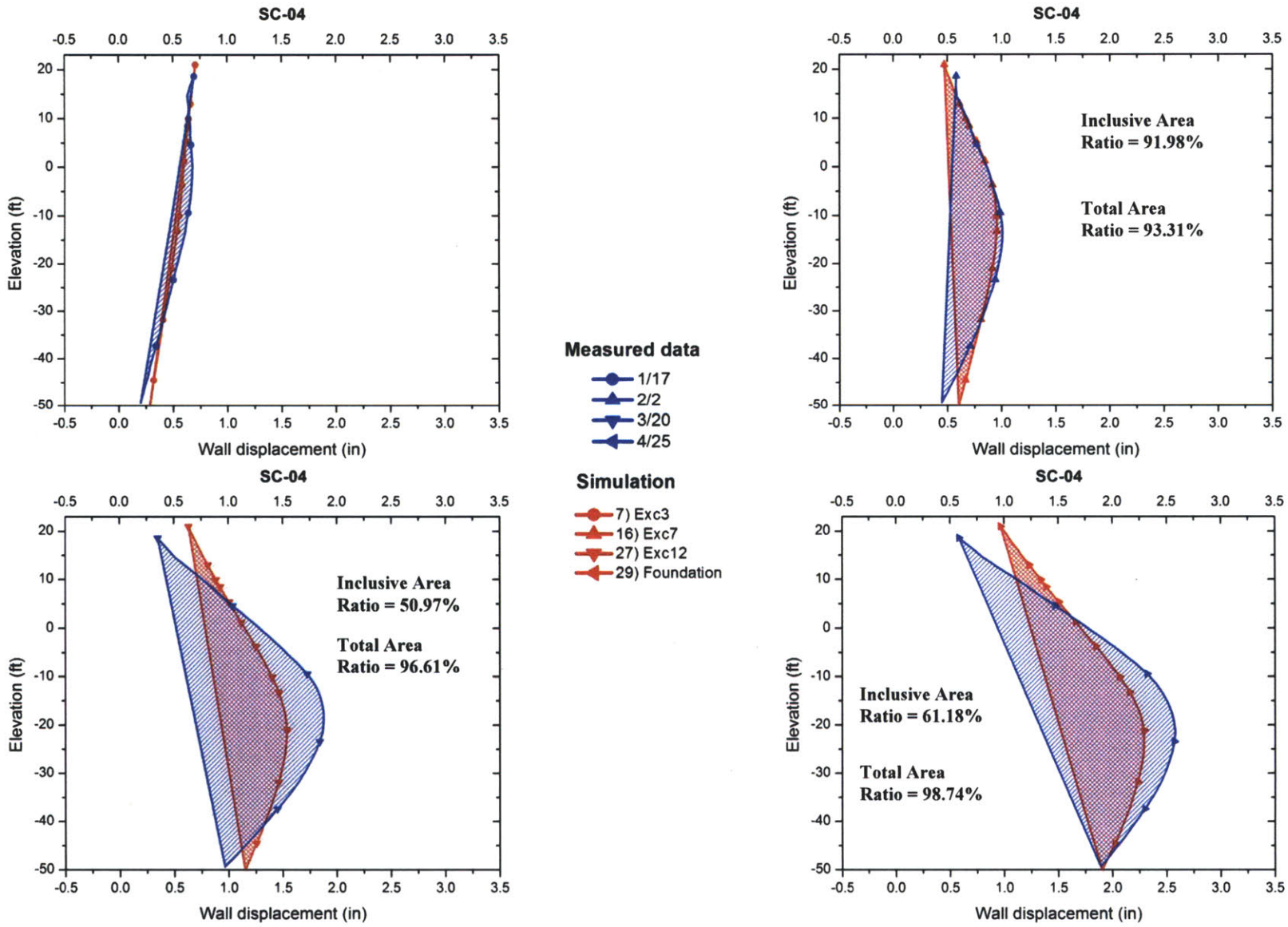

Figure 4-19: Wall Deflections Comparison Technique for the East Wall - Measured Data vs. Simulation (Base Case A)

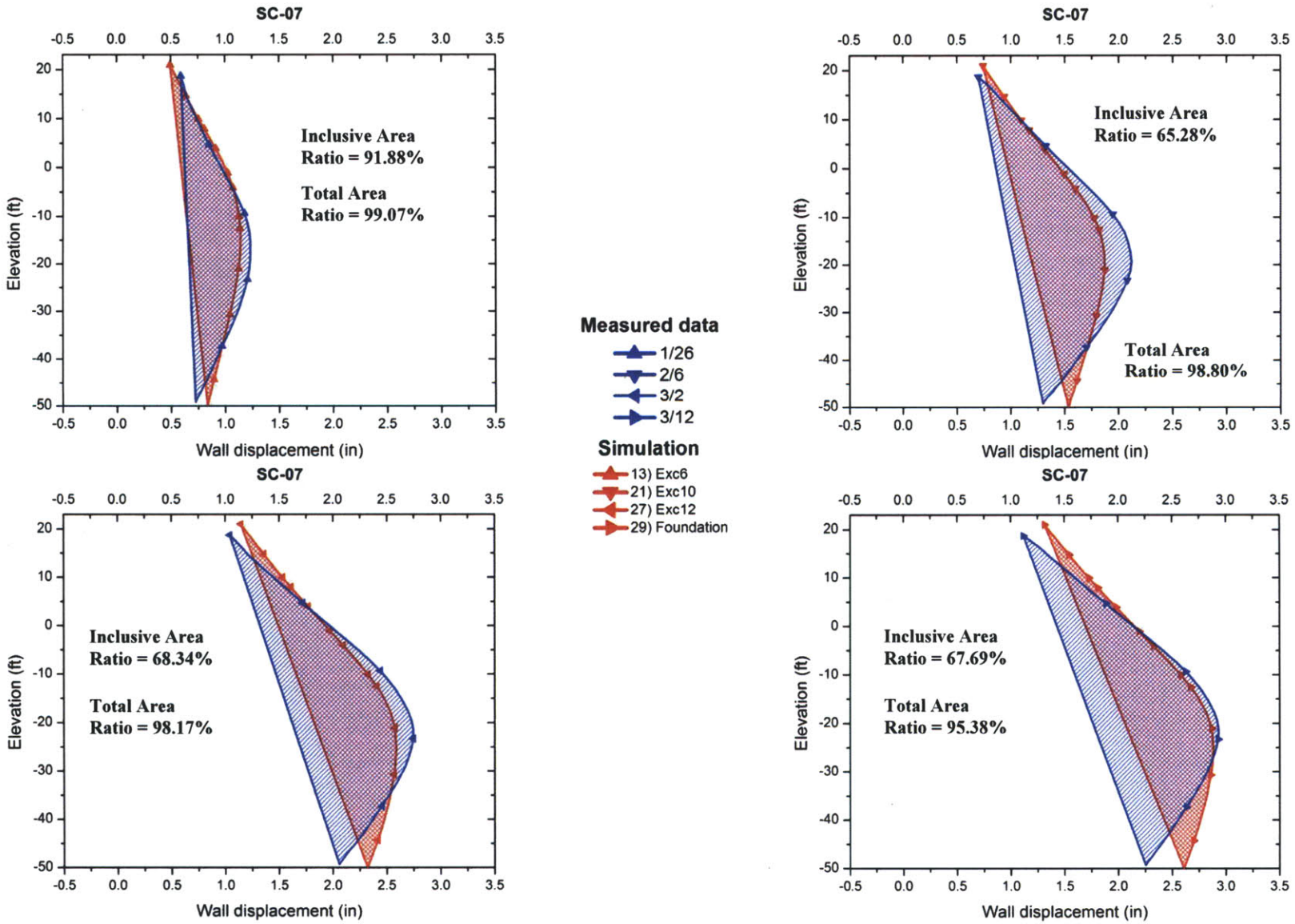

Figure 4-20: Wall Deflections Comparison Technique for the South Wall - Measured Data vs. Simulation (Base Case A)

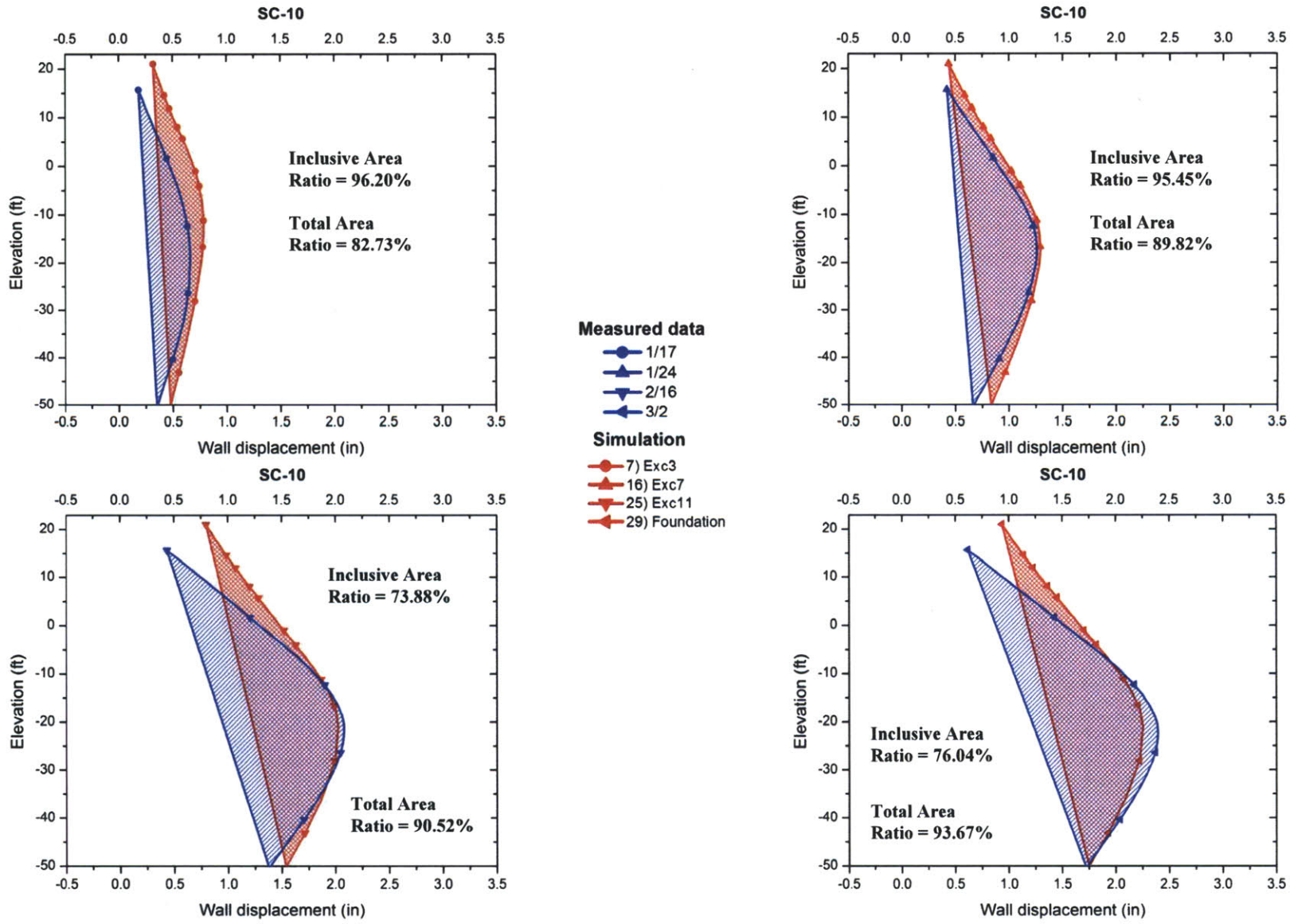

Figure 4-21: Wall Deflections Comparison Technique for the West Wall - Measured Data vs. Simulation (Base Case A)

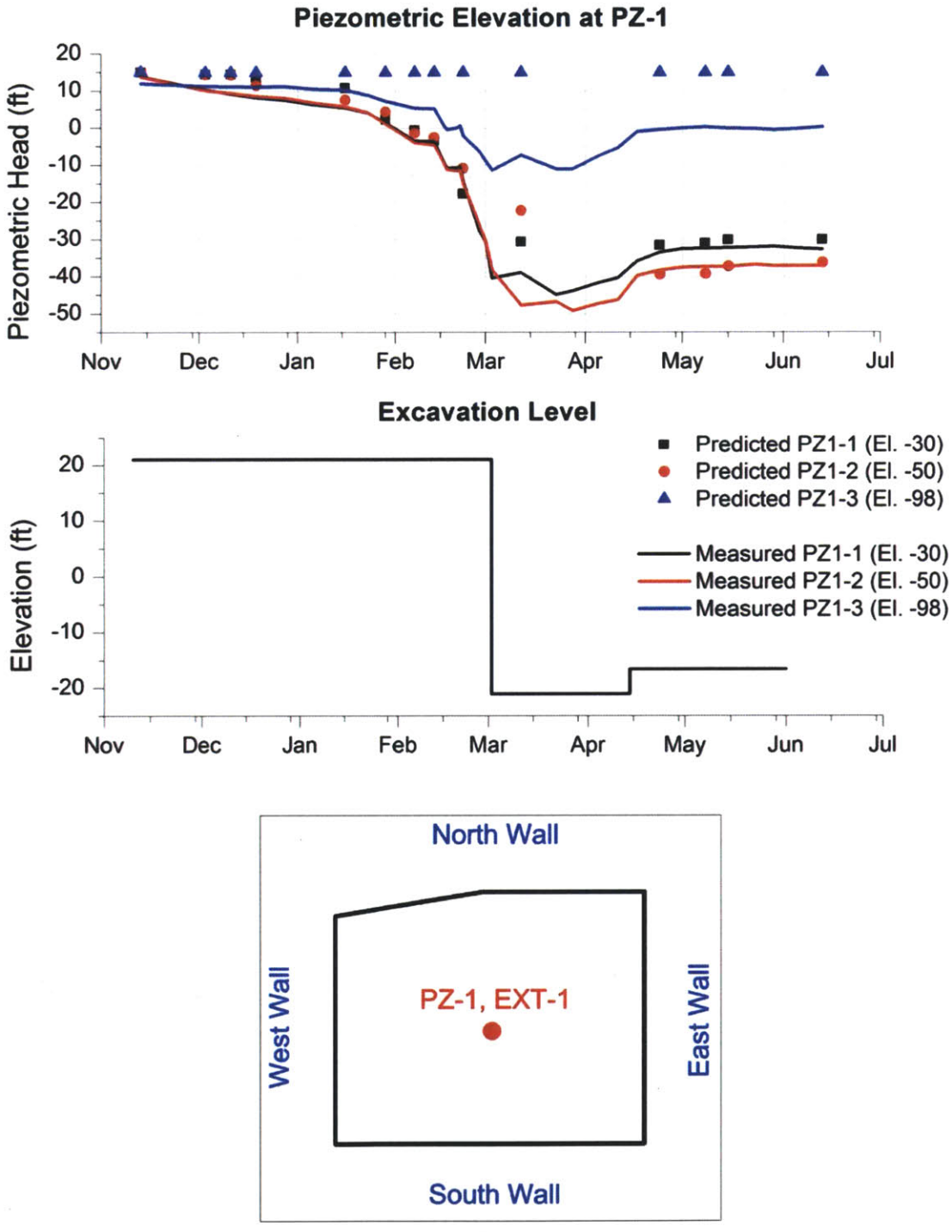

Figure 4-22: Piezometric elevations measured by PZ-1 vs. 3D Finite Element Analysis predictions (Base Case A)

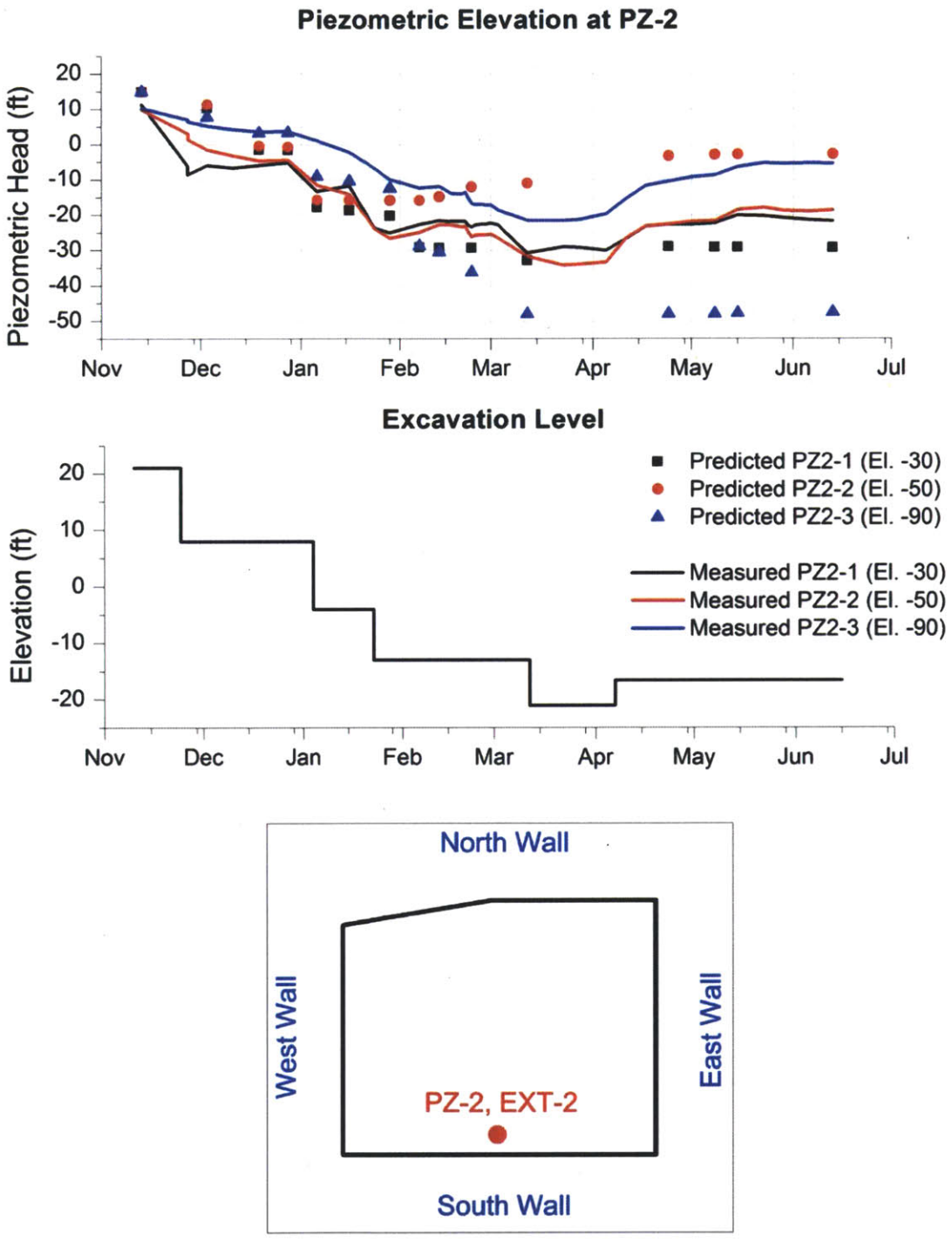

Figure 4-23: Piezometric elevations measured by PZ-2 vs. 3D Finite Element Analysis predictions (Base Case A)

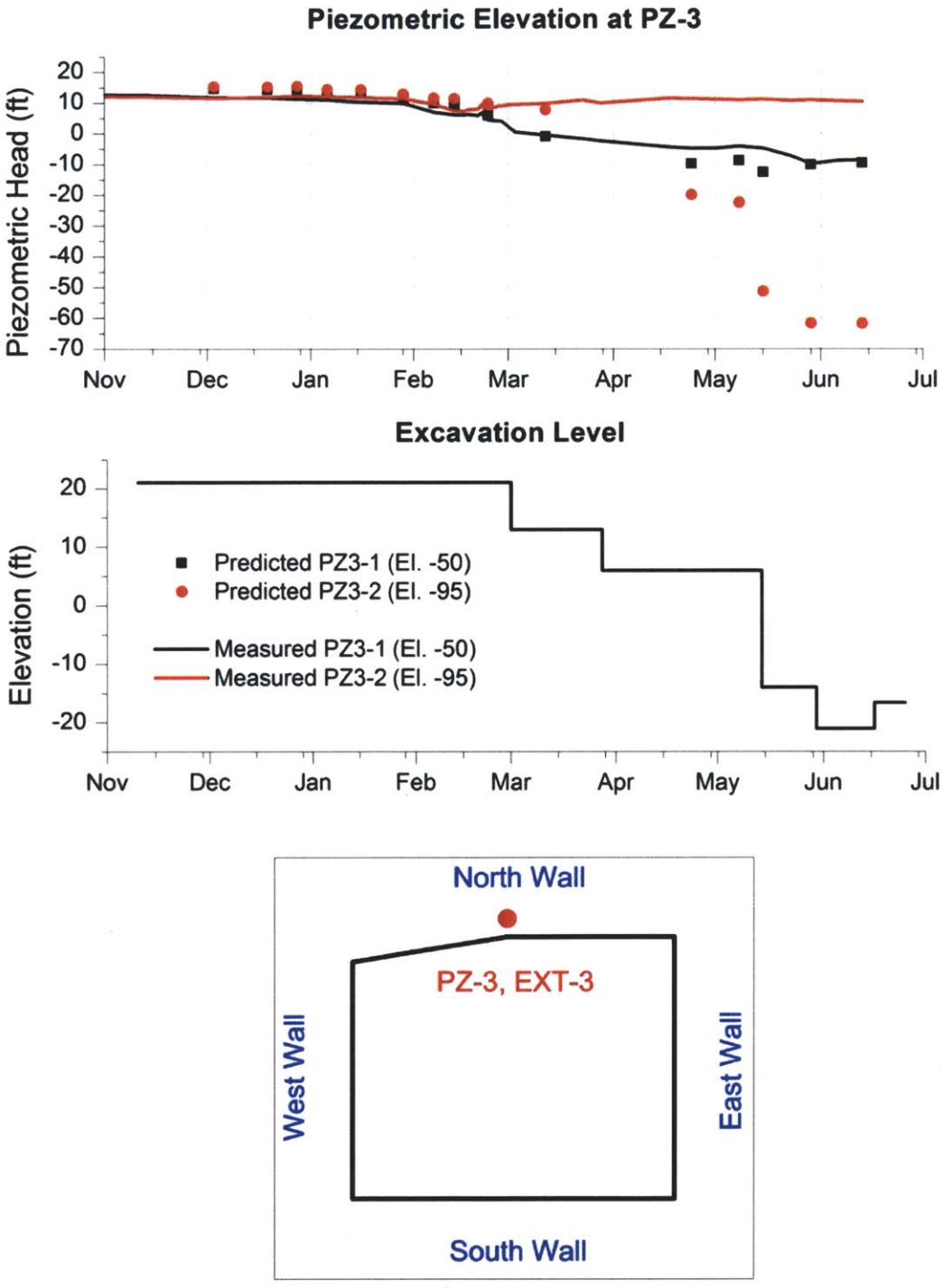

Figure 4-24: Piezometric elevations measured by PZ-3 vs. 3D Finite Element Analysis predictions (Base Case A)

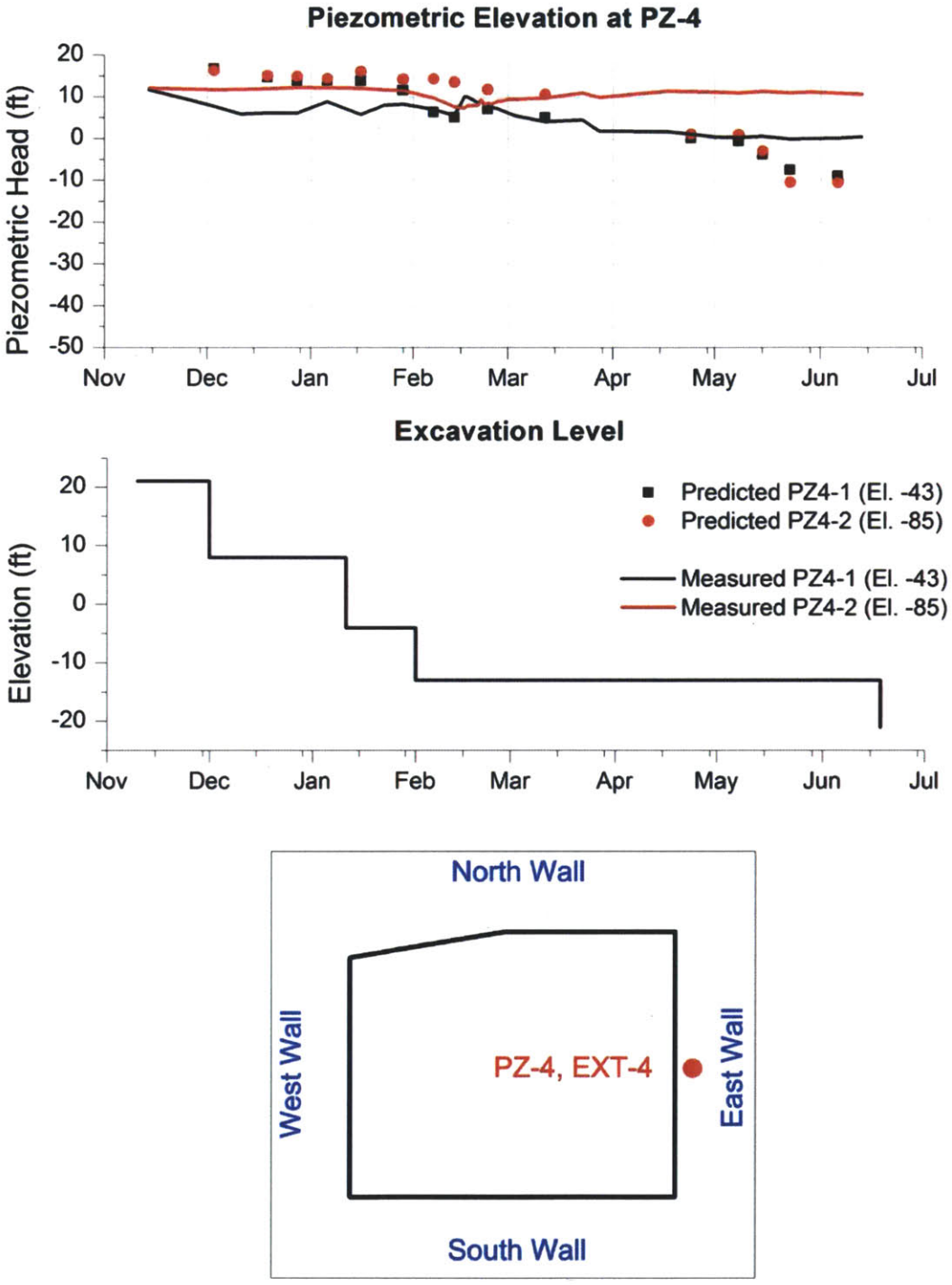

Figure 4-25: Piezometric elevations measured by PZ-4 vs. 3D Finite Element Analysis predictions (Base Case A)

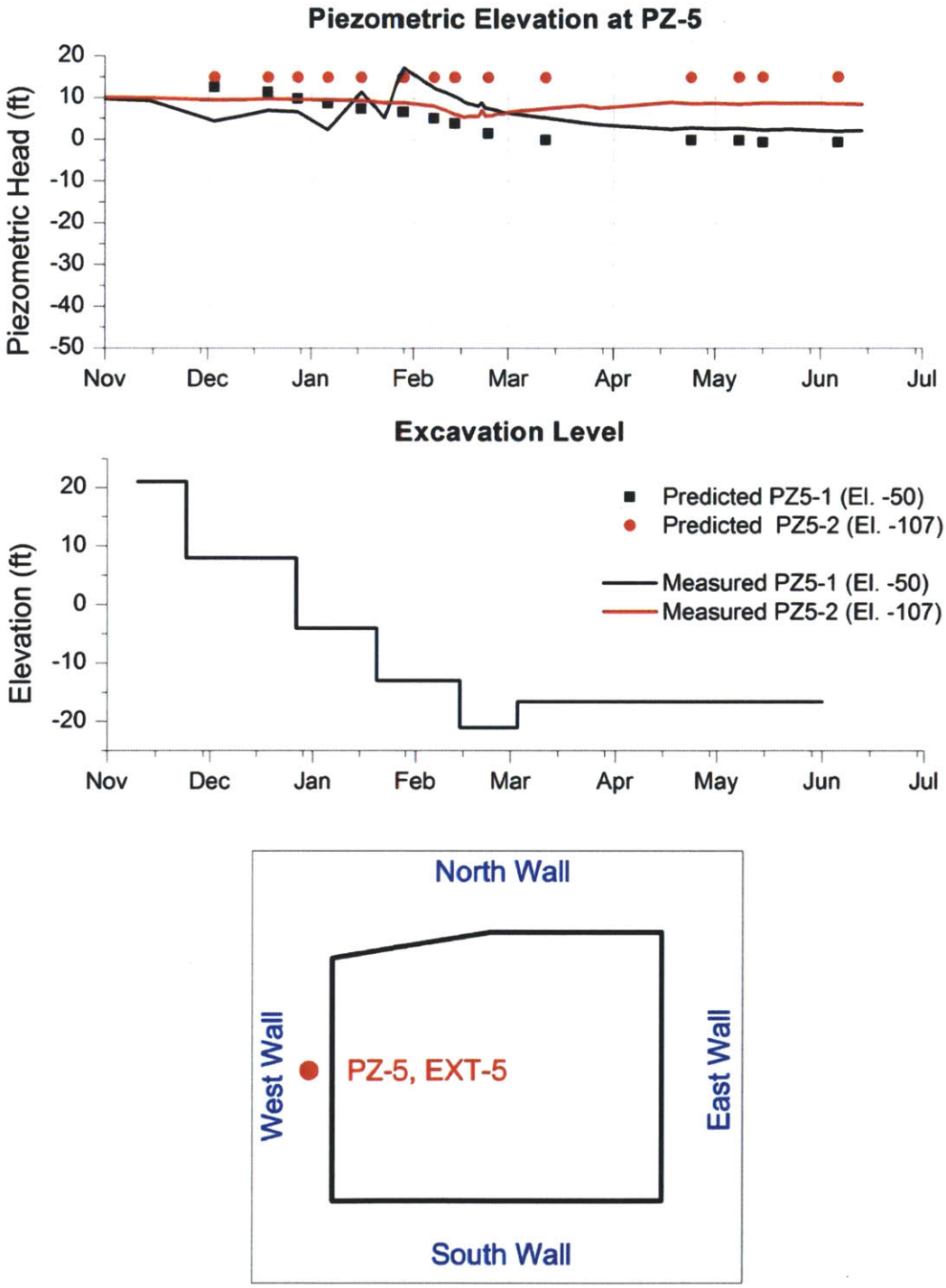

Figure 4-26: Piezometric elevations measured by PZ-5 vs. 3D Finite Element Analysis predictions (Base Case A)

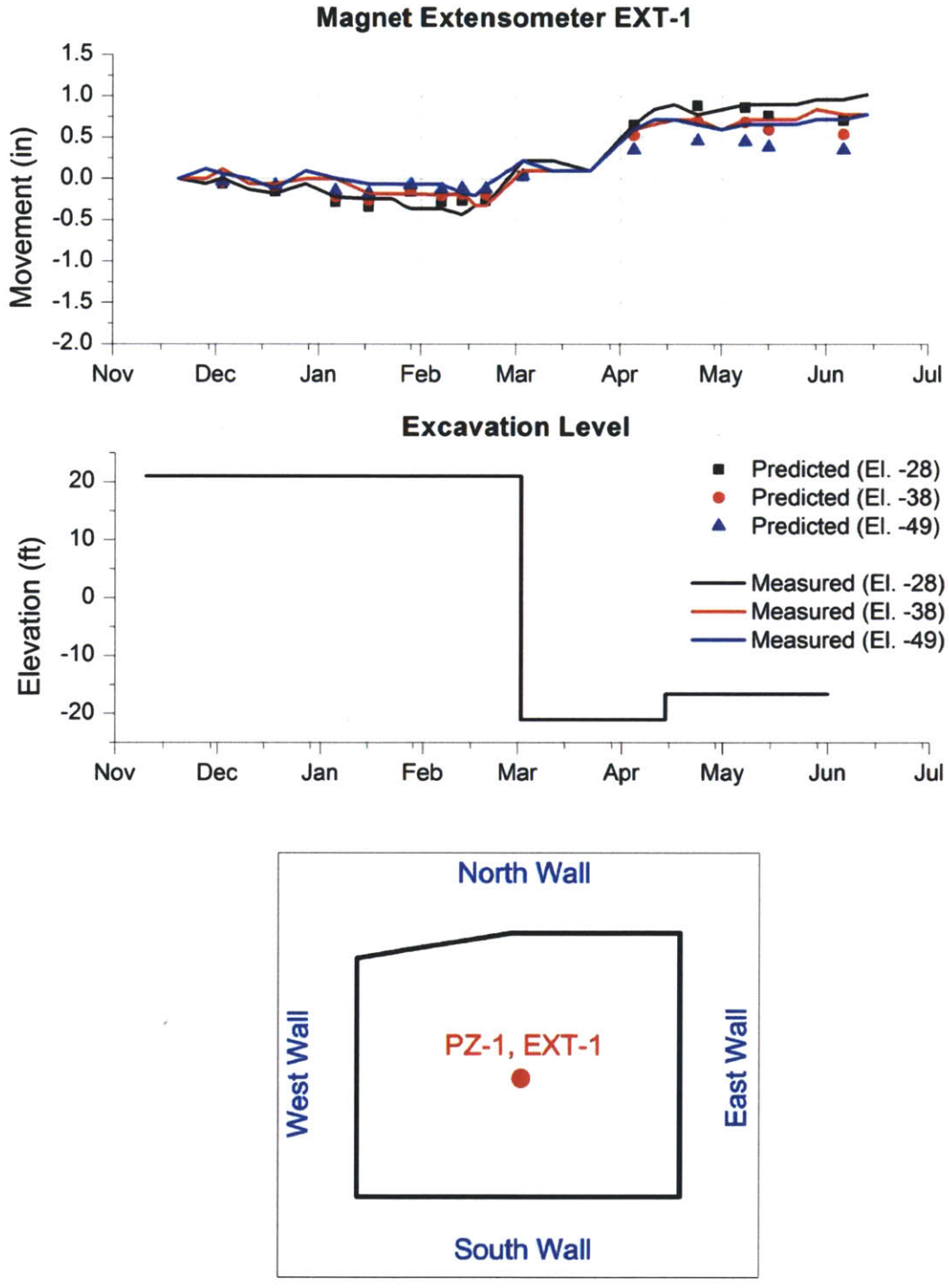

Figure 4-27: Vertical Ground Movements measured by EXT-1 (upper level) vs. 3D Finite Element Analysis predictions (Base Case A)

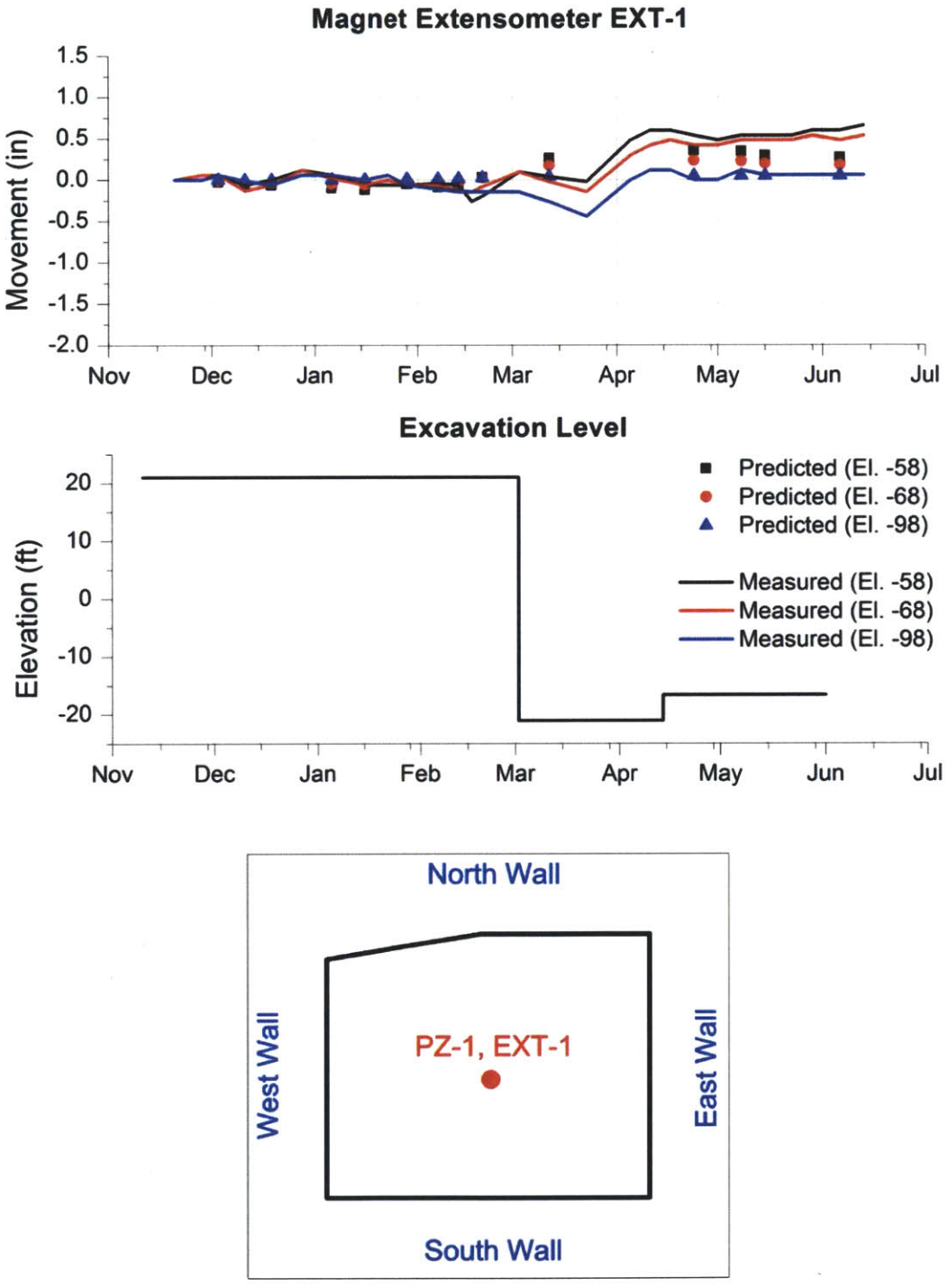

Figure 4-28: Vertical Ground Movements measured by EXT-1 (lower level) vs. 3D Finite Element Analysis predictions (Base Case A)

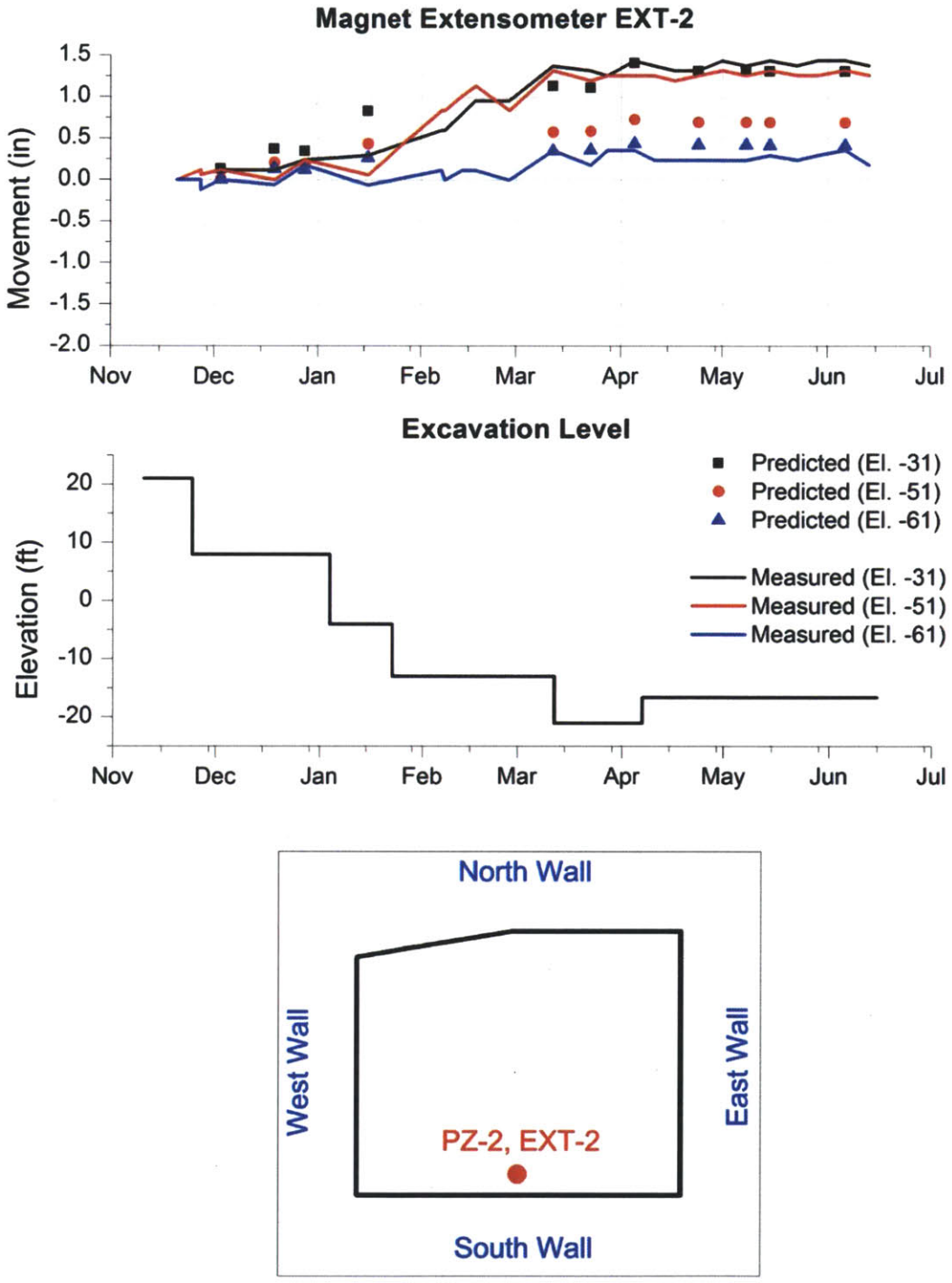

Figure 4-29: Vertical Ground Movements measured by EXT-2 (upper level) vs. 3D Finite Element Analysis predictions (Base Case A)

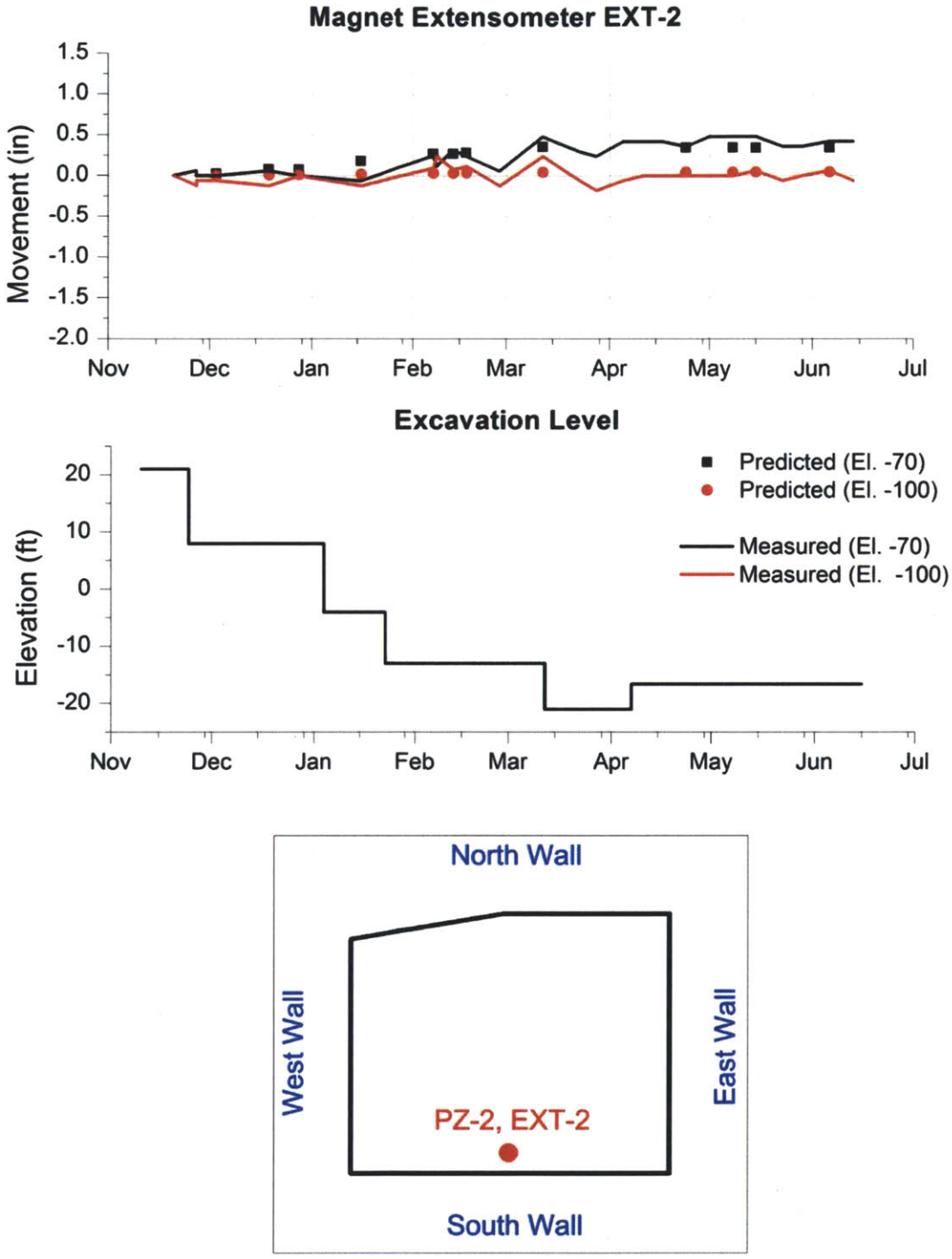

Figure 4-30: Vertical Ground Movements measured by EXT-2 (lower level) vs. 3D Finite Element Analysis predictions (Base Case A)

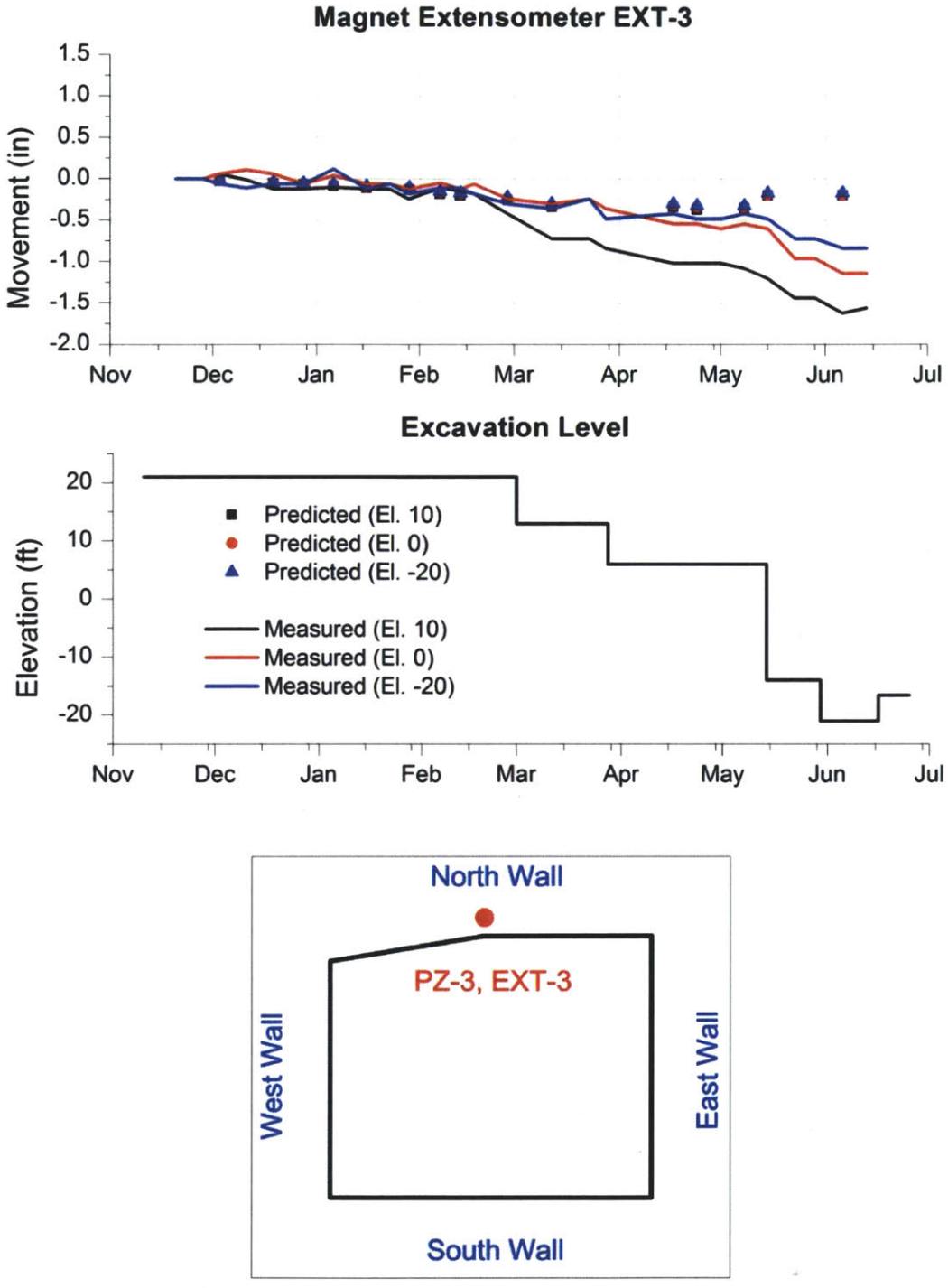

Figure 4-31: Vertical Ground Movements measured by EXT-3 (upper level) vs. 3D Finite Element Analysis predictions (Base Case A)

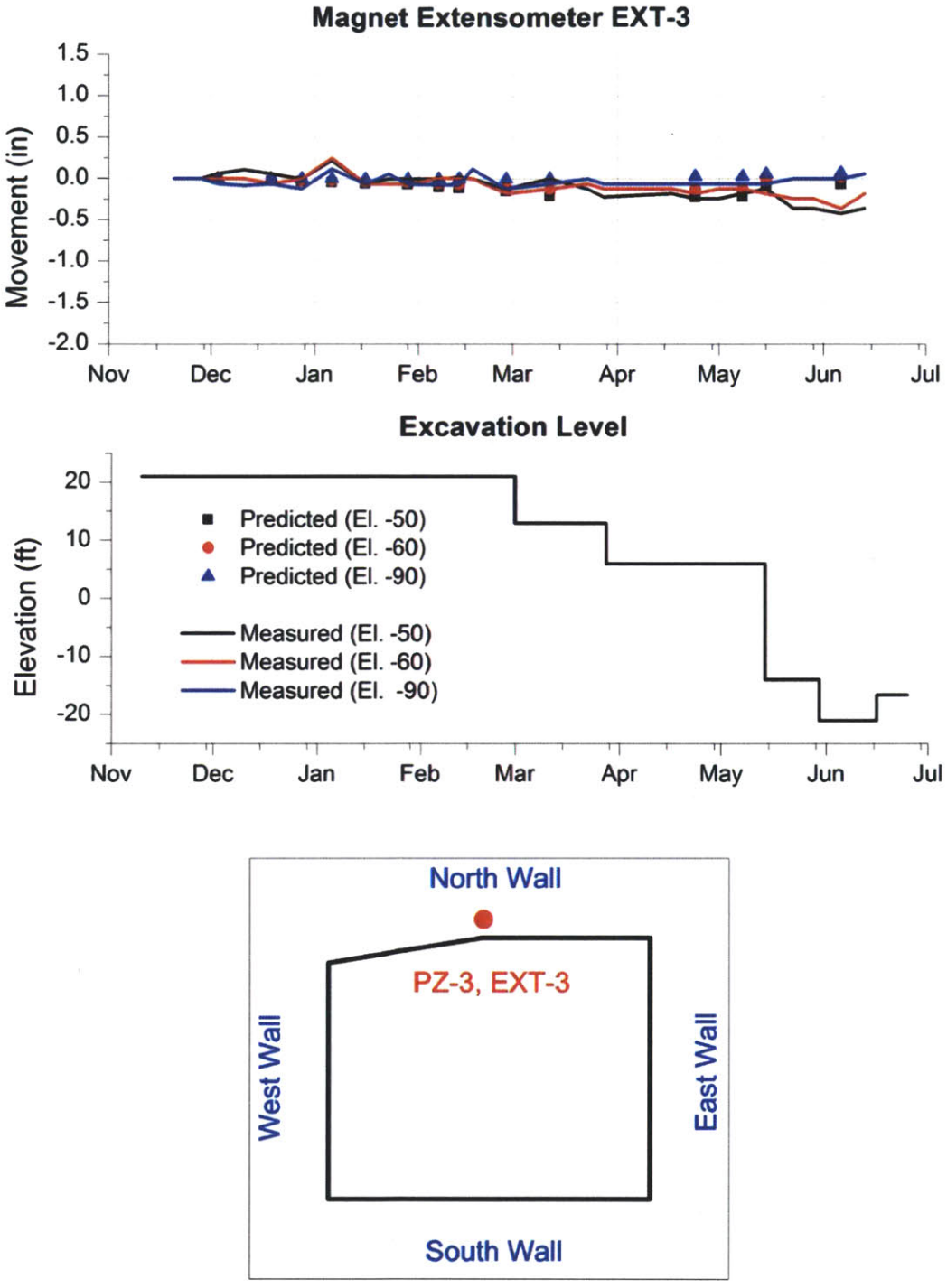

Figure 4-32: Vertical Ground Movements measured by EXT-3 (lower level) vs. 3D Finite Element Analysis predictions (Base Case A)

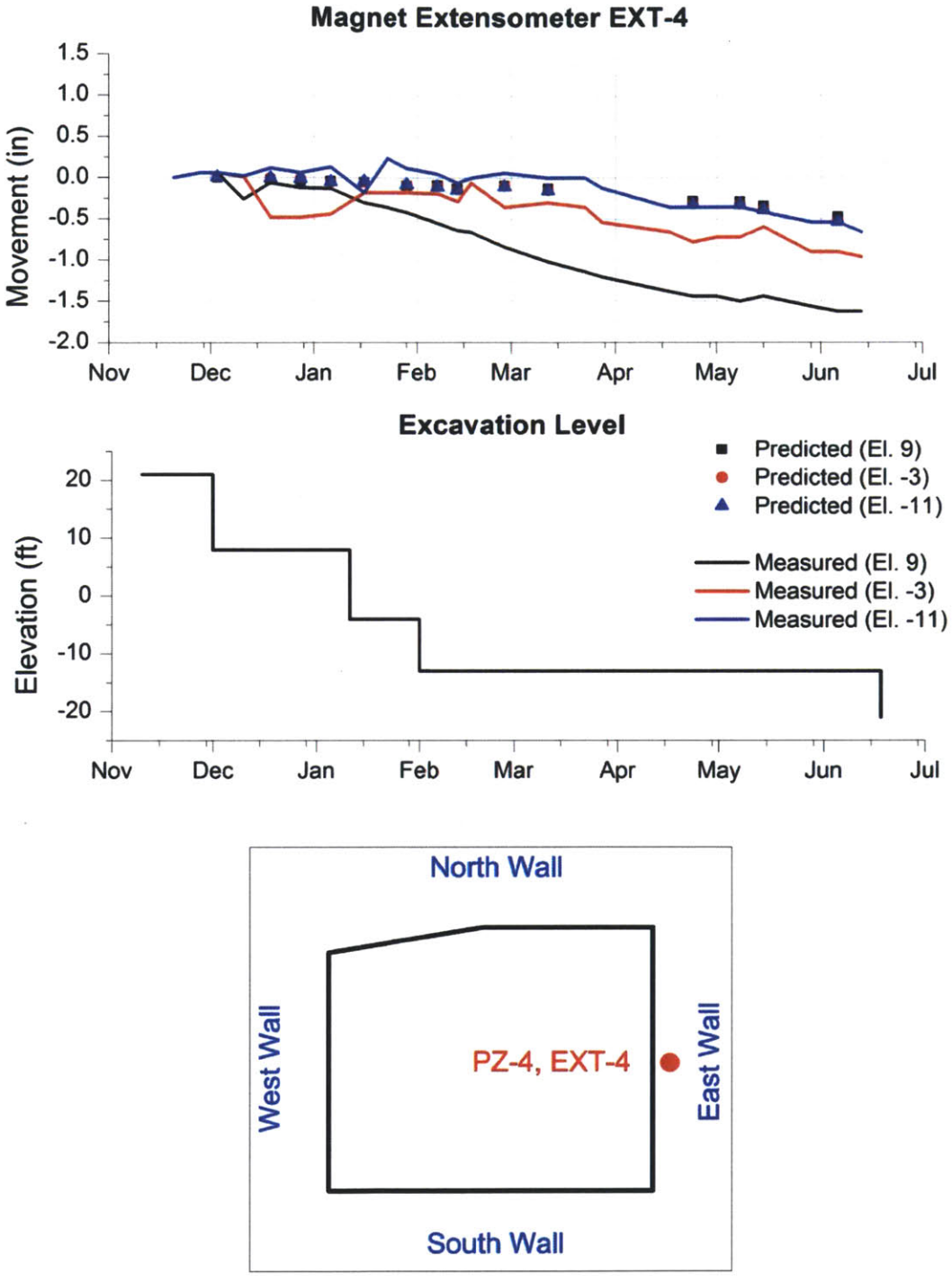

Figure 4-33: Vertical Ground Movements measured by EXT-4 (upper level) vs. 3D Finite Element Analysis predictions (Base Case A)

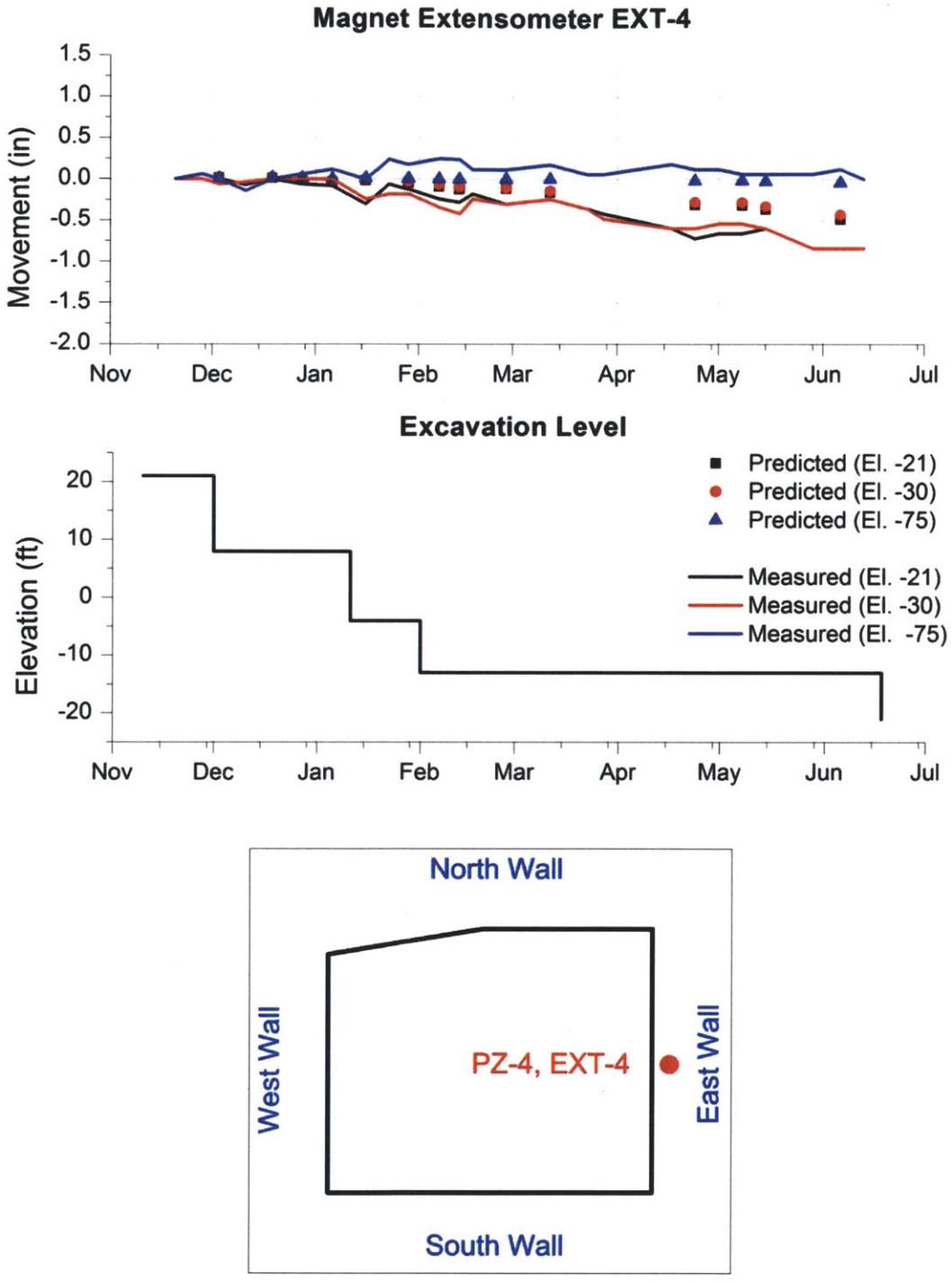

Figure 4-34: Vertical Ground Movements measured by EXT-4 (lower level) vs. 3D Finite Element Analysis predictions (Base Case A)

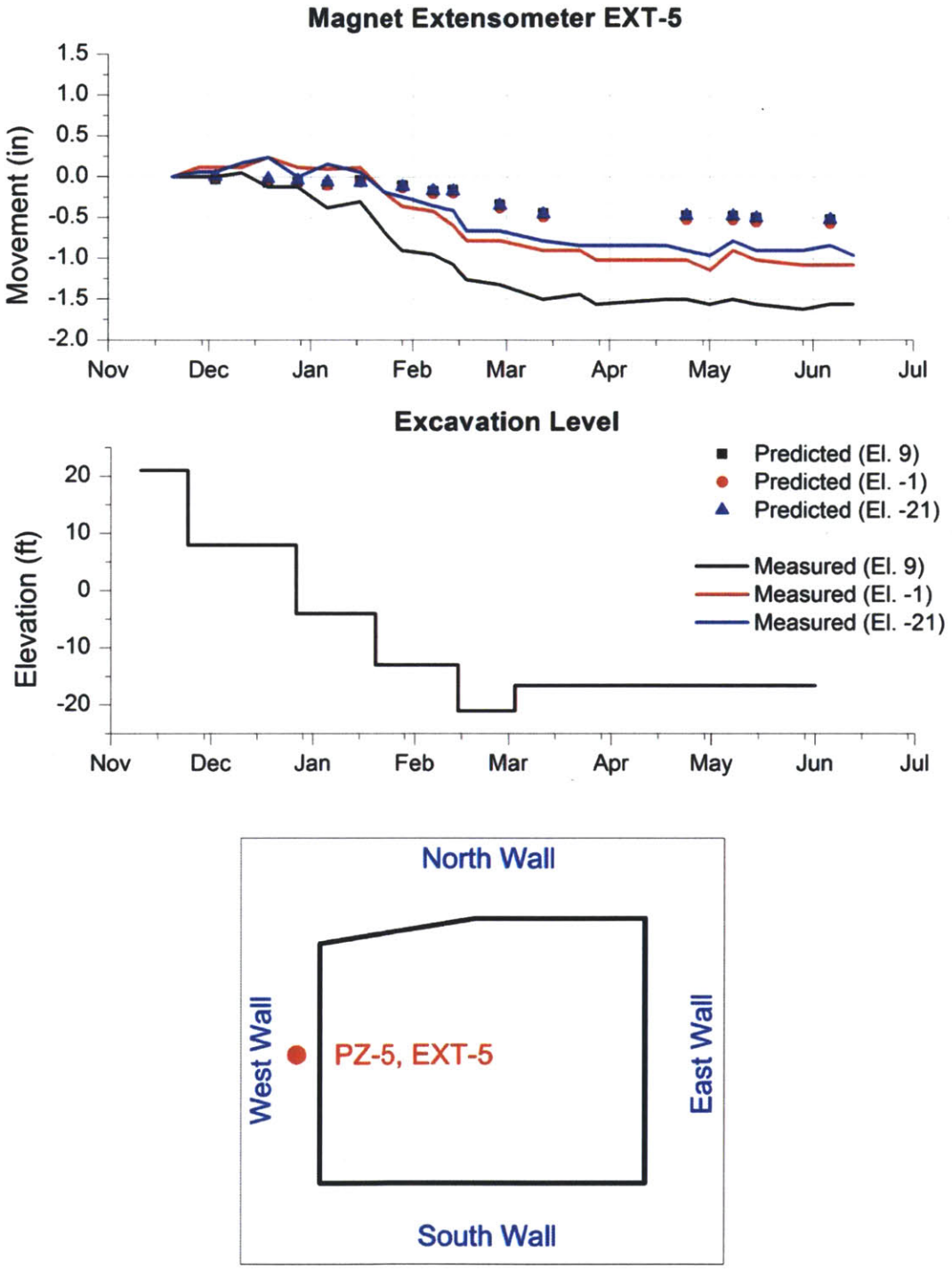

Figure 4-35: Vertical Ground Movements measured by EXT-5 (upper level) vs. 3D Finite Element Analysis predictions (Base Case A)

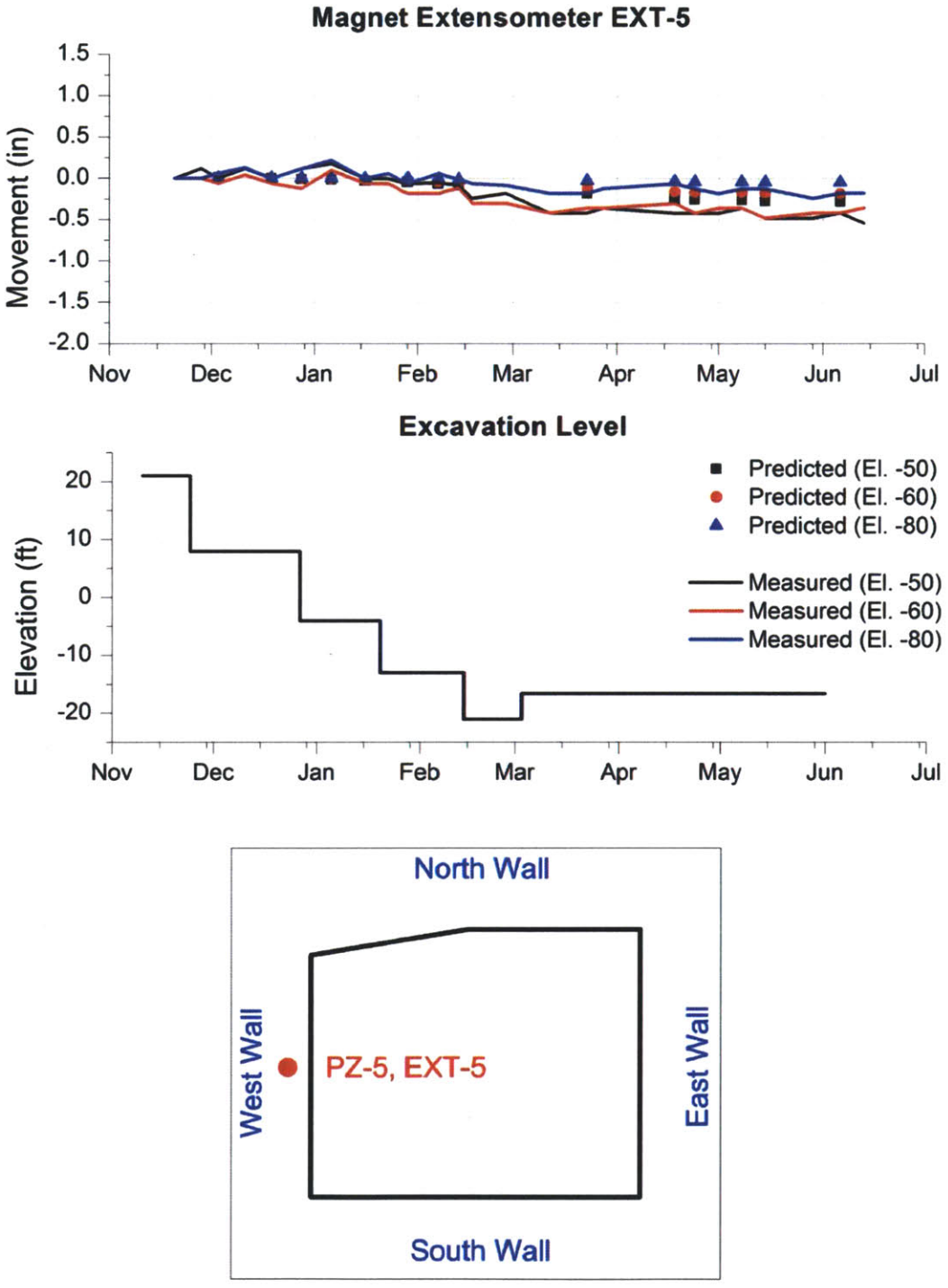

Figure 4-36: Vertical Ground Movements measured by EXT-5 (lower level) vs. 3D Finite Element Analysis predictions (Base Case A)

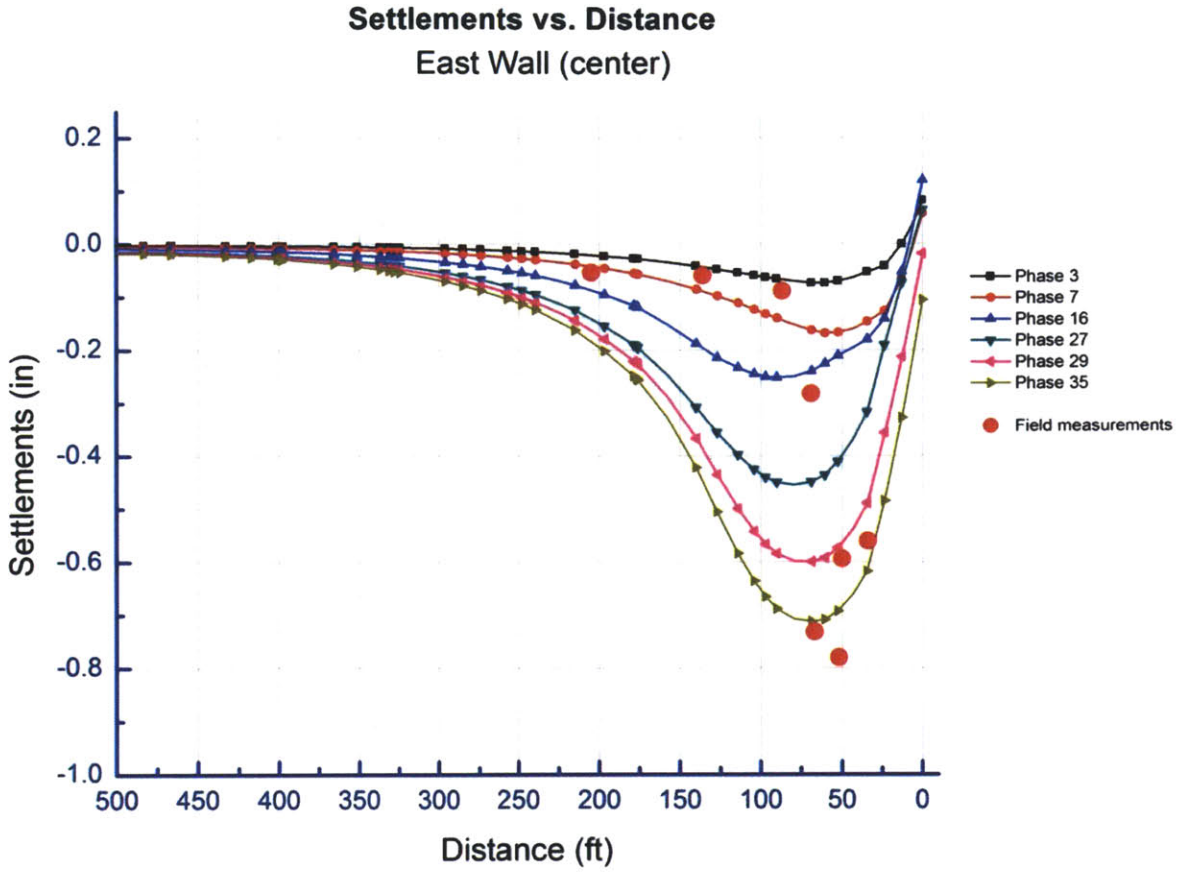

Figure 4-37: 3D Finite Element Analysis predictions (Base Case A) of surface settlements behind the East wall vs. measured data (June 1, 2001)

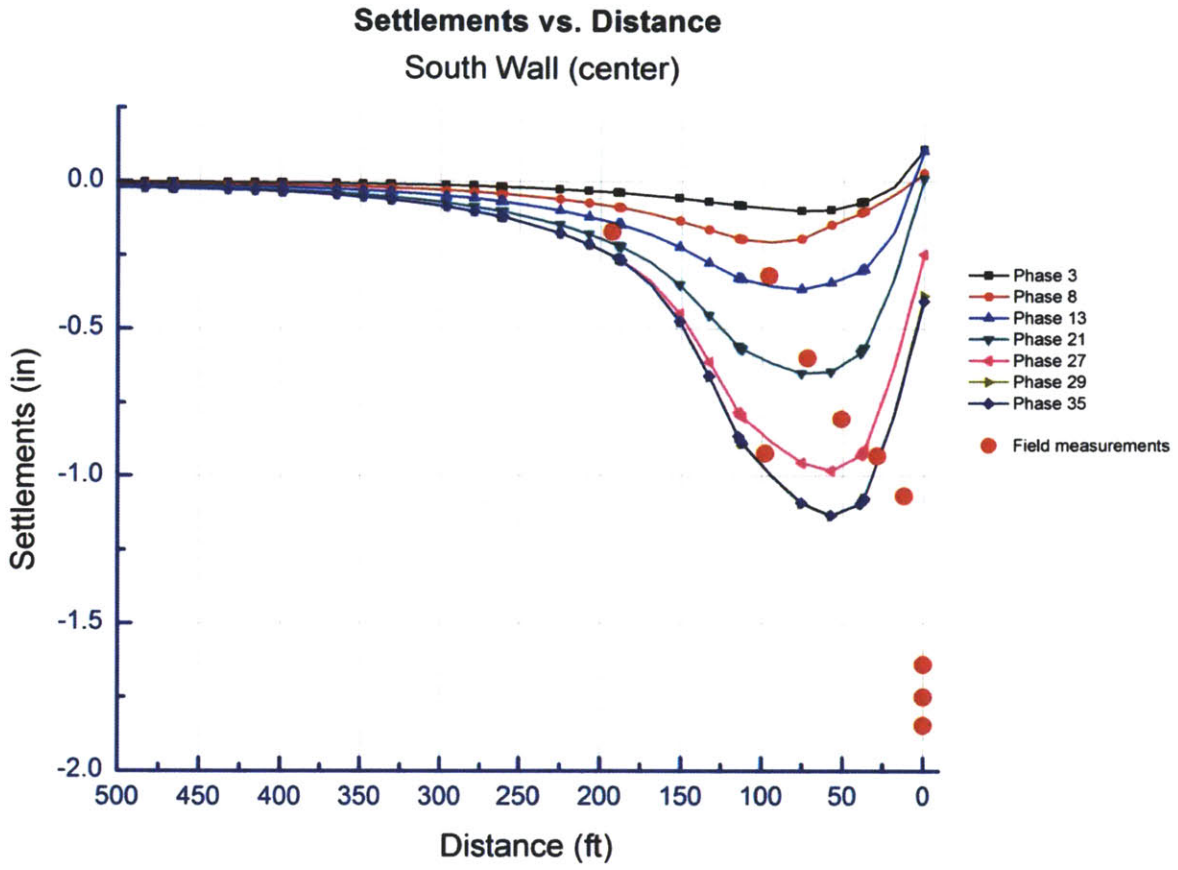

Figure 4-38: 3D Finite Element Analysis predictions (Base Case A) of surface settlements behind the South wall vs. measured data (June 1, 2001)

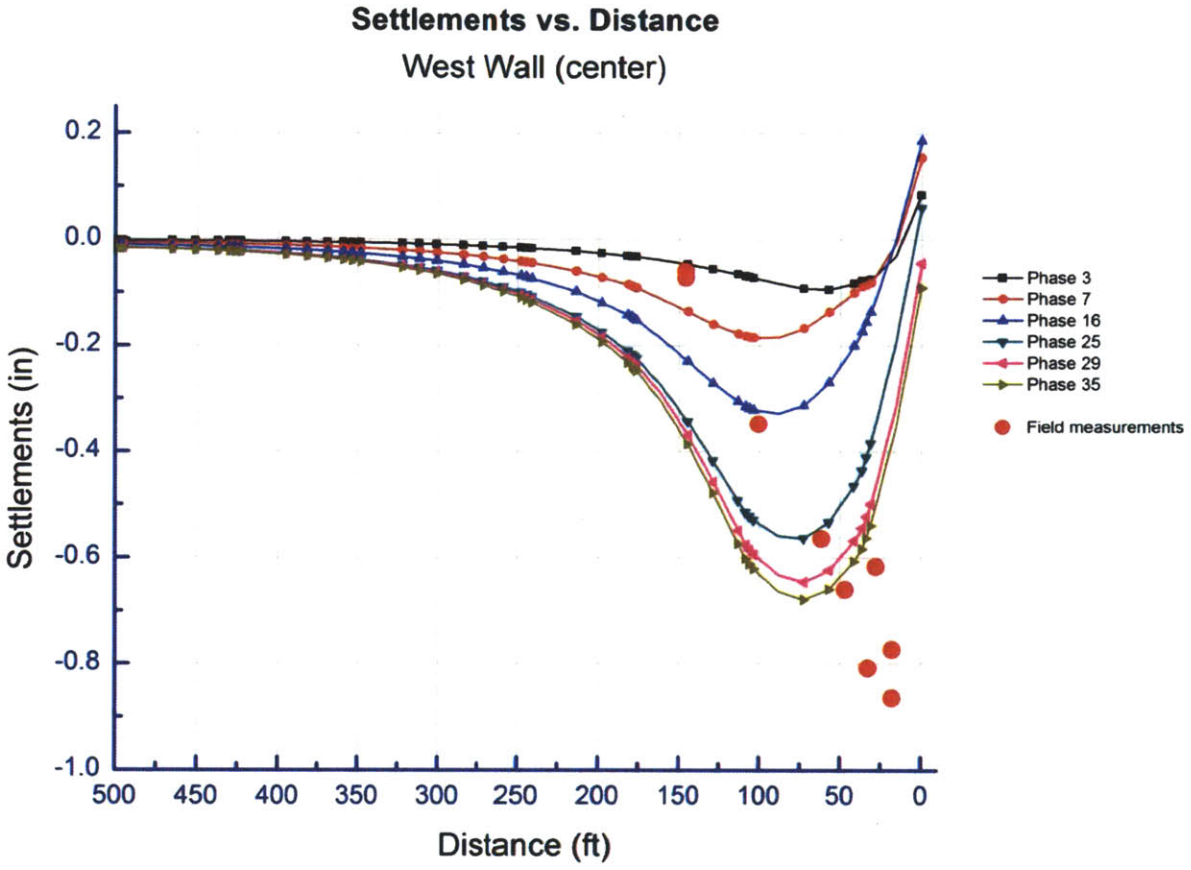

Figure 4-39: 3D Finite Element Analysis predictions (Base Case A) of surface settlements behind the West wall vs. measured data (June 1, 2001)

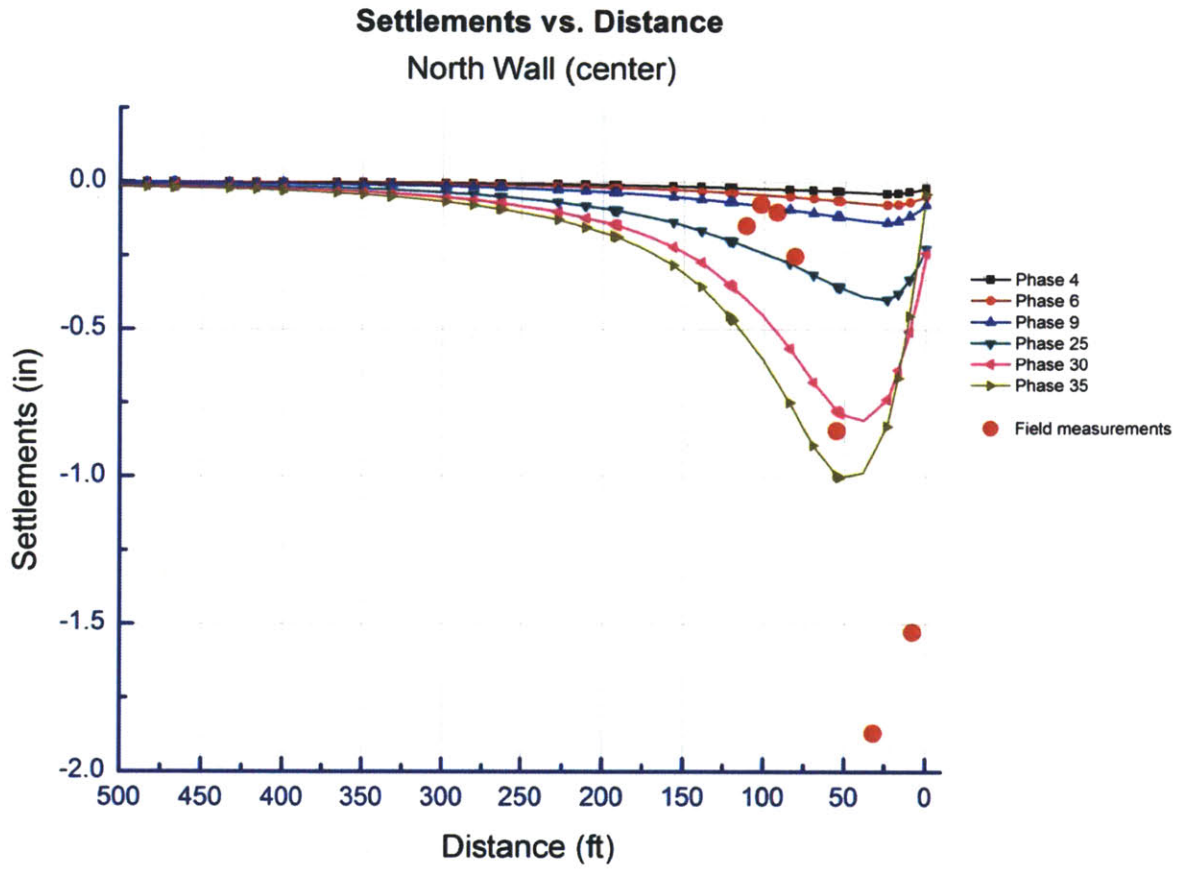

Figure 4-40: 3D Finite Element Analysis predictions (Base Case A) of surface settlements behind the North wall vs. measured data (June 1, 2001)

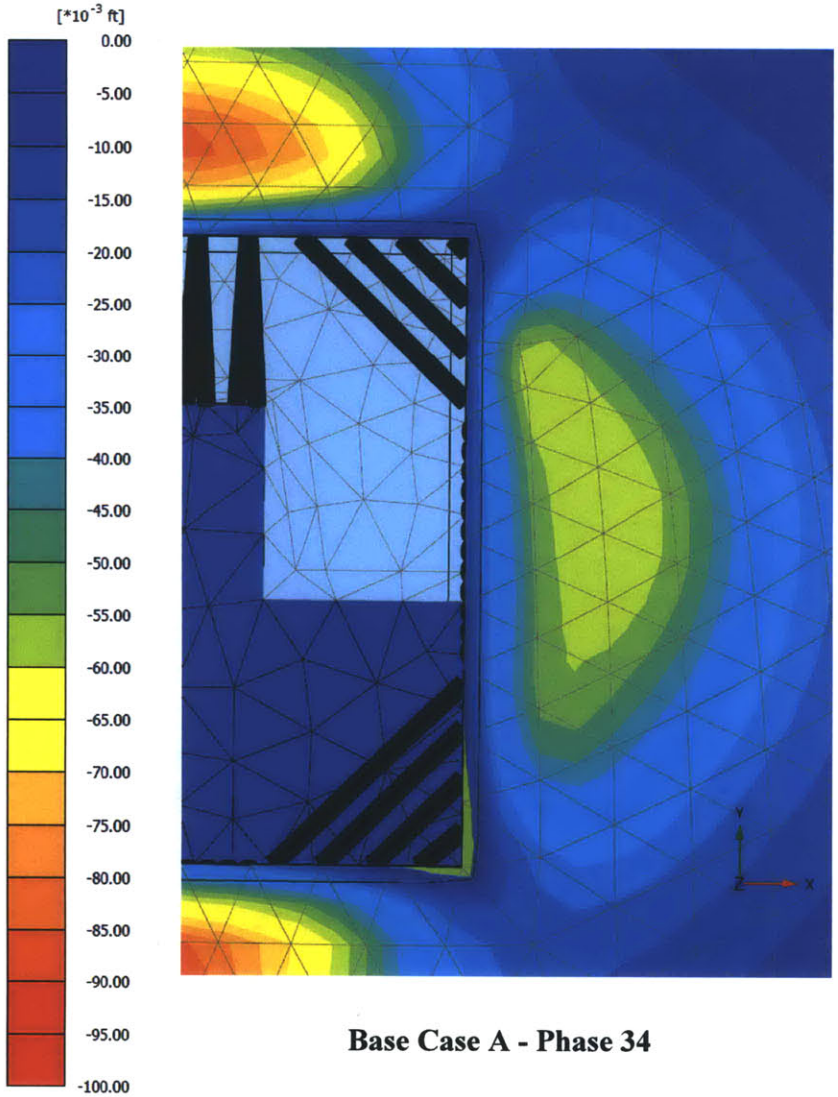

Base Case A - Phase 34

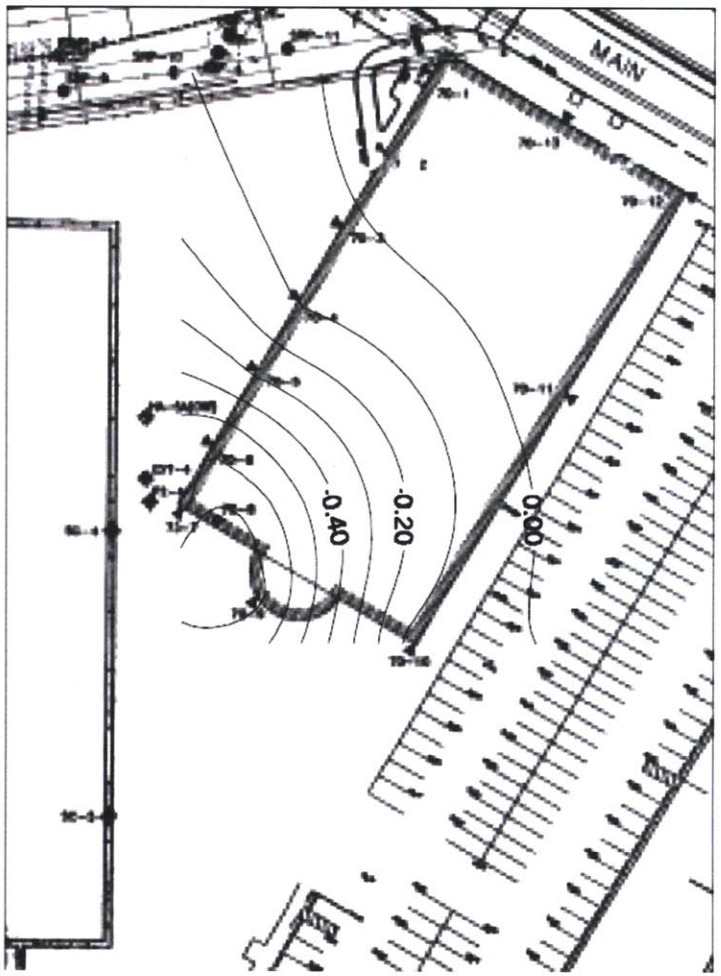

Field data - June 1, 2001

Figure 4-41: Settlement contours for the East wall based on compiled data from the surface settlement points (after Olsen, 2001) vs. 3D Finite Element Analysis predictions (Base Case A)

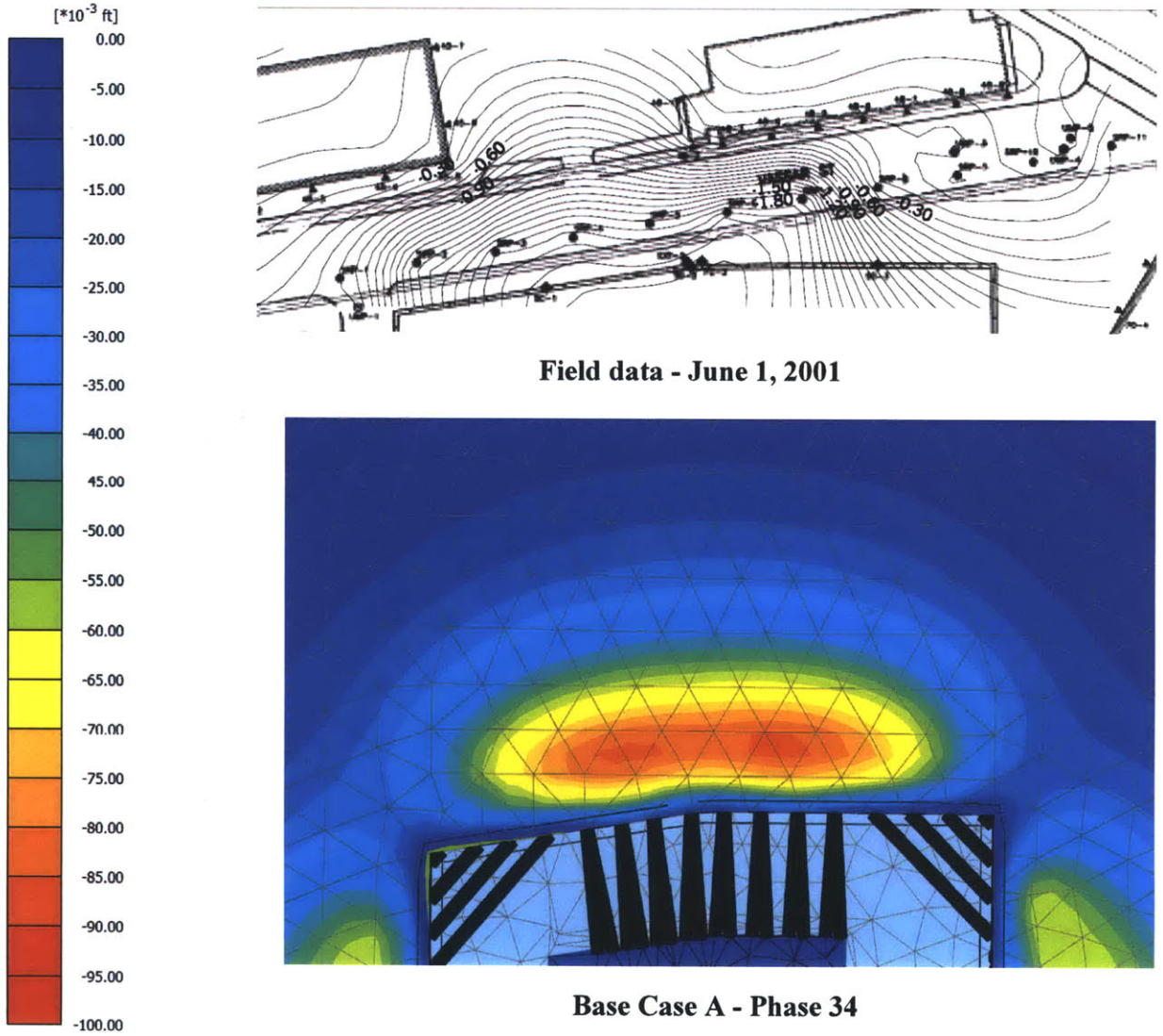

Figure 4-42: Settlement contours for the North wall based on compiled data from the surface settlement points (after Olsen, 2001) vs. 3D Finite Element Analysis predictions (Base Case A)

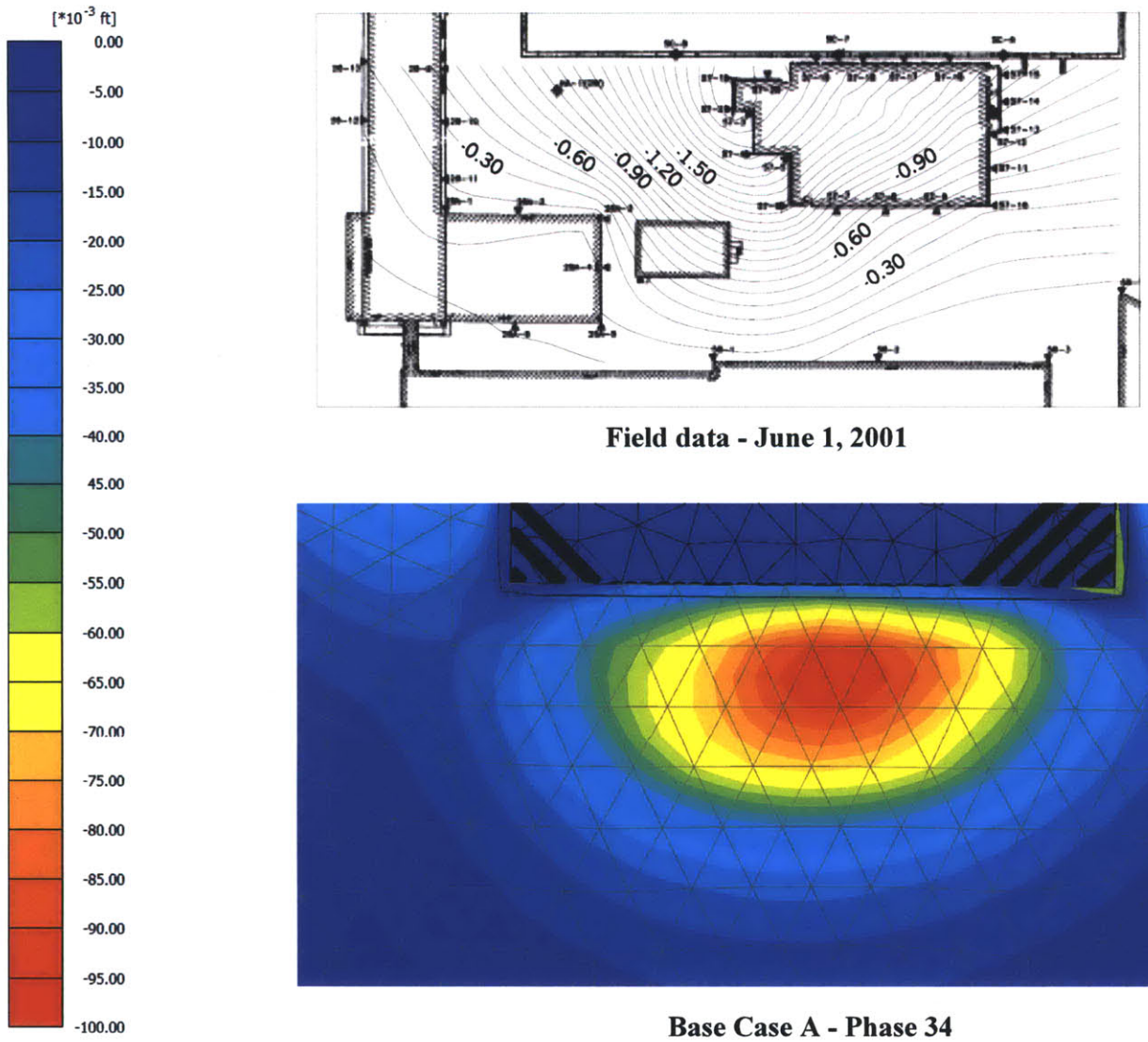

Figure 4-43: Settlement contours for the North wall based on compiled data from the surface settlement points (after Olsen, 2001) vs. 3D Finite Element Analysis predictions (Base Case A)

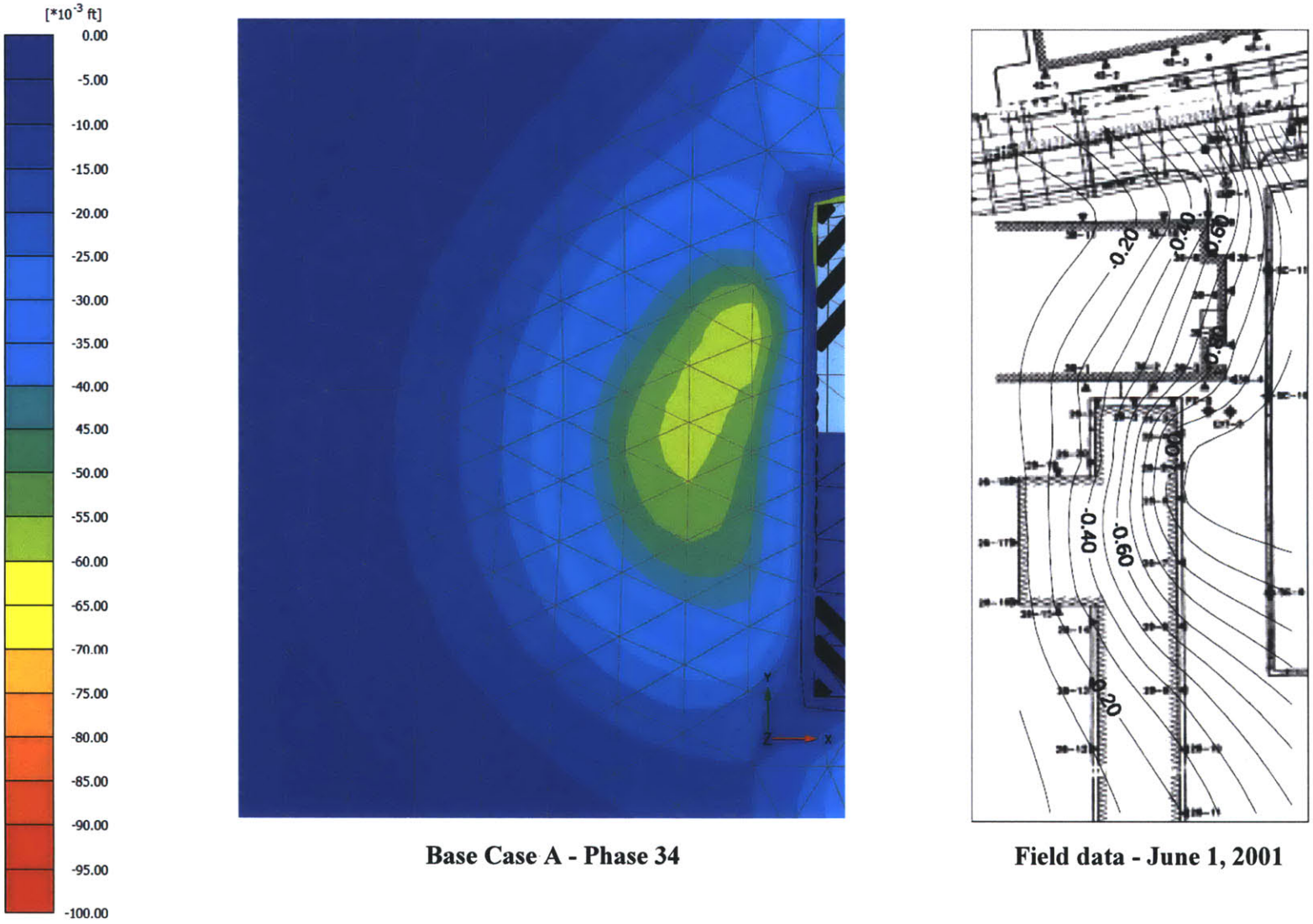

Base Case A - Phase 34

Field data - June 1, 2001

Figure 4-44: Settlement contours for the West wall based on compiled data from the surface settlement points (after Olsen, 2001) vs. 3D Finite Element Analysis predictions (Base Case A)

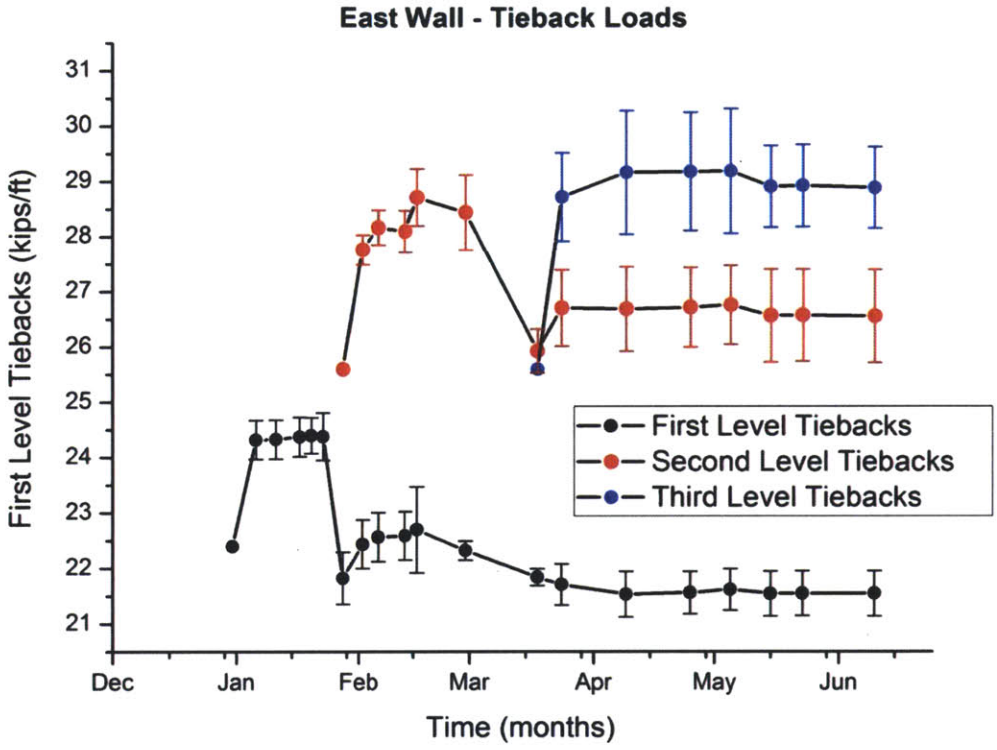

Figure 4-45: 3D Finite Element Analysis predictions (Base Case A) of tieback loads vs. time along the East wall

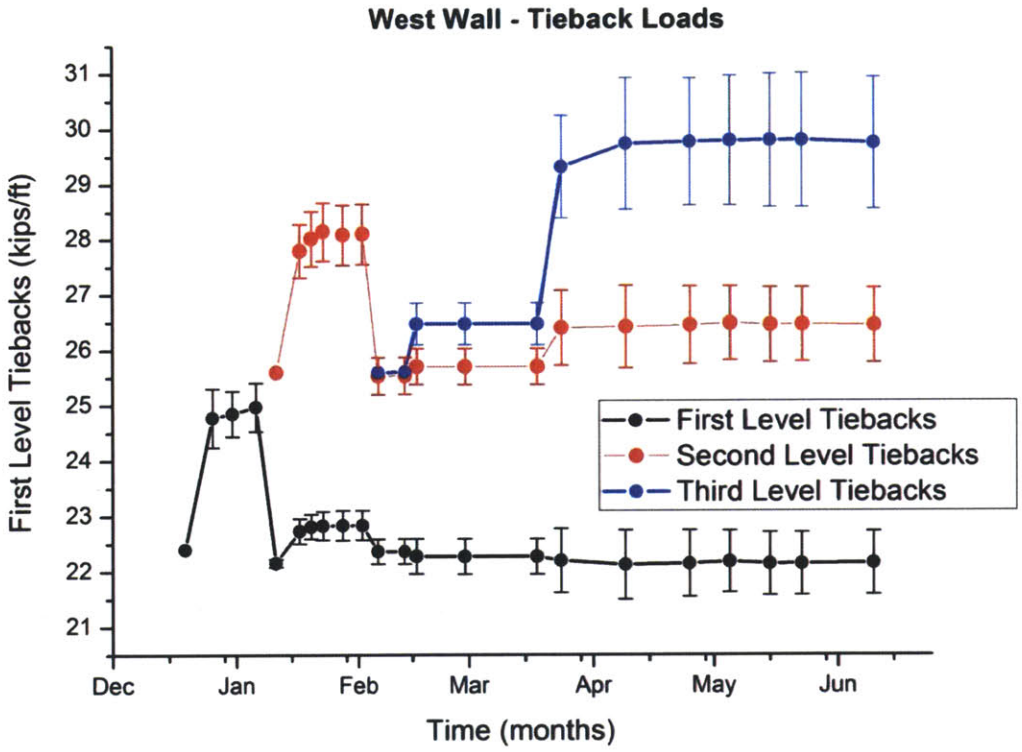

Figure 4-46: 3D Finite Element Analysis predictions (Base Case A) of tieback loads vs. time along the West wall

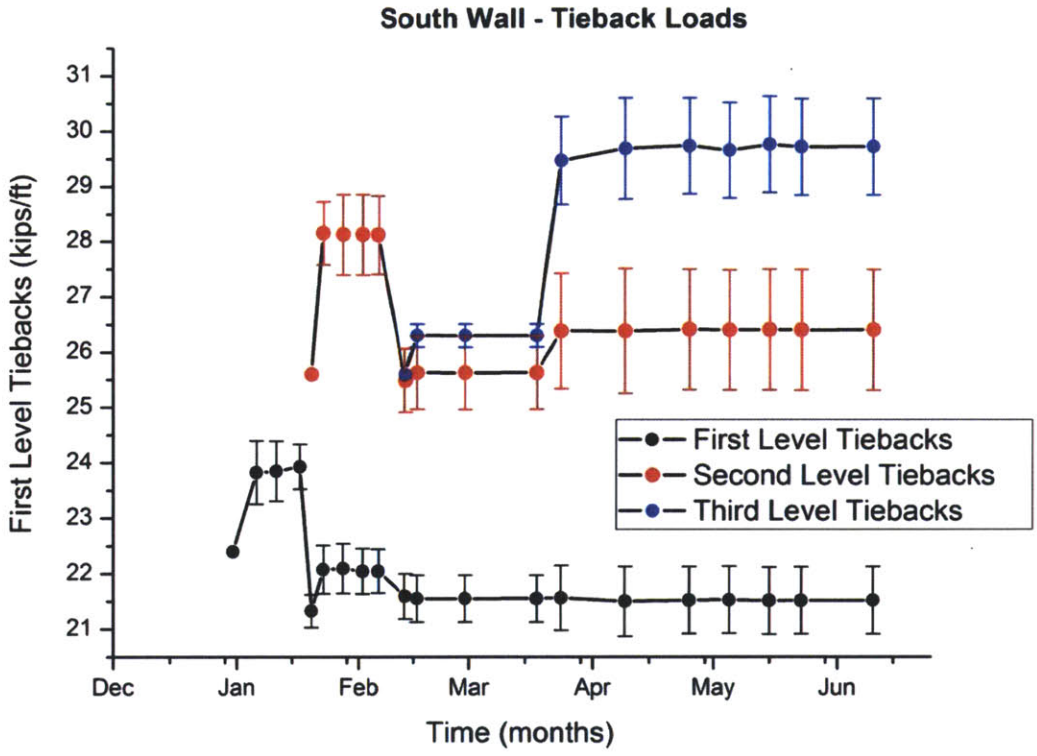

Figure 4-47: 3D Finite Element Analysis predictions (Base Case A) of tieback loads vs. time along the South wall

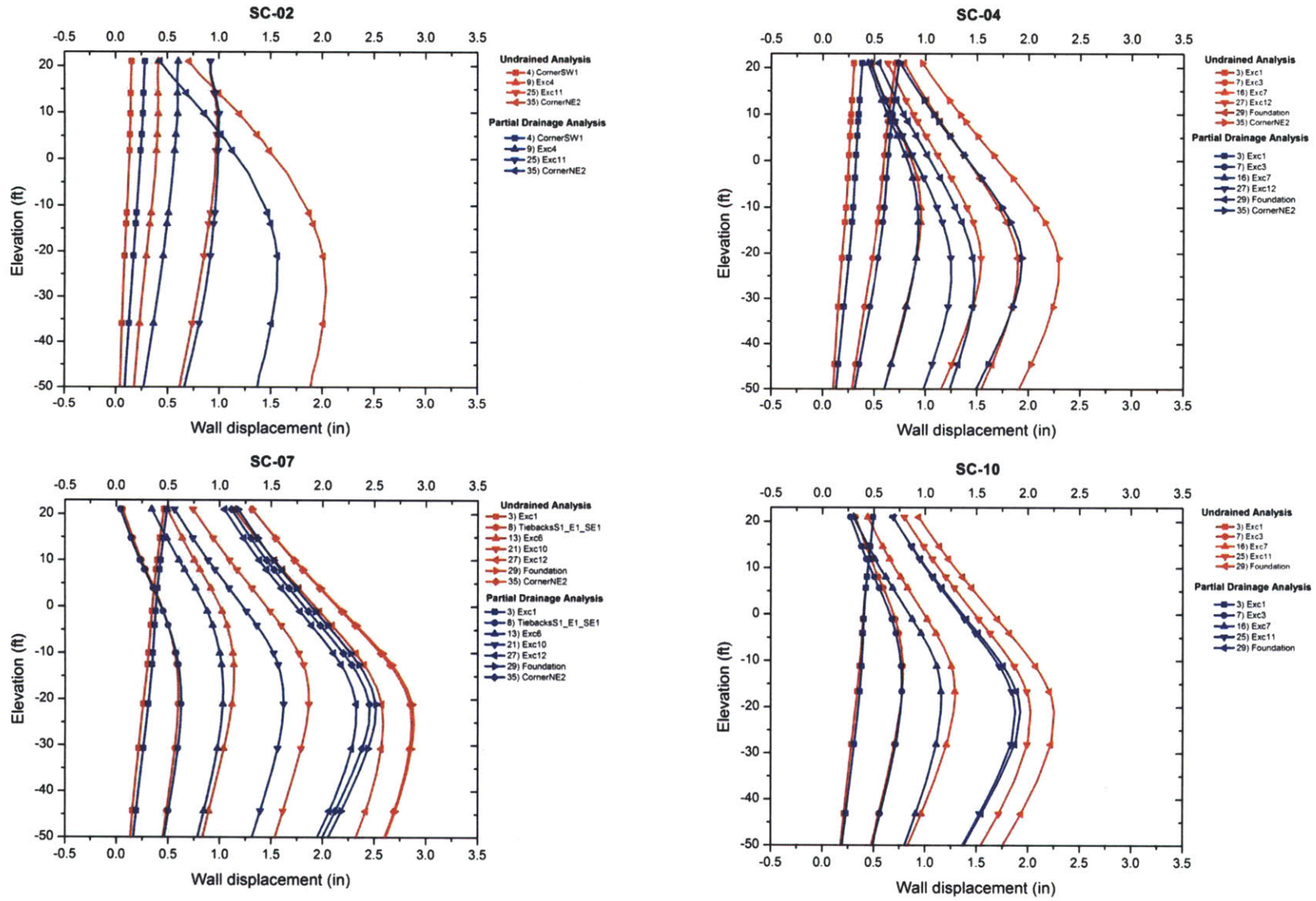

Figure 4-48: 3D Finite Element Analysis predictions-Case B (Partial Drainage Analysis) vs. Base Case A (Undrained Analysis)

5 SUMMARY AND CONCLUSIONS

5.1 Summary

The thesis demonstrated the application of the three-dimensional finite element analysis (using a commercial Finite Element Analysis code, Plaxis 3D 2011) to the Ray and Maria Stata Center excavation project in Cambridge, Massachusetts. This study has shown that the three-dimensional finite element analysis can be effectively used for a such complex excavation projects and is capable to achieve consistent predictions of wall deflections, ground movements, and pore pressures for tieback, corner-braced, and raker supported diaphragm walls. The three-dimensional finite element analysis results showed a good agreement with the measured data despite of simplifications in the Base Case model.

The non-uniform ground excavation resulted in the three-dimensional effects which were well captured in the Base Case model predictions (Figures 4-31 through 4-42). The three-dimensional effects noticed in the model were similar to the effects described by Finno (2007) where smaller ground movements occurred near the corners and larger ground movements towards the middle of the wall due to the higher stiffness of the corner bracing system.

In order to quantitatively assess the obtained predictions from the Base Case model and consistently compare them with the field data, a "curve integration" method was used. The principle of this method was to obtain and compare the areas under each curves on the "elevation vs. wall deflection" plots. The results showed on average 93% in total and 76% in inclusive areas agreement with the measured data (integrated wall deflections curves).

The effects of partial drainage (Case B analysis, which incorporated the actual construction time from the calendar plan) on wall deflections were also discussed. The full

results of the analysis and detailed directions to reproduce the Base Case model predictions were provided.

5.2 Conclusion

This work is the first use of the fully coupled three-dimensional flow-deformation analysis in Plaxis 3D 2011 for a such complex, well-instrumented three-dimensional case study. The results of the analysis provided answers to the questions on the practical usage of three-dimensional finite element analysis for complex excavation projects, quantitative assessment of the three-dimensional predictions, and the effects of partial drainage on wall deflections. The following possible explanations for some observed discrepancies in the model predictions were given:

1. The Base Case analysis assumed a constant height of the diaphragm wall with the top at the ground surface (El. +21 ft) while the actual top elevation varied from El. 15.4 ft to El. 19.0 ft.
2. The material properties of the diaphragm wall were assumed to be isotropic and linear. In reality, the reinforcement of the wall is not continuous across wall panels; hence, bending properties are expected to be anisotropic.
3. The soil layers in geological profile were assumed to be horizontal, and a simple elastic-perfectly plastic constitutive soil model was used.
4. The groundwater table was assumed to be at El. +15 ft around the excavation site and was lowered inside the impermeable diaphragm wall each time to match the current maximum level of excavation and to produce steady-state seepage.
5. The adjacent Building 57 was simulated only as a surcharge load at the tip of the caissons.

In addition, the following factors seem to have an important effect on the excavation performance: the three-dimensional effects resulting from a non-uniform soil excavation and corner bracing, geological profile, plan geometry of the wall, consolidation within the clay and groundwater conditions.

Further studies using more accurate constitutive representation of the soil such as advanced effective stress model MIT-E3 (Whittle, 1987) is recommended to assess the importance of soil constitutive behavior on the observed field performance of the support system for the Stata Center basement.

Although the first three-dimensional model required a great deal of time and computational resources, with gained experience, it is now possible to construct the three-dimensional models with any levels of complexity in a short amount of time. The author also developed a program in MS Visual Basic to analyze the Plaxis 3D[1] output data and prepare it for plotting automatically. Due to the size of the mesh and complex geometry, the whole model calculation lasted almost 20 hours on a quad-core personal computer. However, with the use of multi-core solver on a powerful machine, the computational time could be further substantially reduced to even more practical values.

[1] During the course of this research, a software bug in the Plaxis 3D program producing hidden excessive lateral water loads was found and reported to the Plaxis Development Team. It helped them to identify the problem and release a workaround solution for the previous version of Plaxis. The complete fix for the identified issue has been implemented in the latest software update.

REFERENCES

Arabshahi, M. (2010). Three Dimensional Bearing Capacity of Shallow Foundations Adjacent to Slopes Using Discrete Element Method. *International Journal of Engineering*, *4*(2), 160-178.

Athanasopoulos, G. A., Vlachakis, V. S., Pelekis, P. C. (2011). Installation and Performance of a Steel Sheet Pile Wall for Supporting an Excavation in Urban Environment. *Geo Frontiers 2011: Advances in Geotechnical Engineering.*

Aukema, E. J., Joling, A. G. (1997) *A 3D Numerical Simulation of Oblique Bending in a Steel Sheet Pile Wall.* Thesis, Department of Civil Engineering and Geosciences, Delft University of Technology.

Blackburn, J., Finno, R. (2007). Three-dimensional responses observed in an internally braced excavation in soft clay. *Journal of Geotechnical and Geoenvironmental Engineering.*

Berman, D. R., (1993), *Characterization of the Engineering Properties of Boston Blue Clay at the MIT Campus*. Thesis, Department of Civil and Environmental Engineering, Massachusetts Institute of Technology, Cambridge, MA.

Bolton, M. (2007). Back analysis of three case histories of braced excavations in Boston Blue Clay using MSD method. *Soft Soil Engineering*, 755-764.

Bolton, M. D., Lam, S. Y., Vardanega, P. J. (2010). Predicting and controlling ground movements around deep excavations. *Geotechnical Challenges in Urban Regeneration, the 11th International Conference of the DFI-EFFC.* London.

Chen, S. L., Ho, C., Kuo, Y. C. (2011). Three-Dimensional Numerical Analysis of Ground Surface Settlement Induced by the Excavation of Shield Tunnels. *ASCE, 2011 Geo Human International Conference* (pp. 80-87). ASCE.

Chen, S., Ho, C., Li, C., Gui, M. (2011). Efficiency of buttress walls in deep excavations. *Journal of Geotechnical and Geoenvironmental Engineering*, *6*(3), 145-156.

Cheng, N., Kung, G. (2010). Finite Element Analysis of Wall Deflection and Ground Movements Caused by Braced Excavations. *Finite Element Analysis* (pp. 611-636).

Clough, G. W., (1985), Effects of Excavation Induced Movements in Clays on Adjacent Structures, *Proceedings of the First ICSMFE*, Cambridge, Vol. 3, 60-64.

Clough, G. W., and J. M. Duncan, (1971), Finite Element Analysis of Retaining Wall Behavior, *Journal of Soil Mechanics and Foundations Engineering*, ASCE, (97), 1657-1673.

Clough, G. W., E. M. Smith, and B. P. Sweeney, (1989), Movement Control of Excavation Support Systems by Iterative Design, *Proceedings of the Congress on Foundation Engineering: Current Principles and Practices*, ASCE, Vol. 2, New York, 869-882.

Corral, G. A., (2010), *Re-analysis of Deep Excavation Collapse Using a Generalized Effective Stress Soil Model.* Thesis, Department of Civil and Environmental Engineering, Massachusetts Institute of Technology, Cambridge, MA.

Finno, R., Blackburn, J. (2007). Three-dimensional effects for supported excavations in clay. *Journal of Geotechnical and Geoenvironmental Engineering*, 30-36.

Finno, R., Roboski, J. (2005). Three-dimensional responses of a tied-back excavation through clay. *Journal of Geotechnical and Geoenvironmental Engineering*, 273-282.

Galavi, V. (2010). *Groundwater flow, fully coupled flow deformation and undrained analyses in PLAXIS 2D and 3D.*, Internal Report, Plaxis BV

Gourvenec, S. M., Powrie, W. (1999). Three-dimensional finite-element analysis of diaphragm wall installation. *Géotechnique*, *49*(6), 801-823.

Gourvenec, S., Powrie, W., De Moor, E. K. (2002). Three-dimensional effects in the construction of a long retaining wall. *Proceedings of the ICE - Geotechnical Engineering*, *155*(3), 163-173.

Gourvenec, M., Powrie, W. (2000). Three-dimensional finite element analyses of embedded retaining walls supported by discontinuous earth berms. *Canadian Geotechnical Journal*, *37*(5), 1062-1077.

Haley & Aldrich, (2000), Report on Geotechnical Investigations and Foundation Design Recommendations the Ray and Maria Stata Center Massachusetts Institute of Technology Cambridge, Massachusetts, Submitted to contractor.

Haley & Aldrich, (2000), Test Boring Exploration Program, Submitted to contractor.

Haley & Aldrich, (2001), Daily Field Reports, Ray and Maria Stata Center, report numbers 153-318. Submitted to contractor.

Haley & Aldrich, (2001), Geotechnical Instrumentation Reports, Reports 1-43, Submitted to contractor.

Hashash, Y. M. A., Song, H., Osouli, A. (2011). Three-dimensional inverse analyses of a deep excavation in Chicago clays. *International Journal for Numerical and Analytical Methods in Geomechanics*.

Hashash, Y. M. A. and A. J. Whittle, (1996), Ground Movement Prediction for Deep Excavations in Soft Clay, *Journal of Geotechnical Engineering*, ASCE, 122(6), 474-486.

Hewitt, R. D., Haley, M. X. Stata Center - Deep Excavation Meets MIT's Needs. *Structure magazine*, 20-23.

Hewitt, R. D., Haley, M. X., Kinner, E. B. (2003). Case History of Deep Excavation on an Urban Campus. *Proc., 12th Panamerican Conf. on Soil Mechanics and Geotechnical Engineering, Soil Rock America*. Boston.

Horn, H. M., and T. W. Lambe, (1964), Settlement of buildings on the MIT Campus, ASCE, *Journal of the Soil Mechanics and Foundations Division*, Vol. 90, No. SM5, pp. 181-195.

Hou, Y. M., Wang, J. H., Zhang, L. L. (2008). Finite-element modeling of a complex deep excavation in Shanghai. *Geotechnica*, *4*(1), 7-16.

Ikar, J. (2010). 3D analysis of the influence of primary support stiffness on the surface movements during tunnel construction. *RMZ - Materials and Geoenvironment*, *57*(2), 237-250.

Jen, L. C., (1998), *The Design and Performance of Deep Excavations in Clay*. Thesis, Department of Civil and Environmental Engineering, Massachusetts Institute of Technology, Cambridge, MA.

Johnson, E. G., (1989), Geotechnical Characteristics of the Boston Area, *Civil Engineering Practice*, Boston Society of Civil Engineers, 4(1), 53-64.

Joyce, N. E., Gehry, F. O., Sobol, R. M. (2004). *Building Stata: the design and construction of Frank O. Gehry's Stata Center at MIT.*

Konstantakos, D. C., (2000), *Measured Performance of Slurry Walls*. Thesis, Department of Civil and Environmental Engineering, Massachusetts Institute of Technology, Cambridge, MA.

Kouwenberg, P. (2009). *3D subsurface modeling and geotechnical risk analysis for the tunnel construction of the A2- project Maastricht*. Thesis, Department of Civil Engineering and Geosciences, Delft University of Technology.

Krabbenhoft, K., Lyamin, A. V., (2008). Finite-Element Limit Analysis of Mohr–Coulomb Materials in 3D Using Semi definite Programming. *Journal of Engineering Mechanics*, *134*(4), 255-260.

Ladd, C. C., and A. J. Whittle, (1993), Design and Performance of Deep Excavations, Schnabel, H. J., (1982), Tiebacks in Foundation Engineering and Construction, McGraw-Hill, Inc, New York.

Lee, F., Hong, S., Gu, Q., Zhao, P. (2011). Application of Large Three-Dimensional Finite-Element Analyses to Practical Problems. *International Journal of Geomechanics*, *11*(6), 529-539.

Liew, S. S., Choo, E. L. (2004). Bending moment interpretation of structural element with measured deflection profile. *Malaysian Geotechnical Conference.*

Liu, J., He, J., Ding, B. Y. (2006). 3D Finite Element Analysis on Bearing Capacity Characteristics of the Composite Ground. *ASCE, Sessions of GeoShanghai* (pp. 305-312).

Lyamin, A. V., Salgado, R., Sloan, S. W., Prezzi, M. (2007). Two-and three-dimensional bearing capacity of footings in sand. *Géotechnique, 57*(8), 647 –662.

Masin, D. (2009). 3D Modeling of an NATM Tunnel in High K0 Clay Using Two Different Constitutive Models. *Journal of Geotechnical and Geoenvironmental Engineering, 135*(9), 1326-1335.

Munoz, J., Bonet, J., Huerta, A., Peraire, J. (2008). Bounds and adaptivity for 3D limit analysis. *7th Workshop on Numerical Methods in Applied Science and Engineering (NMASE 08).*

Ng, C., Yan, R. (1999). Three-dimensional modeling of a diaphragm wall construction sequence. *Géotechnique, 49*(6), 825-834.

Olsen, M. B. (2001). *Measured Performance of a Large Excavation on the MIT Campus.* Thesis, Department of Civil and Environmental Engineering, Massachusetts Institute of Technology, Cambridge, MA.

Persson, H., Sigstrom, D. (2010). *Staged excavation in soft clay supported by a cantilever sheet pile wall.* Chalmers University of Technology.

Plaxis (2011). Plaxis 3D 2011 - Reference Manual. http://www.plaxis.nl/.

Sadek, M., Shahrour, I. (2004). A three dimensional embedded beam element for reinforced geomaterials. *International Journal for Numerical and Analytical Methods in Geomechanics, 28*(9), 931-946. doi:10.1002/nag.357

Salgado, R., Lyamin, A., Sloan, S. (2004). Two-and three-dimensional bearing capacity of foundations in clay. *Géotechnique, 54*(5), 297-306.

Sen, K. K., Alostaz, Y., Pellegrino, G., Hagh, A. (2004). Support of Deep Excavation in Soft Clay : A Case History Study. *Fifth International Conference on Case Histories in Geotechnical Engineering.* New York.

Simpson, B., Ng, C. W., Nash, D. F., Lings, M. L. (1995). An approximate analysis of the three-dimensional effects of diaphragm wall installation. *Géotechnique, 45*(3), 497-507.

Taylor, D. W., (1944), An unusual Foundation Problem: The Alumni Pool Building, *J. Boston Society of Civil Engineers*, October.

Terra Drilling Company, Inc., (2000), Tieback Installation at MIT-Ray and Maria Stata Center, Submitted to contractor.

Terzaghi, K., R. B. Peck, and G. Mesri, (1996), *Soil Mechanics in Engineering Practice*, 3rd Edition, Wiley and Sons, New York.

Trevi Icos Corporation, (2000), Grouting Submittal for Building 57, Submitted to contractor.

Wang, Z., Zhou, J. (2011). Three-dimensional numerical simulation and earth pressure analysis on double-row piles with consideration of spatial effects. *Journal of Zhejiang University SCIENCE A*, *12*(10), 758-770.

Weidlinger & Associates, (2000), Excavation Support System Slurry Wall Design, reports 1-4, Submitted to contractor.

Whittle, A. J., Davies, R. V. (2006). Nicoll Highway collapse: evaluation of geotechnical factors affecting design of excavation support system. *International Conference on Deep Excavations*.

Whittle, A. J., Kavvadas M. J., (1994), Formulation of MIT-E3 Constitutive Model for Overconsolidated Clays, *Journal of Geotechnical Engineering*, ASCE, 120(1), (173-198).

Wilson, E. L. (2002). Three-Dimensional Static and Dynamic Analysis of Structures. *Computers and Structures, Inc.*

Xanthakos, P. P., (1991), Ground Anchors and Anchored Structures, A Wiley Interscience Publication, John Wiley and Sons, New York.

Xue, F., Ma, J., (2011). Three-dimensional FEM Analysis of Bridge Pile Group Settlement in Soft Soils. *The 2011 Geo Human International Conference* (pp. 135-143).

Young, R. P., Collins, D., Hazzard, J., Heath, A. (2003). An Innovative 3-D Numerical Modeling Procedure for Simulating Repository-Scale Excavations in Rock – SAFETI. *The CLUSTER Conference on Impact of the EDZ on the performance of radioactive waste geological repositories*. Luxembourg.

APPENDIX 1

Information about the mesh

FE elements - 10-Noded
Number of soil elements - 111886
Number of nodes - 173787

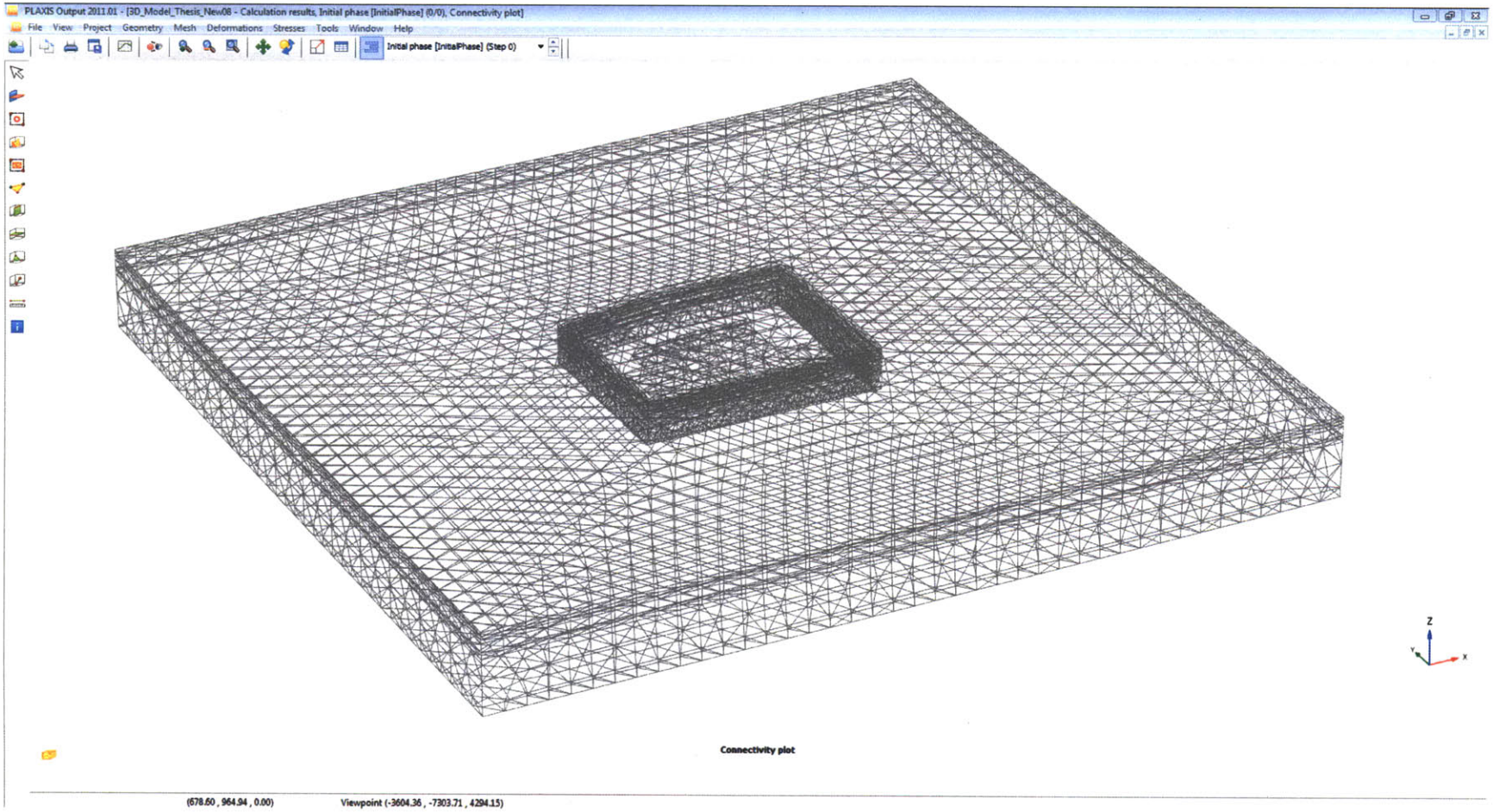

APPENDIX 2

Main input commands to rebuild the model in Plaxis 3D 2011

```
==========
Wall:
_surface 0 0 21 0 281 21 184 311 21 381 311 21 381 0 21
==========
Corner NW1 +10:
_n2nanchor 0 274 10 7.144 282.2 10
_n2nanchor 0 249 10 32.24 286.3 10
_n2nanchor 0 225 10 55.11 290 10
_n2nanchor 0 200 10 80.13 294.1 10
==========
Corner NW2 -10:
_n2nanchor 0 274 -10 7.144 282.2 -10
_n2nanchor 0 249 -10 32.24 286.3 -10
_n2nanchor 0 225 -10 55.11 290 -10
_n2nanchor 0 200 -10 80.13 294.1 -10
==========
Corner NE1 +10:
_n2nanchor 381 304 10 374 311 10
_n2nanchor 381 279 10 349 311 10
_n2nanchor 381 254 10 324 311 10
_n2nanchor 381 229 10 299 311 10
==========
Corner NE2 -10:
_n2nanchor 381 304 -10 374 311 -10
_n2nanchor 381 279 -10 349 311 -10
_n2nanchor 381 254 -10 324 311 -10
_n2nanchor 381 229 -10 299 311 -10
==========
Corner SW1 +10:
_n2nanchor 0 7 10 7 0 10
_n2nanchor 0 32 10 32 0 10
_n2nanchor 0 54 10 54 0 10
==========
Corner SW2 -10:
_n2nanchor 0 7 -10 7 0 -10
_n2nanchor 0 32 -10 32 0 -10
_n2nanchor 0 54 -10 54 0 -10
==========
Corner SE1 +10:
_n2nanchor 360 0 10 381 18 10
_n2nanchor 337 0 10 381 43 10
_n2nanchor 312 0 10 381 68 10
_n2nanchor 288 0 10 381 90 10
==========
Corner SE2 -10:
_n2nanchor 360 0 -10 381 18 -10
_n2nanchor 337 0 -10 381 43 -10
_n2nanchor 312 0 -10 381 68 -10
_n2nanchor 288 0 -10 381 90 -10
==========
Tiebacks W1 (x12):
_n2nanchor 0 70 10 -47 70 -7
_embeddedpile -47 70 -7 -85 70 -21
==========
Tiebacks W2:
_n2nanchor 0 70 -1 -19 70 -8
_embeddedpile -19 70 -8 -66 70 -25
==========
Tiebacks W3:
_n2nanchor 0 70 -10 -10 70 -14
_embeddedpile -10 70 -14 -57 70 -31
==========
```

```
================================================================================
Tiebacks S1 (x22):
_n2nanchor 66 0 10 66 -47 -7
_embeddedpile 66 -47 -7 66 -85 -21
================================================================================
Tiebacks S2:
_n2nanchor 66 0 -1 66 -19 -8
_embeddedpile 66 -19 -8 66 -66 -25
================================================================================
Tiebacks S3:
_n2nanchor 66 0 -10 66 -10 -14
_embeddedpile 66 -10 -14 66 -57 -31
================================================================================
Tiebacks E1 (x12):
_n2nanchor 381 105 10 428 105 -7
_embeddedpile 428 105 -7 466 105 -21
================================================================================
Tiebacks E2:
_n2nanchor 381 105 -1 400 105 -8
_embeddedpile 400 105 -8 447 105 -25
================================================================================
Tiebacks E3:
_n2nanchor 381 105 -10 391 105 -14
_embeddedpile 391 105 -14 438 105 -31
================================================================================
Rakers R1:
_n2nanchor 124 216 -21 105.6 298.2 10
_n2nanchor 144 219 -21 129.5 302.1 10
_n2nanchor 163 222 -21 151.3 305.7 10
_n2nanchor 183 225 -21 176.2 309.7 10
_n2nanchor 203 227 -21 198 311 10
_n2nanchor 228 227 -21 223 311 10
_n2nanchor 253 227 -21 248 311 10
_n2nanchor 278 227 -21 273 311 10
================================================================================
Rakers R2:
_n2nanchor 114 214 -21 105.3 298.2 -10
_n2nanchor 134 217 -21 129.2 302.1 -10
_n2nanchor 154 220 -21 151.1 305.6 -10
_n2nanchor 173 224 -21 175.9 309.7 -10
_n2nanchor 193 227 -21 198 311 -10
_n2nanchor 218 227 -21 223 311 -10
_n2nanchor 243 227 -21 248 311 -10
_n2nanchor 268 227 -21 273 311 -10
================================================================================
South Building (1.28ksf):
_surfload 130 -6 -10 297 -6 -10 297 -97 -10 130 -97 -10
================================================================================
North Street (0.6ksf):
_surfload 0 335 21 0 395 21 381 395 21 381 335 21
================================================================================
Foundation Slab:
_surface 0 0 -21 0 150 -21 80 150 -21 80 212 -21 180 228 -21 282 228 -21 282 130 -21 381 130 -21 381 0 -21
================================================================================
Water Levels:
_waterlevel -500 -500 15 -500 811 15 0 0 15 0 281 15 184 311 15 381 311 15 381 0 15 881 811 15 881 -500 15
_waterlevel -500 -500 15 -500 811 15 0 0 8 0 281 8 184 311 8 381 311 8 381 0 8 881 811 15 881 -500 15
_waterlevel -500 -500 15 -500 811 15 0 0 -4 0 281 -4 184 311 -4 381 311 -4 381 0 -4 881 811 15 881 -500 15
_waterlevel -500 -500 15 -500 811 15 0 0 -14 0 281 -14 184 311 -14 381 311 -14 381 0 -14 881 811 15 881 -500 15
_waterlevel -500 -500 15 -500 811 15 0 0 -21 0 281 -21 184 311 -21 381 311 -21 381 0 -21 881 811 15 881 -500 15
================================================================================
Hydraulic Boundaries:
_surfgwfbc -500 -500 -110 -500 811 -110 881 811 -110 881 -500 -110
_surfgwfbc -500 811 -110 -500 811 21 -500 -500 21 -500 -500 -110
_surfgwfbc 881 811 -110 881 811 21 881 -500 21 881 -500 -110
_surfgwfbc -500 -500 21 -500 -500 -110 881 -500 -110 881 -500 21
_surfgwfbc -500 811 21 -500 811 -110 881 811 -110 881 811 21
================================================================================
```

APPENDIX 3

The source codes of the output preparation program in Visual Basic

```
========WALL DEFLECTIONS - NEW_FILE_IMPORT========
Dim i As Integer
For i = 1 To 33
ActiveWorkbook.Worksheets.Add After:=Sheets(Sheets.Count)
With ActiveSheet.QueryTables.Add(Connection:= _
"TEXT;C:\Data\Wall deflections\SC-11\" & i & ".TXT", _
Destination:=Range("$A$1"))
.Name = "1"
.FieldNames = True
.RowNumbers = False
.FillAdjacentFormulas = False
.PreserveFormatting = True
.RefreshOnFileOpen = False
.RefreshStyle = xlInsertDeleteCells
.SavePassword = False
.SaveData = True
.AdjustColumnWidth = True
.RefreshPeriod = 0
.TextFilePromptOnRefresh = False
.TextFilePlatform = 866
.TextFileStartRow = 1
.TextFileParseType = xlDelimited
.TextFileTextQualifier = xlTextQualifierDoubleQuote
.TextFileConsecutiveDelimiter = False
.TextFileTabDelimiter = True
.TextFileSemicolonDelimiter = False
.TextFileCommaDelimiter = False
.TextFileSpaceDelimiter = False
.TextFileColumnDataTypes = Array(1, 1, 1, 1, 1, 1, 1, 1, 1)
.TextFileTrailingMinusNumbers = True
.Refresh BackgroundQuery:=False
End With
Columns("A:I").Select
Range("I1").Activate
Selection.NumberFormat = "0.000000"
Selection.ColumnWidth = 15
Next i
========/WALL DEFLECTIONS - NEW_FILE_IMPORT=========

========INCLINOMETER-north=========================
Dim i As Integer
For i = 1 To 33
Windows("1.xlsx").Activate
Sheets("Sheet" & i).Select
Range("K2").Select
ActiveCell.FormulaR1C1 = "=RC[-4]*(-12)"
Range("K2").Select
Selection.AutoFill Destination:=Range("K2:K66"), Type:=xlFillDefault
Range("K2:K66").Select
Selection.Copy
Windows("WallDisplacements.xlsx").Activate
```

```
Sheets("SC-1").Select
ActiveCell.Offset(0, 1).Select
Selection.PasteSpecial Paste:=xlPasteValues, Operation:=xlNone, SkipBlanks _
:=False, Transpose:=False
Next i
========/INCLINOMETER-north=======================

=======INCLINOMETER-east==========================
Dim i As Integer
For i = 1 To 33
Windows("4.xlsx").Activate
Sheets("Sheet" & i).Select
Range("K2").Select
ActiveCell.FormulaR1C1 = "=RC[-5]*(-12)"
Range("K2").Select
Selection.AutoFill Destination:=Range("K2:K83"), Type:=xlFillDefault
Range("K2:K83").Select
Selection.Copy
Windows("WallDisplacements.xlsx").Activate
Sheets("SC-4").Select
ActiveCell.Offset(0, 1).Select
Selection.PasteSpecial Paste:=xlPasteValues, Operation:=xlNone, SkipBlanks _
:=False, Transpose:=False
Next i
=========/INCLINOMETER-east=======================

========INCLINOMETER-south=======================
Dim i As Integer
For i = 1 To 33
Windows("6.xlsx").Activate
Sheets("Sheet" & i).Select
Range("K2").Select
ActiveCell.FormulaR1C1 = "=RC[-4]*(12)"
Range("K2").Select
Selection.AutoFill Destination:=Range("K2:K71"), Type:=xlFillDefault
Range("K2:K71").Select
Selection.Copy
Windows("WallDisplacements.xlsx").Activate
Sheets("SC-6").Select
ActiveCell.Offset(0, 1).Select
Selection.PasteSpecial Paste:=xlPasteValues, Operation:=xlNone, SkipBlanks _
:=False, Transpose:=False
Next i
=========/INCLINOMETER-south======================

==========INCLINOMETER-west======================
Dim i As Integer
For i = 1 To 33
Windows("9.xlsx").Activate
Sheets("Sheet" & i).Select
Range("K2").Select

ActiveCell.FormulaR1C1 = "=RC[-5]*(12)"
Range("K2").Select
Selection.AutoFill Destination:=Range("K2:K61"), Type:=xlFillDefault
Range("K2:K61").Select
Selection.Copy
```

```
Windows("WallDisplacements.xlsx").Activate
Sheets("SC-9").Select
ActiveCell.Offset(0, 1).Select
Selection.PasteSpecial Paste:=xlPasteValues, Operation:=xlNone, SkipBlanks _
:=False, Transpose:=False
Next i
================/INCLINOMETER-west================

============PORE PRESSURES - NEW_FILE_IMPORT======
Dim i As Integer
For i = 1 To 33
ActiveWorkbook.Worksheets.Add After:=Sheets(Sheets.Count)
With ActiveSheet.QueryTables.Add(Connection:= _
"TEXT;C:\PredictedData\2) Pore Pressures\PZ-5\"
& i & ".TXT", _
Destination:=Range("$A$1"))
.Name = "1"
.FieldNames = True
.RowNumbers = False
.FillAdjacentFormulas = False
.PreserveFormatting = True
.RefreshOnFileOpen = False
.RefreshStyle = xlInsertDeleteCells
.SavePassword = False
.SaveData = True
.AdjustColumnWidth = True
.RefreshPeriod = 0
.TextFilePromptOnRefresh = False
.TextFilePlatform = 866
.TextFileStartRow = 1
.TextFileParseType = xlDelimited
.TextFileTextQualifier = xlTextQualifierDoubleQuote
.TextFileConsecutiveDelimiter = False
.TextFileTabDelimiter = True
.TextFileSemicolonDelimiter = False
.TextFileCommaDelimiter = False
.TextFileSpaceDelimiter = False
.TextFileColumnDataTypes = Array(1, 1, 1, 1, 1, 1)
.TextFileTrailingMinusNumbers = True
.Refresh BackgroundQuery:=False
End With
Cells.Select
Selection.ColumnWidth = 15
Selection.NumberFormat = "0.000000"
Next i

==========/PORE PRESSURES - NEW_FILE_IMPORT======

==========================PP1==================
Dim i As Integer
For i = 1 To 33
Windows("PZ-1.xlsx").Activate
Sheets("Sheet" & i).Select
Range("F2,F8,F22").Select
Selection.Copy
Windows("PorePressures.xlsx").Activate
Sheets("PZ-1").Select
```

```
ActiveCell.Offset(1, 0).Select
Selection.PasteSpecial Paste:=xlPasteAll, Operation:=xlNone, SkipBlanks:= _
False, Transpose:=True
Next i
==========================/PP1==================

==========================PP2==================
Dim i As Integer
For i = 1 To 33
Windows("PZ-2.xlsx").Activate
Sheets("Sheet" & i).Select
Range("F2,F17,F28").Select
Selection.Copy
Windows("PorePressures.xlsx").Activate
Sheets("PZ-2").Select
ActiveCell.Offset(1, 0).Select
Selection.PasteSpecial Paste:=xlPasteAll, Operation:=xlNone, SkipBlanks:= _
False, Transpose:=True
Next i
==========================/PP2==================

============EXTENSOMETERS - NEW_FILE_IMPORT=======
Dim i As Integer
For i = 1 To 33
ActiveWorkbook.Worksheets.Add After:=Sheets(Sheets.Count)
With ActiveSheet.QueryTables.Add(Connection:= _
"TEXT;C:\PredictedData\3)Extensometers\EXT-1-1\" & i & ".TXT", _
Destination:=Range("$A$1"))
.Name = "1"
.FieldNames = True
.RowNumbers = False
.FillAdjacentFormulas = False
.PreserveFormatting = True
.RefreshOnFileOpen = False
.RefreshStyle = xlInsertDeleteCells
.SavePassword = False
.SaveData = True

.AdjustColumnWidth = True
.RefreshPeriod = 0
.TextFilePromptOnRefresh = False
.TextFilePlatform = 866
.TextFileStartRow = 1
.TextFileParseType = xlDelimited
.TextFileTextQualifier = xlTextQualifierDoubleQuote
.TextFileConsecutiveDelimiter = False
.TextFileTabDelimiter = True
.TextFileSemicolonDelimiter = False
.TextFileCommaDelimiter = False
.TextFileSpaceDelimiter = False
.TextFileColumnDataTypes = Array(1, 1, 1, 1, 1, 1)
.TextFileTrailingMinusNumbers = True
.Refresh BackgroundQuery:=False
End With
Cells.Select
Selection.ColumnWidth = 15
Selection.NumberFormat = "0.000000"
```

```
Next i
============/EXTENSOMETERS - NEW_FILE_IMPORT===========

============================EXT-1-1=====================
Dim i As Integer
For i = 1 To 33
Windows("EXT-1-1.xlsx").Activate
Sheets("Sheet" & i).Select
Range("F2,F3,F6,F10").Select
Selection.Copy
Windows("Heave.xlsx").Activate
Sheets("EXT-1-1").Select
ActiveCell.Offset(1, 0).Select
Selection.PasteSpecial Paste:=xlPasteAll, Operation:=xlNone, SkipBlanks:= _
False, Transpose:=True
Next i
============================/EXT=========================

============================EXT-1-2=====================
Dim i As Integer
For i = 1 To 33
Windows("EXT-1-2.xlsx").Activate
Sheets("Sheet" & i).Select
Range("F2,F13").Select
Selection.Copy
Windows("Heave.xlsx").Activate
Sheets("EXT-1-2").Select
ActiveCell.Offset(1, 0).Select
Selection.PasteSpecial Paste:=xlPasteAll, Operation:=xlNone, SkipBlanks:= _
False, Transpose:=True
Next i

============================/EXT=========================

=========SETLLEMENTS - NEW_FILE_IMPORT==================
Dim i As Integer
For i = 1 To 33
ActiveWorkbook.Worksheets.Add After:=Sheets(Sheets.Count)
With ActiveSheet.QueryTables.Add(Connection:= _
"TEXT;C:\PredictedData\4) Settlements\East\" &
i & ".TXT", _
Destination:=Range("$A$1"))
.Name = "1"
.FieldNames = True
.RowNumbers = False
.FillAdjacentFormulas = False
.PreserveFormatting = True
.RefreshOnFileOpen = False
.RefreshStyle = xlInsertDeleteCells
.SavePassword = False
.SaveData = True
.AdjustColumnWidth = True
.RefreshPeriod = 0
.TextFilePromptOnRefresh = False
.TextFilePlatform = 866
.TextFileStartRow = 1
.TextFileParseType = xlDelimited
```

```
.TextFileTextQualifier = xlTextQualifierDoubleQuote
.TextFileConsecutiveDelimiter = False
.TextFileTabDelimiter = True
.TextFileSemicolonDelimiter = False
.TextFileCommaDelimiter = False
.TextFileSpaceDelimiter = False
.TextFileColumnDataTypes = Array(1, 1, 1, 1, 1, 1)
.TextFileTrailingMinusNumbers = True
.Refresh BackgroundQuery:=False
End With
Cells.Select
Selection.ColumnWidth = 15
Selection.NumberFormat = "0.000000"
Next i
==========/SETLLEMENTS - NEW_FILE_IMPORT==========

==========Settlements - East==========
Dim i As Integer
For i = 1 To 33
Windows("East.xlsx").Activate

Sheets("Sheet" & i).Select
Range("H2").Select
ActiveCell.FormulaR1C1 = "=RC[-5]-381"
Selection.AutoFill Destination:=Range("H2:H85"), Type:=xlFillDefault
Range("I2").Select
ActiveCell.FormulaR1C1 = "=RC[-3]*(12)"
Range("I2").Select
Selection.AutoFill Destination:=Range("I2:I85"), Type:=xlFillDefault
Columns("I:I").Select
Selection.Copy
Windows("Surface_Settlements.xlsx").Activate
Sheets("East").Select
ActiveCell.Offset(0, 1).Select
Selection.PasteSpecial Paste:=xlPasteValues, Operation:=xlNone, SkipBlanks _
:=False, Transpose:=False
Next i
==========/End==========

==========Settlements - West==========
Dim i As Integer
For i = 1 To 33
Windows("West.xlsx").Activate
Sheets("Sheet" & i).Select
Range("I2").Select
ActiveCell.FormulaR1C1 = "=RC[-3]*(12)"
Range("I2").Select
Selection.AutoFill Destination:=Range("I2:I85"), Type:=xlFillDefault
Columns("I:I").Select
Selection.Copy
Windows("Surface_Settlements.xlsx").Activate
Sheets("West").Select
ActiveCell.Offset(0, 1).Select
Selection.PasteSpecial Paste:=xlPasteValues, Operation:=xlNone, SkipBlanks _
:=False, Transpose:=False
Next i
==========/West==========
```

```
==========================Settlements - South==============
Dim i As Integer
For i = 1 To 33
Windows("South.xlsx").Activate
Sheets("Sheet" & i).Select
Range("I2").Select
ActiveCell.FormulaR1C1 = "=RC[-3]*(12)"
Range("I2").Select
Selection.AutoFill Destination:=Range("I2:I85"), Type:=xlFillDefault
Columns("I:I").Select
Selection.Copy
Windows("Surface_Settlements.xlsx").Activate

Sheets("South").Select
ActiveCell.Offset(0, 1).Select
Selection.PasteSpecial Paste:=xlPasteValues, Operation:=xlNone, SkipBlanks _
:=False, Transpose:=False
Next i
==========================/West============================

==========================Settlements - North==============
Dim i As Integer
For i = 1 To 33
Windows("North.xlsx").Activate
Sheets("Sheet" & i).Select
Range("H2").Select
ActiveCell.FormulaR1C1 = "=RC[-4]-311"
Selection.AutoFill Destination:=Range("H2:H91"), Type:=xlFillDefault
Range("I2").Select
ActiveCell.FormulaR1C1 = "=RC[-3]*(12)"
Range("I2").Select
Selection.AutoFill Destination:=Range("I2:I91"), Type:=xlFillDefault
Columns("I:I").Select
Selection.Copy
Windows("Surface_Settlements.xlsx").Activate
Sheets("North").Select
ActiveCell.Offset(0, 1).Select
Selection.PasteSpecial Paste:=xlPasteValues, Operation:=xlNone, SkipBlanks _
:=False, Transpose:=False
Next i
==========================/End=============================
```